To my family

MULTIPLEXED CELL-BASED DIAGNOSTIC DEVICES FOR THE DETECTION OF KIDNEY DISEASE PATHOLOGICAL MARKERS

A THESIS SUBMITTED TO

THE GRADUATE SCHOOL OF ENGINEERING AND SCIENCE

OF BILKENT UNIVERSITY

IN PARTIAL FULFILLMENT OF THE REQUIREMENTS FOR

THE DEGREE OF

MASTER OF SCIENCE

IN

MATERIALS SCIENCE AND NANOTECHNOLOGY

By

SILA KÖSE

DECEMBER 2020

MULTIPLEXED CELL-BASED DIAGNOSTIC DEVICES FOR THE DETECTION OF KIDNEY DISEASE PATHOLOGICAL MARKERS

By Sıla Köse

December 2020

We certify that we have read this dissertation and that in our opinion it is fully adequate, in scope and in quality, as a thesis for the degree of Master of Science.

_____

Urartu Özgür Şafak Şeker (Advisor)

_____

Fatih İnci

_____

Adil Denizli

Approved for the Graduate School of Engineering and Science:

_____

Ezhan Karaşan

Director of the Graduate School

ABSTRACT

MULTIPLEXED CELL-BASED DIAGNOSTIC DEVICES FOR THE DETECTION OF KIDNEY DISEASE PATHOLOGICAL MARKERS

Sıla Köse

MSc in Materials Science and Nanotechnology

Advisor: Urartu Özgür Şafak Şeker

December, 2020

Development of accurate, inexpensive and fast-screening devices has been a big vacancy in the field of medical diagnostics. Close monitoring and diagnosis of various diseases are generally conducted by typical analytical techniques which require intensive efforts and qualified personnel. Therefore, there is an urgent need for more convenient and reliable alternatives that are highly specific, cost-efficient and rapid. One of the approaches in solving this problem is using naturally-derived proteins and nucleic acid molecules that can respond to various types of metabolites. Synthetic biology utilizes these components to assemble biological systems that can probe and control metabolic state of a host. In this context, biosensors can be considered highly specific, cost-effective and can be implemented in point-of-care bioanalytical tools for effective healthcare. Here, we have developed biosensors that are responsive to medically relevant biomarkers namely; urea and uric acid. Furthermore, a multi-input version that can sense and respond to both biomarkers simultenously and another multiplexed biosensor that can mimic the AND-logic were developed. Biosensors were designed to respond to their respective

target analyte presence through an increase in the fluorescence intensity which can be measured with spectrophotometric devices. To do so, native promoter and transcription factors from different organisms were assembled inside a gene circuit to express a fluorescent protein in the presence of the respective biomarker. For urea biosensor, UreR transcriptional activator and the complete intergenic region inside the urease operon of the organism *Proteus mirabilis* were utilized. The system was optimized to have the desired dose- response curve using post trancriptional regulation elements and protein engineering. For the uric acid biosensor, transcriptional repressor HucR and the transcription factor binding site inside the uricase operon from the organism *Deinococcus radiodurans* were assembled in a gene circuit as well as a Uric Acid Transporter (UACT). Using promoter engineering and copy number modifications the response curve of the system was optimized. Next, biological components of the biomarkers were assembled in a multiplexed system to respond both molecules simultenously. Furthermore, a logic gate operating system was developed using promoter engineering that performs AND-logic to be implemented in a medically relevant algorithm A framework for stabilization of biosensors on low-cost portable paper discs through biofilm-cellulose interactions, and entrapment of whole-cell biosensors inside biocompatible, biodegradable and mechanically strong gelatin beads was provided for remote detection of the pathological biomarkers. Finally, the robustness of the developed whole cell biosensors was tested with human clinical samples.

Keywords: whole-cell biosensors, bio-diagnostic device, gene circuit optimization, logic gate implementation.

ÖZET

BÖBREK HASTALIKLARININ TAKİBİNDE KULLANILABİLİR ÇOK KATMANLI TÜM HÜCRE SENSÖRLERİ İLE OLUŞTURULMUŞ BİYOTEŞHİS CİHAZLARI

Sıla Köse

Malzeme Bilimi ve Nanoteknoloji, Yüksek Lisans

Tez Danışmanı: Urartu Özgür Şafak Şeker

Aralık, 2020

Kesin sonuç veren, ucuz ve hızlı tarama yapabilen sensör cihazlarının geliştirilememesi, tıbbi teşhis alanında büyük bir problem oluşturmaktadır. Çeşitli hastalıkların yakından izlenmesi ve teşhisi genellikle yoğun çaba ve kalifiye personel gerektiren tipik analitik tekniklerle yapılır. Bu nedenle, son derece spesifik, düşük maliyetli ve hızlı olan daha uygun ve güvenilir alternatiflere acil bir ihtiyaç vardır. Birçok organizma, doğal metabolitlere yanıt verebilen çeşitli proteinler ve nükleik asit molekülleri bulunmaktadır. Sentetik biyoloji, bu bileşenleri kullanarak belirlenen fonksiyonları yerine getiren özgün biyolojik sistemler geliştirebilir. Bu bağlamda, biyosensörler son derece spesifik, uygun maliyetli ve etkin biyoanalitik araçlar olarak sağlık takibi prosedürlerinde rutin olarak uygulanabilecek potansiyele sahiptir. Bu çalışmada, medikal testlerde sıklıkla takip edilen biyolojik belirteçlerden olan üreye ve ürik asite yanıt veren biyosensörler geliştirdik. Ayrıca, bu biyobelirteçleri eşzamanlı olarak algılayabilen ve bunlara yanıt verebilen bir biyosensör versiyonu ve VE-mantığını mimik edebilen bir hücresel biyosensör de geliştirildi. Biyosensörler, ilgili hedef analit varlığına floresan

yoğunluğundaki bir artış yoluyla yanıt verecek şekilde tasarlanmıştır. Böylece analitler spektrofotometrik cihazlarla ölçülebilmektedir. Bu amaç ile, farklı organizmalardan gelen doğal promoter ve transkripsiyon faktörleri, sentetik gen devrelerinde biyobelirteçlerin varlığına floresan protein üretecek şekilde birleştirildi. Üre biyosensörü için *Proteus mirabilis* organizmasının UreR transkripsiyonel aktivatörü ve promotör olarak da üreaz operonu içindeki tam intergenik bölge kullanıldı. Sistem, post-transkripsiyonel modifikasyon elementleri ve protein mühendisliği kullanılarak istenen doz-yanıt eğrisine sahip olacak şekilde optimize edildi. Ürik asit biyosensörü için, *Deinococcus radiodurans* organizmasından transkripsiyonel baskılayıcı HucR ve ürikaz operon içindeki transkripsiyon faktörü bağlanma bölgesi, bir gen devresinin yanı sıra bir Ürik Asit Taşıyıcı (UACT) içinde birleştirildi. Promotör mühendisliği ve kopya sayısı modifikasyonları kullanılarak sistemin doz-yanıt eğrisi optimize edildi. Daha sonra, biyobelirteçlerin biyolojik bileşenleri, her iki moleküle aynı anda yanıt verebilen için çoklu bir sistemde bir araya getirildi. Ek olarak, medikal algoritmalarda uygulanabilir VE-mantık kapısı işletimini gerçekleştiren bir sistem promotör mühendisliği kullanılarak geliştirildi. Patolojik biyobelirteçlerin uzaktan tespiti için biyofilm-selüloz etkileşimleri yoluyla, biyosensörlerin düşük maliyetli ve taşınabilir kâğıt diskler üzerinde stabilizasyonu ve tam hücre biyosensörlerinin biyo-uyumlu, biyolojik olarak parçalanabilir ve mekanik güce sahip jelatin boncuklar içinde tutulması için deney düzenekleri oluşturulmuştur. Son olarak, geliştirilen tam hücre biyosensörlerinin sağlamlığı klinik insan numuneleri ile test edilmiştir.

Anahtar kelimeler: hücresel biyosensörler, biyo-teşhis cihazı, gen devre optimizasyonu, mantık kapısı uygulaması.

ACKNOWLEDGEMENTS

I would like to thank my advisor, Assoc. Prof. Dr. Urartu Özgür Şafak Şeker for being very helpful and supportive during the time I spent here. I thank him for all the advices he has given me and for the great learning experience I gained here. Next, I would like to thank my thesis tracking committee; Asst. Prof. Fatih İnci and Prof. Dr. Adil Denizli for being my jury members and their valuable feedback.

Luckily, I was surrounded by very hardworking and ambitious colleagues during my stay in this lab. These people made my stay here very enjoyable during the hardest days. Starting with my supportive partners in the project İlkay Çisil Köksaldı and Recep Erdem Ahan, I would like to thank all the current and former members of SBL: Dr. Ebru Aras, Ebru Şahin Kehribar, Merve Erden, Murat Alp Güngen, Nedim Hacıosmanoğlu, Ahmet Hınçer, Gökçe Özkul, Anooshay Khan, Eray Ulaş Bozkurt, and former SBL members, Dr. Esra Yüca, Dr. Ebuzer Kalyoncu, Dr. Tolga Tarkan Ölmez, Dr, Elif Duman, Dr. Behide Saltepe, Musa Efe Işılak.

Spending so much time at the lab, I gained precious friendships which I am grateful for. I would like to thank my close friends Julian Ostaku, Özge Beğli and Merve Yavuz for their companionship and all the things they have done for me. I thank Julian Ostaku for his patience and sharing a quarter-life existensial crisis with me. Özge Beğli for making late-night studying so much more fun with cheesy pop music and quality jokes. Merve Yavuz for all the coffee breaks and conversations we shared. Also I thank Büşra Merve Kırpat and Özge Beğli for the lively night-in’s at their house.

Finally, I would like to thank my family and friends. I am so proud and lucky to be the daughter of Uğur and Hatice Köse. They are the most supportive, knowledgable and kindest people that I know, I would not be here without them. Furthermore, I would like to thank my little sister, Güneş Köse for being my real-life stress ball, she is the greatest. I would like to thank my better half Ozan Umut Zor for the times we shared together and his support. Finally, I thank Funda Uzun for being my best friend for more than 13 years, I am grateful that we grew up together.

This study is supported by TÜBİTAK Project Number 115Z217.

Table of Contents

List of Figures

List of Tables

CHAPTER 1
Introduction

1.1 Whole-Cell Biosensors and Synthetic Biology

The similarities between electronic circuits and biological parts namely connectivity and collective processing logical operations have resulted in the emergence of the field synthetic biology with the fundamental goal of engineering biological circuitry. Synthetic biology was founded with engineering principles such as modularization, rationalization and modelling and it has been one of the fastest growing fields of biology [1].These rational and systematic approaches have resulted in rapid evolution of sensors, control circuits, and actuators as tailor-made biosystems for the detection of specific molecules. Therefore, the field is increasingly transitioning to the clinics with the broad goal of developing novel, versatile, programmable and autonomous diagnostic devices since the clinical industry suffers from limited number of comprehensive diagnosis of patient pathophysiology and personalized medicine techniques[2].

Mainly based on analytical chemistry techniques or antibody-based platforms, conventional diagnostic technologies inherently do not accomodate for detection of dynamic biomarker signatures, precise processing of localized information, or non-invasive monitoring with point-of-care systems. Other drawbacks of traditional approaches include; high-cost, requiring extensive infrastructure and technical expertise and time consumption.Therefore,

developing new modes of detection for complex and dynamic biomarkers has drawn the attention of synthetic biologists over the years.

The rise of synthetic biology has led to construction of various novel gene circuits and biological parts such as toggle switches, ring oscillators, cell-cell communication and biomolecular Boolean logic. These advances are then used to build sensor, counter, multiplexed, and memory systems[3]. Synthetic biology-enabled technologies have applications areas in the production of chemicals, industrial enzymes, biofuels and natural products[4]. Developments in the synthetic biology have also expanded in clinical applications, from designing detection systems, building engineered tissues to developing new drugs and vaccines[5].

One of the new molecular diagnostics approach with synthetic biology that can be used for real-time monitoring of difficult-to-trace metabolites is achieved through transcriptional gene switches based on prokaryotic transcription factors[6]. These systems, namely whole cell biosensors, utilize the natural biorecognition elements in a genetic circuit to drive the expression of various physical or chemical signals in response to a selected target analyte[7]. The incredible diversity of sensors and regulators found in all organisms opens the way for designing novel synthetic architectures with desired criteria. Furthermore; the whole-cell biosensors compared to their traditional counterparts provide versatility, high accuracy and high-throughput screening while being low-cost and rapid. Over the years various cell-based biosensors have been developed for diagnosis of medical conditions including but not limited to inflammation[8, 9], cancer[10, 11], detection of micronutrients[12-14] and pathological agents[15-19].

1.2 Transcription Factor-Based Biosensors

With cellular biosensors, intracellular detection of various natural metabolites can be exploited and conversion this detection into a measurable output in can be achieved. As the sensory unit; metabolite-sensing proteins such as transcription factors, enzymes, periplasmic-binding proteins or with regulatory RNA aptamers can be used. This sensing unit of the biosensor can then be combined with the processing unit and the actuator unit. The processing unit is resposible for modulating the expression of the chosen reporter molecule which can be a fluorescent, bioluminicent or a pigment reporter and a selection marker[20, 21].

Generally, a transcription-factor based biosensor is composed of as its name suggessts; a transcription factor (TF), an operator or the transcription factor binding site (TFBS) on the promoter and the gene of output signal of choice. Simply, the TF with its ligand-binding domain (LBD) binds to the desired analyte and with its DNA-binding domain (DBD) regulates the interactions with the processing unit depending on the conformational change induced by LBD. Processing unit in return affects RNA polymerase (RNAP)-promoter association to affect the transcription of the chosen output signal molecule[22].

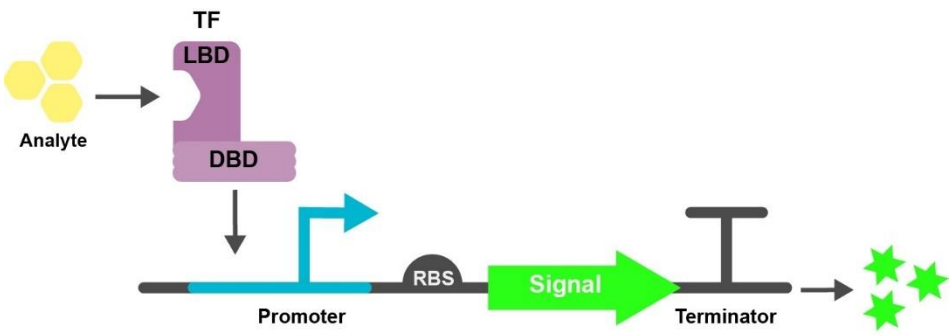

Figure 1: Schematics of a TF-based Biosensor

Transcriptional factors can regulate the transcription in one of two ways; by repressing or activating. Transcriptional repressors bind to their cognate binding regions on the operon when the effector metabolite is not present. When bound, repressors can block the RNA polymerase interaction with the operon hamper transcription progression. Target metabolite binding to the repressor results in its release from the operon which results in transcription activation of the reporter molecule. There is a different mode of regulation can for TFs called aporepressors, in which aporepressor can only bind to its TFBS and inhibit transcription only when bound to its effector[23]. Finally, the activators act by recruiting RNA polymerase to the promoter or forming active RNA pol-promoter complexes when bound to the target molecule. Regulation by the transcriptional activators are considered more eleborate and less clear requiring processes such as DNA bending and the making specific contacts with RNA polymerase or its subunits available[23]. Biosensors can have combinations of architectures depending on the desired interactions of the sensing and regulation module as described in the Figure 2 [24].

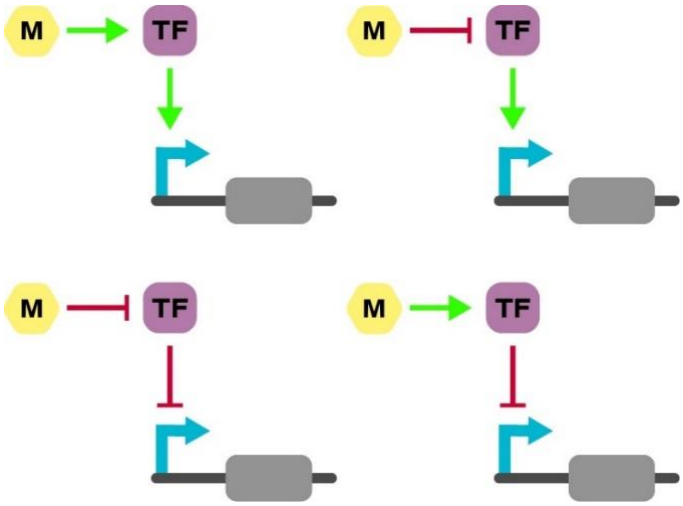

Figure 2: General arhitectures of TF-based Biosensors. (A) Activated-activator[25], Repressed-Activator[26], Activated-Repressor[27], Repressed-Repressor[28]

One of the tunable characteristics of TF-based biosensors is its specificity for the corresponding ligand molecule. Specificity can be defined as the relative increase in the signal molecule before and after target ligand binding to the transcription factor compared to other potential non-targets in the setting. The eligible TF should have high sensitivity to its target molecule and should not bind to other molecules that can be found under the testing conditions.

The other most common engineered characteristic of the TF-based biosensors is the dose-response curve, which can be extrapolated from the proportion of the input concentration to the output signal level. Parameters considered in the response curve include; half-maximal threshold, the dynamic range and the sensitivity or the slope. Operational range of a biosensor is the concentration range of the target molecule in which output signal levels are considered significantly different from the uninduced state. The half-maximal threshold is as its name suggests, the ligand concentration needed for the half maximal

output to be reached.The dynamic range on the other hand is the signal range of the biosensor between the ON and OFF states of the biosensor. The slope of the response function shows the sensitivity of the biosensor to the chosen analyte. Depending on the binding kinetics, the response can show analog or digital behaviour. This behaviour is influenced by the various underlying regulatory mechanisms in the circuit. One problem needed to be tuned in biosensing systems is the leaky expression which leads to a high background meaning the gene circuit's activation or the lack of repression when the target analyte is absent in the system.

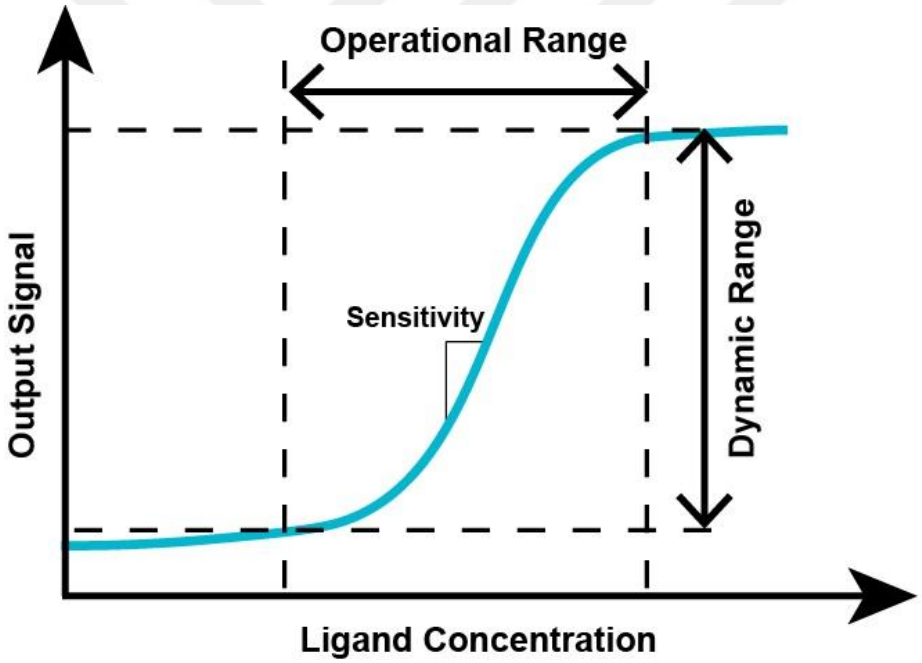

Figure 3: The parameters of a cellular biosensor

1.3 Tuning the Transcription-Based Biosensor

Functional genetic networks are mainly have two forward engineering approaches; trial-and-error or computer-aided design. To address patient-specific medical conditions or environmental monitoring, standardized natural

and in vitro-evolved biological parts are assembled in a plug-and-play fashion[29].

Trial-and-error circuit implementation for TF-based biosensors, generally target the sensing and regulation modules seperately and require iterative testing and refinement cycles. Modifying the binding kinetics between the effector and the transcription factor or the transcription factor and its promoter through trial-and-error methods such as saturation mutagenesis and FACS screening might mitigate unpredictable issues or result in failure[29, 30]. One important factor should be taking into consideration is the fact that changes in component can affect all parameters of the dose−response curve simultaneously. Thus, multicomponent systems require combinatorial fine-tuning of component expression strengths[31].

Automatic or computer-aided designs have proved their tremendous value for circuit assembly over the recent years(ref). While the circuit performance predictive design. While circuit design software holds great potential to test assembles extensively and enable precise manipulation, capabilities of such tools remain limited and in vitro debugging is inevitable[32].

1.4 Kidney Related Pathological Biomarkers: Urea

Urea is a small organic compound comprised of two amino groups (NH_2) linked to a carbamyl (C-O). Being the principal end product of protein metabolism, urea is mainly excreted through the kidneys. The so-called “urea cycle” in the protein metabolism converts the toxic product ammonia to non-toxic urea with series of five enzymatically controlled reactions in the body (Figure 5) [33].

Therefore, urea has been an important biomarker when it comes to monitoring kidney functions and detecting kidney related diseases [34, 35].

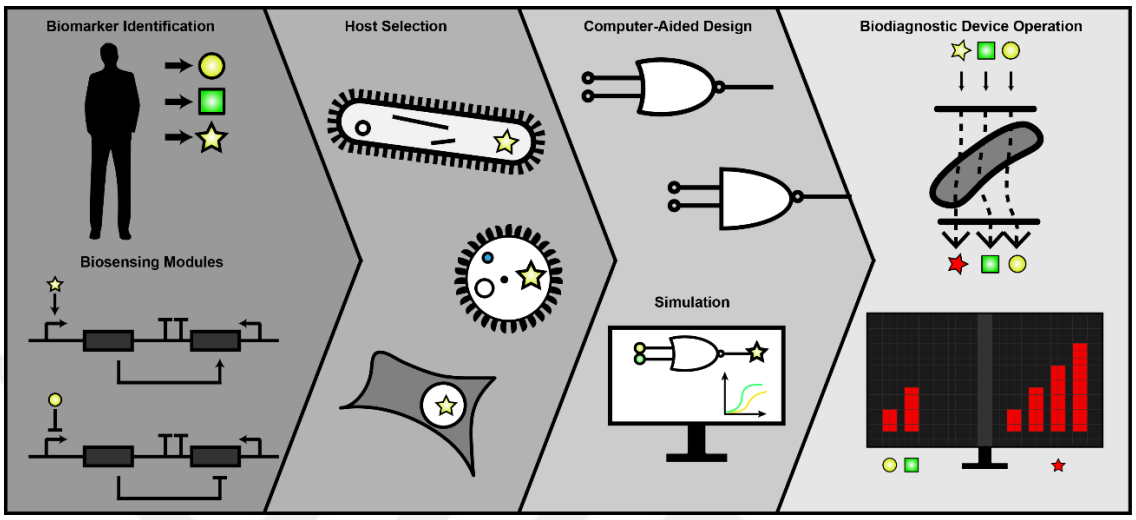

Figure 4: Workflow of synthetic biology-enabled next-generation diagnostics.

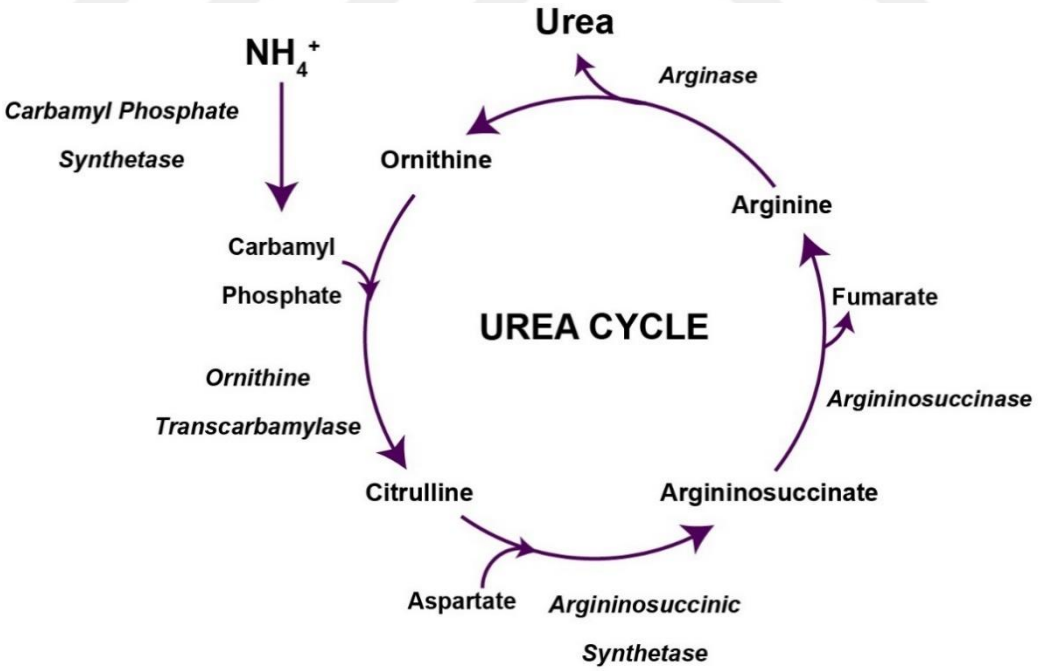

Figure 5: Simplified Urea Cycle[36].

To measure Blood Urea Nitrogen (BUN) in routine laboratory tests, generally kinetic assays are used with immobilized urease enzyme. The enzyme urease is used to cleave urea into ammonium and hydrogencarbonate.The enzymatic reaction is then monitored using conventional methods including; potentiometry with pH electrodes [37] and NH_4^+ selective electrodes [38], UV-visible spectrophotometry and ammonium ion-selective field effect transistor, coulometry and amperometry [39].The intrisinc problems with these techniques are influence of the buffering capacity of the sample on the response, interferences in biological solutions, lack of point-of-care measurement capability, relative slow response and high detection limit [39, 40].

1.5 Kidney Related Pathological Biomarkers: Uric Acid

Uric acid ($C_5H_4N_4O_3$) is a heterocyclic organic compound and in humans it is the end product of catabolism of pürine products which are the monomeric precursors of nucleic acids. Uric acid is a weak acid at physiological pH and mainly exists as urate, the salt of uric acid. The elevated levels of urate in the blood results in uric acid crystal formation. Since humans lack the enzyme uricase, uric acid oxidation to more soluble allantoin does not occur. Furthermore, the solubility of uric acid in water is low, approximately 6-8 mg/dL and humans have uric acid levels close to the solubility limit on average. The reference range of uric acid in blood is 1.5-7.0 mg/dL (0.09-0.42 mM). Many enzymes are involved in the conversion of adenine and guanine, to uric acid (Figure 6)[41].

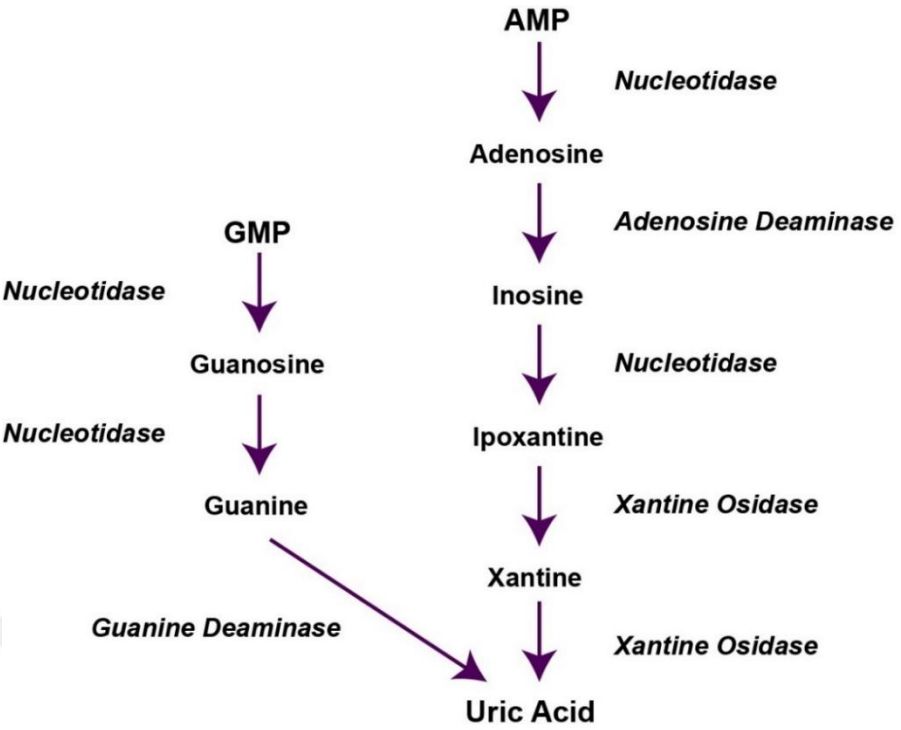

Figure 6: Simplified Purine Metabolism[41].

The kidneys excrete the two-thirds of uric acid while the rest is eliminated through the gastrointestinal tract[41]. Therefore, high uric acid levels in the body can be strong indicators of renal failure and cardiovascular disease[42, 43] as well as othe syndromes such as gout, dyslipidemia, insulin resistance, tumor lysis syndrome,crdiovascular disease and Lesch–Nyhan syndrome[42, 44, 45]. In addition to being a biomarker of renal dysfunction, uric acid is suggested to be effector of the development and progression of renal disease by the recent studies [46-48].Since uric acid is a critical biomarker with connections to various metabolic abnormalities, it is one of the routinely screened biomarkers in blood tests.

The main methods for uric acid determination in the clinical laboratory are phosphotungistic acid methods (PTA), high-performance liquid chromatography methods and enzymatic quantification. In the non-enzymatic

methods, the blood serum was mixed with phosphotungstic acid which results in a color change. Although, this method has been used in medical tests, it is generally considered an overestimation of true uric acid levels since the results are affected by the presence of other molecules such as ascorbic acid[49]. As an enzymatic quantification method, uricase oxidase can be utilized to catalyze blood uric acid decomposing into allantoin. While higher sensitivity can be achieved this technique than colorimetric methods, the enzymatic quantification methods have the high cost drawback[50].

1.6 Aim of this study

The appeal of cell-based biosensors as low-cost, rapidly deployable and on-site diagnostics alternatives to conventional bio-diagnostic methods has been well-understood over the last two decades[51]. While the transfer of these systems to real world applications has been slow, we aimed to accelarate this process by developing cellular biosensors with medically relevant biomarkers. With the state-of-art gene circuit optimization methods, we have showed the desired sensitivity and the dose-response curves expected from a medical diagnostic device can be achieved. Furthermore, we have developed multiplexed systems that can be used for diagnosis of diseases where a combination of several markers is needed by aiding medical decision-making. Finally, we have showed potential integration methods of cellular systems on point-of-care devices to enable routine testing. The developed next-generation diagnostic devices aim to meet clinical specifications and attain more widespread application globally.

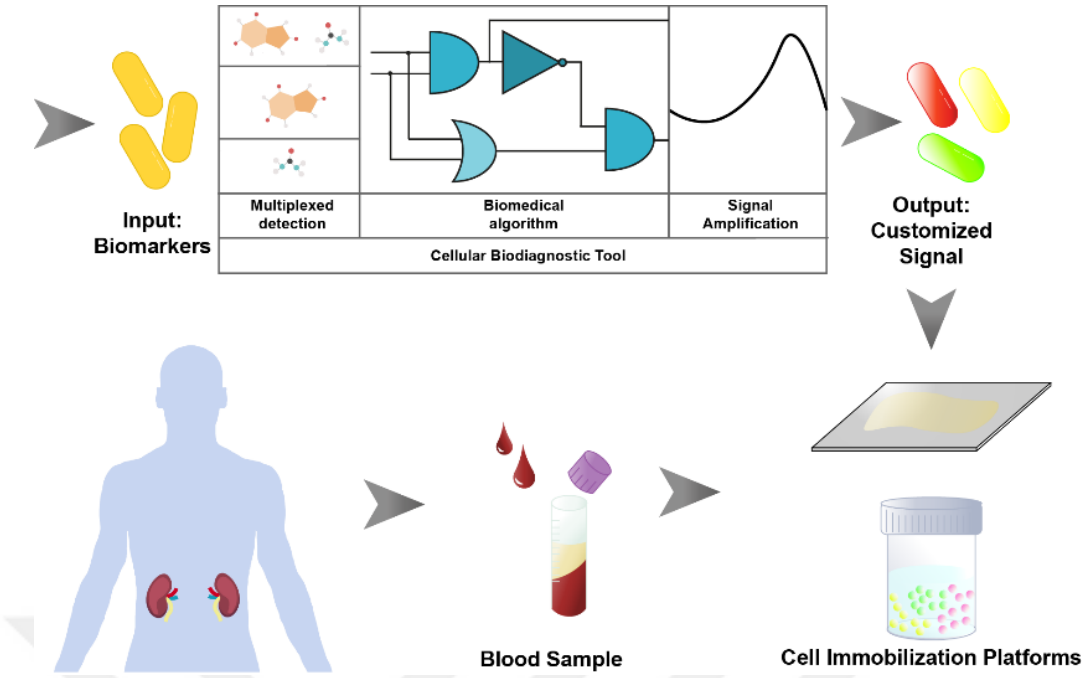

Figure 7: Summary of the development of cellular bioisensors for kidney related diseases and the application strategies for real-life applications.

CHAPTER 2
Materials and Methods

2.1 Bacterial Strains, Growth and Maintenance

For the cloning and characterization assays, *Escherichia coli (E. coli)* DH5α PRO strain was used as the chasis. This strain contains a cassette for constitutive expression of TetR, LacI and spectinomycin resistance gene as well as certain endonuclease mutations for an efficient plasmid vector storage. For biofilm immobilization studies, *E. coli* DH5 alpha Δcsga was utilized. Cell stocks were maintained in a solution mixed in equal volumes of Lysogeny Broth (LB) medium and 50%(v/v) glycerol solution followed by at -80 ˚C storage. Overnight cultures were prepared by inoculation of cell stocks in fresh LB medium with corresponding antibiotics (1:1000) and grown at 37 ˚C for 16 hours at 200 rpm.

2.2 Preparation of Chemically Competent Cells and Transformation

Cells were inoculated from -80 ˚C cell stock as mentioned previously and grown overnight. Next, the growth was diluted (1:100) in fresh LB and grown in same conditions of overnight growth until their OD_{600} reached 0.2-0.5. Then the cell suspension was cooled on ice for 10 minutes followed by centrifugation at 3000 rpm for 10 minutes. Supernatant was removed and the cell pellet was then resuspended in 1:10 growth volume of TSS Buffer. Resuspended cells were aliquoted to have 100µl per sample and stored -80 ˚C until use.

For transformation, competent cells that are taken from -80 ˚C were thawed on ice, before mixing them with the 100 ng of intact target plasmid or the total volume of the completed Gibson assembly reaction or T4 ligation mixture. Then cells were kept on ice 20 more minutes before the heatshock. Heatshock was done at 42 ˚C for 45 seconds followed by immediate incubation on ice for 2 minutes. After that, 250µl of LB was added onto each sample and samples were incubated at 37 ˚C, 200 rpm for 45 minutes. When the incubation was completed, cells were centrifuged at 5500 g for 6 minutes. 250µl of the supernatant was removed and pellet was dissolved in the remaining volume before spreading onto LB-agar plate with appropriate antibiotics

2.3 Plasmid Construction and Cloning

Prior to cloning, PCR amplified product and restriction digested part sizes were verified by gel-electrophoresis with loading the PCR or restriction digestion reaction in %1 agarose gel respectively. Gels were run 25-45 minutes at constant 120-140V. The correct sized products were isolated from agarose using MN PCR clean-up kit according to manufacturer's protocol. Isolated products were then assembled with home-made Gibson Assembly reaction mix (details are given in Appendix E) by mixing 50 ng digested vector, the equal molar of insert and ddH_2O (when necessary) with 7.5 µl of 1,33x Gibson reaction mix to have the final 10 µl reaction volume. The reaction mix was then incubated at 50 ˚C for 1 hour. At the end of 1 hour, assembled vectors were transformed to chemically competent E. coli DH5α PRO as described above.

Sequences of the constructed vectors were verified by Sanger Sequencing (GENEWIZ). All Sequences used in here can be found in Table A1, and all

constructed vector maps were indicated in Appendix C with their respective sequencing verification results in Appendix D.

2.4 Construct Design and Sequence Alignment with Benchling Software

For all construct designs, online Benchling software (http://benchling.com) was used. Sequencing result files were obtained as ab1 or seq files and uploaded to benchling alignment tool from the control panel of the server. Corresponding constructs were used as template to analyze the sequencing results with MAFFT (Multiple Alignment using Fast Fourier Transform) algorithm. Standard parameters used during the analyses.

2.5 Biosensor Characterization Assays

2.5.1 Urea and Uric Acid Induction with Whole-Cell Biosensors

Overnight grown samples were diluted (1:100) into 10 mL fresh LB medium with the appropriate antibioticsand and grown at 37°C, 200 rpm until their optical density(OD_{600}) reached to 0.4-0.6. After that, samples were induced with freshly prepared 5M urea and 10 mM uric acid solution. Unless other otherwise stated, induction conditions were 37°C, 200 rpm for 8 hours or specified time intervals such as 0,2,4,6,8 and 16 hours. Duration of specific assays were chosen from the observed maximum or close to maximum signal time points that would be suitable for further multiplexed biosensor assays. Fort he dynamic range profiling assays 8th hour was chosen as the designated time point, unless otherwise stated.

2.5.2 Fluorescence Measurement and Data Analysis

Fluoresence measurements were done by taking 400 µL of samples to microcentrifuge tubes at the designated time point. Tubes were then centrifuged for 3.5 minutes at 14000 rpm and the supernatant was removed from each sample. Cell pellets were resuspended in equal volume of 1x PBS. 200 µL of the samples were then transferred to Corning 96-well clear flat bottom polystyrene plates to measure fluoresence and OD_{600} values via a microplate reader(SpectraMax M5, Molecular Devices). Excitation and emisson wavelengths for sfGFP protein expression were 485 nm and 538 nm, respectively. For mScarletI protein expression, excitation wavelength of 544 nm and emission wavelength of 612 nm were used. For all samples absorbance was measured at 600 nm.

2.6 Statistical Analysis

For data analysis, normalization was done by subtracting the value of fluorescence and the value of OD_{600} the blank PBS solution from the fluorescence value and OD_{600} of each sample respectively. Then, the fluorescence value of each sample was divided by it OD_{600} value.

All data is displayed as mean ± standard deviation. Depending on the data groups, one-way analysis of variance (ANOVA) or two-way ANOVA with Dunnett's/Tukey's/Sidak's multiple comparison test were used (GraphPad Prism v8). Dynamic range experiments were plotted using One site-Specific binding with Hill slope (GraphPad Prism v8).

2.7 Fluorescence Microscopy

Samples were prepared as described in fluorescent measurement and data analysis. Fluorescent pictures were taken with epifluorescent microscope (Zeiss) for sfGFP Zeiss filter set 49 (excitation; 470/40nm, emission; 525/550).

2.8 Environmental scanning electron microscope (ESEM)

Fixation of the cells were done with addition of 400 µL %2,5 glutaraldehyde solution in PBS onto paper samples. Samples were kept at 4 ˚C overnight. Following the fixation, samples were washed with 400 µL of 1x PBS solution twice for 5 minutes each. Next, samples were washed with 25% ethanol, 50% ethanol ve 75% ethanol solutions for again 5 minutes each. Finally, samples were kept in 100% ethanol for 10 minutes before drying with a critical point dryer (Tousimis). Samples were then coated with 8nm with Au/Pd alloy. The silica wafers were examined under ESEM (Tecnia) at 15 kV, 3.0 spot size.

2.9 Whole-Cell Biosensor Immobilization Assay on Whatman Paper

Overnight grown cells were diluted (1:100) in 10 mL LB with corresponding antibiotics and grown at 37°C, 200 until their OD_{600} reached approximately 0.5. Cells were then centrifuged at 3000 rpm for 10 minutes. Supernatant was removed and the cell pellet was resuspended in 10 mL of fresh M63 minimal medium with corresponding antibiotics.

Whatman paper, Corning 24-well clear flat bottom polystyrene plate, dH_2O, paper napkins and a plastic container were sterilised for 15 minutes under UV-light inside a laminar flow hood. Paper discs were cut fitting to bottoms of the

24-well plate. Another set of samples were prepared by diluting cells that have OD_{600} 0.5 to have OD_{600} of 0.01 in fresh M63 medium with appropriate antibiotics. 2 mL from the parallel sets that have OD_{600} 0.5 and 0.01 were then directly added onto the paper covered wells. A sample that is composed of only paper and sterile M63 medium was used as reference for analysis under ESEM. Samples were either re-induced with 0.2% arabinose solution or the medium was refreshed with proper antibiotics and 0.2% arabinose solution every 3 days. Samples were kept in the plastic container that has paper napkins stuck on its walls which were wetted with sterile dH_2O. Container was tightly closed and kept in 30°C incubater for 6-9 days unless otherwise stated. The medium of the samples were changed with fresh M63 medium with appropriate antibiotics and 0.2% arabinose without disturbing the formed biofilms.

2.10 Biosensor Entrapment inside Hyrogel Beads

Sterile sunflower seed oil was cooled down to -5°C.100% acetone and sterile dH_2O was kept -20°C approximately 1 hour prior to use. edible gelatin sheets(Kenton, Yaprak Jelatin 20g) were softened in warm water and then dissolved in sterile 1xPBS (10%w/v) by vortexing and heating at 55°C. After dissolving, liquid gelatin was kept at 40°C until bead formation. Overnight grown urea or uric acid biosensors were diluted (1:100) into liquid gelatin mixture. Immediately, cell suspension was pipetted into cold oil to form beads. Beads were then transferred to cold 100% acetone to remove the residual oil. After that beads were washed in cold water and drained with a sieve. A transglutaminase(Tito-Transglutaminaz Enzimi-Aktive 100g)-LB mixture was prepared by mixing edible transglutaminase in sterile LB medium with

appropriate antibiotics to have 25%(w/v) concentration. Beads were transferred to transglutaminase-LB mixture and kept at 4°C for 24 hours before induction. Induction was made by transferring beads to 2 mL LB with 100 mM urea containing 24-plate wells and incubated at 37°C for 12 to 24 hours.

2.11 Detection of Biomarkers in Clinical Samples

Blood serum samples were kindly provided by Doç. Dr. Asbürçe Olgaç. Blood Serum Samples were collected from both patients with high levels of urea and/or uric acid and individuals with that have healthy levels of urea and uric acid. Serum samples were stored at -20°C until use. Overnight grown urea or uric acid biosensors were diluted (1:100) into M63 minimal medium with corresponding antibiotics and grown at 37°C, 200 rpm until their optical density (OD_{600}) reached to 0.4-0.6. After that, 300 µL of samples were taken and divided into 1.5 mL volume eppendorfs before inductions. Cells were then centrifuged at 3000 rpm for 10 minutes. Supernatant was removed and the cell pellet was resuspended in appropriate volume of fresh M63 medium to have 300 µL final volume when serum samples are added in the next step. Samples were induced with human serum samples that have different levels of urea and uric acid. Urea biosensors were induced with addition of 15 µL serum sample (serum 1:20 diluted) unless otherwise stated. Uric Acid biosensors were induced with addition of 1.5 µL serum sample (serum 1:200 diluted) unless otherwise stated. Bionsensors were induced for 16 hours unless stated otherwise. Fluorescence measurements were done as described above.

CHAPTER 3

Results and Discussion

3.1. Development and Optimization of the Urea Biosensor

3.1.1 Construction of the Initial Urea Biosensor

For building an urea sensor stage of the project, a synthetic gene circuit was built using the UreR transcription factor as the sensing unit and the pUreR promoter as the transducing unit. Both parts were taken from the organism *Proteus Mirabilis,* a common bacterium that infects urinary tracts[52]. In the presence of urea, the UreR transcription factor can dimerize and enhance the transcription by binding to UreR binding region on the pUreR.

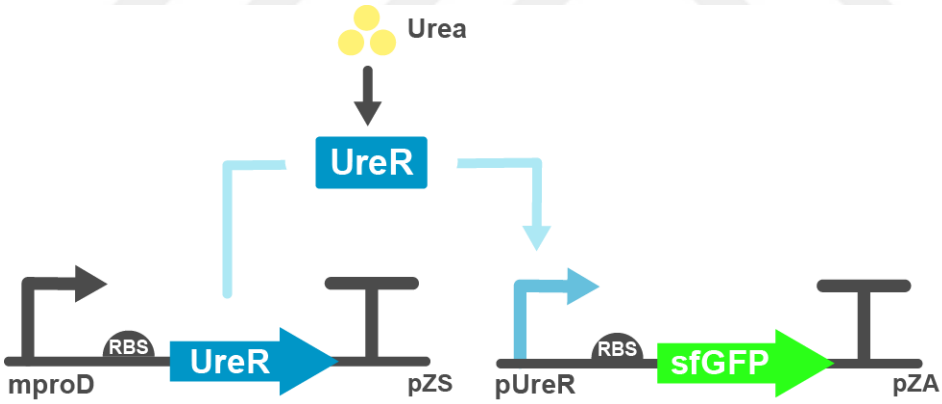

Figure 8: The biological parts and the mechanism used in the urea biosensor. Urea sensitive UreR activator is constituvely expressed via mproD promoter. When urea diffuses inside the cells, UreR first binds to urea and then activates the transcription of sfGFP signal protein via pUreR promoter.

First, constitutive expression of UreR inside the host was established by cloning the TF into the low copy pZS vector downstream of a low-strength

promoter mproD. This was done not to impose a metabolic burden to the host while expressing the sensing unit continiously inside the cell. UreR with the mproD promoter and an RBS (ribosome binding site) sequence was amplified with gibson primers (appendix B) with two PCR reactions.

pZS T7-LacO LuxI plasmid (acquired from Recep Erdem Ahan) was digested with BamhI XbaI restriction enzymes to be used as the backbone. First PCR reaction of mproD-UreR insert was ran on 1%agarose gel, then the bands on the correct size were isolated using MN-gel extraction kit according to manufacturer's instructions (Figure 9.A). The isolated PCR product was then subjected to the second round of PCR using the appropriate primers (appendix B). Then second reaction was again run on 1% agarose and isolated. (Figure 9.B) The isolated pZS backbone and the mproD-UreR were then assembled using the Gibson Assembly method. The success of the cloning was then determined with Sanger sequencing (Appendix D).

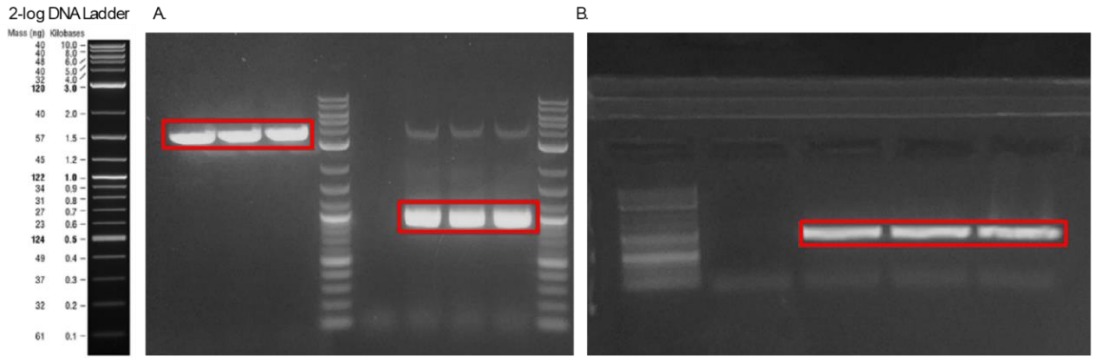

Figure 9: Agarose gel images of the biological parts needed to construct pZS mproD UreR plasmid. A. Digested pZS backbone sized 3297 bp is on the left and the first PCR reaction of mproD UreR insert that is 957 bp is on the right. B. Second PCR reaction product of mproD-UreR amplifications sized 1004 bp.

To generate a fluorescent signal in response the urea, the pUreR promoter was cloned on the upstream of the sfGFP (super-folder green fluorescent protein) reporter. The system was then placed in the pZA plasmid that is a mid-copy vector.

For the construction of pZA pUreR sfGFP plasmid, pZA vector (acquired from Recep Erdem Ahan) was digested with AatII and MluI and the pUreR promoter was amplified with primers from the synthesized DNA segment (Figure 10.A). In addition, sfGFP-rrnb T1 terminator region was amplified with designated primers (Figure 10.B).

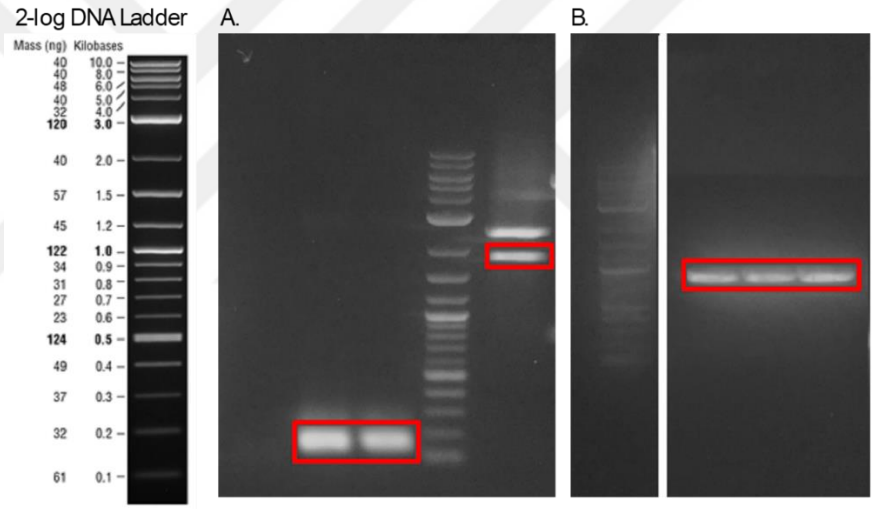

Figure 10: Agarose gel images of the biological parts needed to construct pZA pUreR sfGFP A. PCR-amplified pUreR promoter with the size of 172 bp (left). Pza backbone which is digested with AatII and MluI, 1722 bp (right). B. PCR amplified sfGFP-rrnb T1 DNA insert sized at 882 bp.

The products of the restriction digestion and the PCR reactions were run at 1% Agarose gel before gel extraction. Isolated DNA parts were then assembled

with Gibson Assembly method. The verification of the cloning was done with Sanger sequencing (Appendix D).

3.1.2 Characterization of the Initial Urea Biosensor

The sensivity and response capability of the constructed genetic gates were initially assayed with urea induction experiments. Sensor unit pZS mproD UreR and the transducer unit pZA pUreR sfGFP were first co-transformed to *E.coli* DH5α PRO host. Testing was done on cells prepared as described in Materials and Methods. For the initial screening, urea was dissolved in dH_2O and directly added to appropriately grown cells to have a final concentration of 100 mM. Fluorescence and optical density measurements were conducted at the 8th hour of induction. Cells that carry both the sensor and the transducer plasmids but not induced with any urea solution were used as control. While, urea induced cells have shown significant fluorescence increase in response to urea, fluorescent signal levels were low.

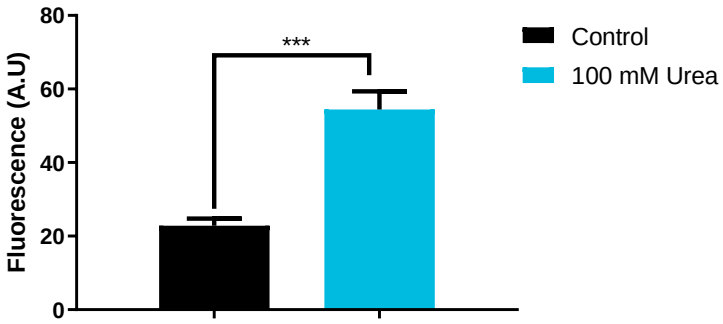

Figure 11: Characterization of the pZA pUreR sfGFP urea biosensor. After induction with 100 mM urea solution. The fluorescence and the optical density oft he samples were measured at the 8th hour. The data shows the normalized values of triplicate samples. Statistical significance was determined with unpaired Two-tailed t-test. (**: $p < 0.01$)

3.1.3 Construction of High Copy Number Urea Transducer Unit Plasmid

To increase the signal levels and expand the operational range of the urea biosensor, components of the transducing unit were cloned in a high copy plasmid. By increasing the number of promoter units per cell its interactions with both the TF and the RNA polymerase were aimed to be heightened. Thus, the p15a origin of replication region of the pZA plasmid was replaced with the pBR 322 origin of replication.

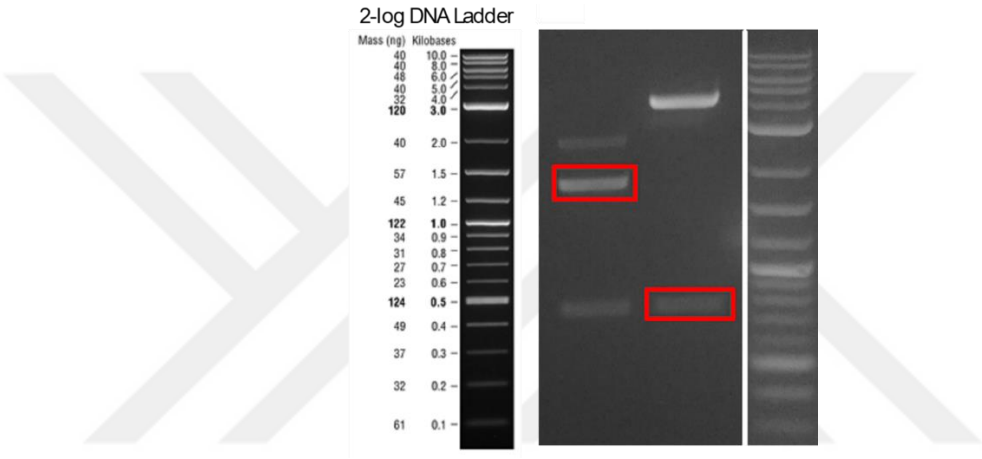

Figure 12: Pictures of the DNA parts needed for the construction of pZE pUreR sfGFP ran on 1% agarose gel. p15A origin of replication was restricted from pZA pUreR sfGFP backbone with SpeI and AvrII enzymes (2630 bp, left). pBR 322 origin of replication digested with SpeI and AvrII enzymes from the pZE palkB GFP plasmid, sized at 814 bp(right)

To do so, pZA pUreR sfGFP plasmid was digested with restriction digestion enzymes AvrII and SpeI which resulted in the removal of p15a origin of replication so that pZA pUreR sfGFP backbone could later be joined with pBR322 ori. Isolation of pBR322 ori was done by digesting pZE palkB GFP plasmid (acquired from Recep Erdem Ahan) with the same restriction digestion enzymes AvrII and SpeI (Figure 12).

After running the restriction digestion reactions on 1% Agarose gel and verifying their expected sizes, digestion products were isolated with MN gel extraction kit following the manufacturer's protocol. Isolated DNA parts were then conjoined wiyh T4 ligation reaction (Materials and Methods). The cloning was verified with Sanger sequencing (Appendix D).

3.1.4 Characterization of the Urea Biosensor in High Copy Vector

Constructed pZE pUreR sfGFP plasmid was first co-transformed to *E.coli* DH5α PRO host with the pZS mproD UreR plasmid. Urea induction assay was conducted as mentioned previously with cells in the log-phase being induced with 100 mM fresh urea solution. Signal amplification of the sensor was determined at the time points 4^{th},6^{th},8^{th} and the 24^{th} hours after the induction. Uninduced cells carrying the pZE pUreR sfGFP and the pZS mproD UreR plasmids were used as control.

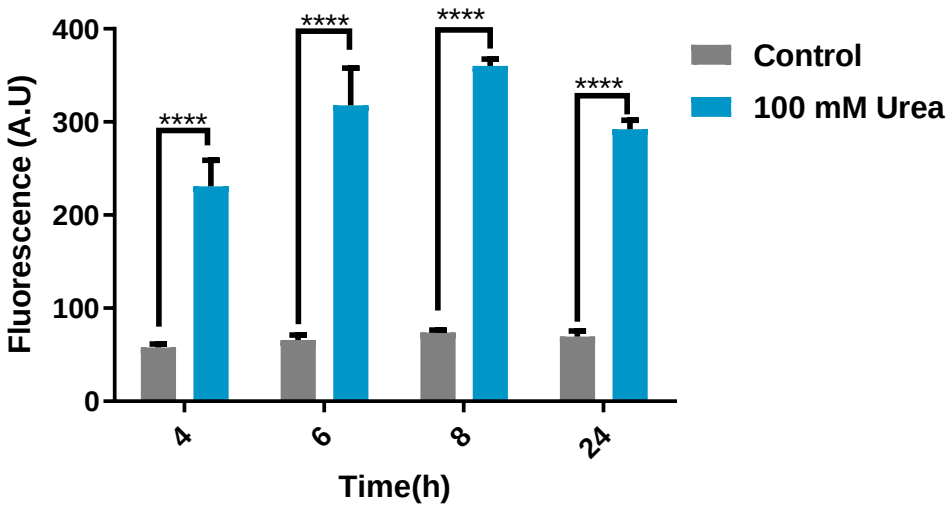

Figure 13: Characterization of the pZE pUreR sfGFP urea biosensor. After induction with 100 mM urea solution the response signal was measured with a microplate reader. Cellular biosensors showed constant increase in

fluorescence over time while dropping slightly after the 8th hour. Experiments were conducted with three replicates and the normalized data was analyzed with two-way ANOVA ($p \leq 0.05$, $p \leq 0.01$, $p \leq 0.001$ and $p \leq 0.0001$ were shown as "*", "**", "***" and "****" respectively).

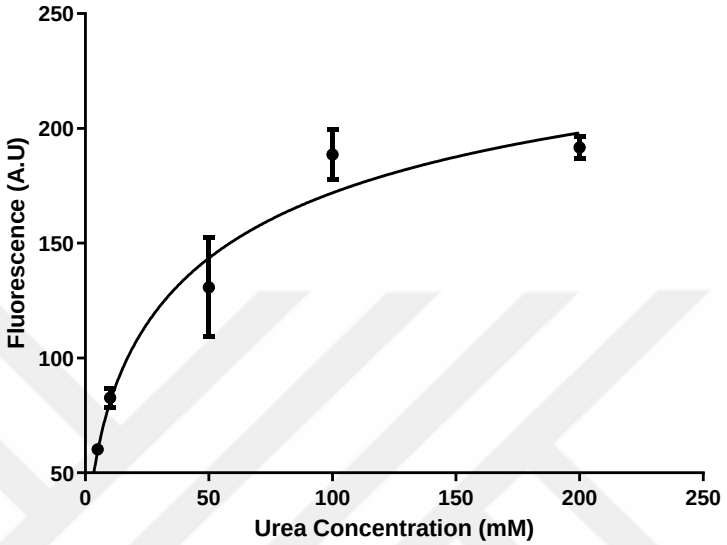

Figure 14: The dynamic range of the pZE pUreR sfGFP-pZS mproD UreR biosensor showing the fluorescence levels among a range of different urea concentrations (0, 5, 10, 50, 100 and 200 mM). Fluorescence and the optical density measurements were taken at the 8th hour of induction. Experiments had three replicates and the normalized data was fitted to one site specific binding graph with Hill Slope (Graphpad Prism8.3).

3.1.5 Signal Optimization of the Urea Biosensor with Promoter Modifications

The operon encoding for urease in the organism *P. Mirabilis* has an intergenic region regulating the transcription of the multiple genes positioned both sides the genome. Even though these unique segment of DNA is not well characterized, it is known that it is comprised of multiple promoters and

regulatory regions[53, 54]. As a result instead of the single promoter pUreR, the whole intergenic region (IR) was synthesized and cloned in front of the signal protein sfGFP.

3.1.6 Construction of Intergenic Region directed at UreR as promoter

To obtain the pZE IR pUreR sfGFP construct, the IR directing the transcription of the UreR gene was amplified with appropriate Gibson Assembly primers (Appendix B) using PCR. Furthermore, pZE pUreR sfGFP plasmid was digested with BamHI and XhoI restriction enzymes to have a pZE backbone with the sfGFP gene. The reactions were then ran on 1% agarose gel and isolated. Isolated DNA fragments were assembled with Gibson Assembly reaction. pZE IR pUreR sfGFP plasmid was later verified with Sanger sequencing (appendix D).

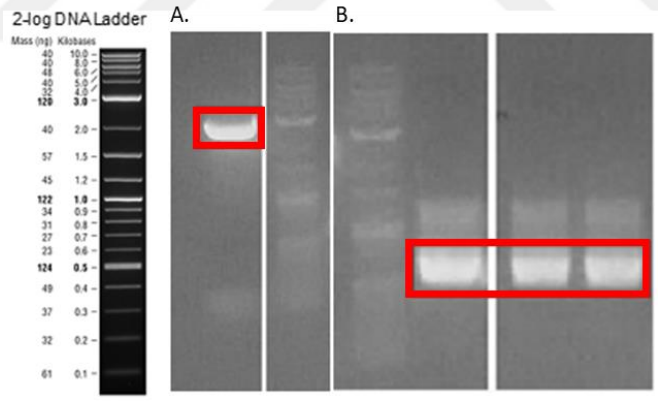

Figure 15: DNA regions needed for the construction of pZE IR pUreR sfGFP ran on 1% agarose gel. A. Restriction digestion of pZE pUreR sfGFP to obtain pZE sfGFP vector sized at 2561 bp. B. PCR-amplified IR region directed at UreR, sized at 577 bp.

3.1.7 Construction of Intergenic Region directed at UreD as promoter

Another approach taken when using IR as the promoter region was to use its direction that is facing genes that forms urease as the promoter. Here, since the first located gene downstream of the IR is UreD the promoters are named pUreD. To obtain the pZE IR pUreD sfGFP construct, again the IR directing the transcription of the UreD gene was amplified with PCR. The same BamHI and XhoI restricted pZE sfGFP vector in Figure 15.A was used as the backbone. Completed PCR reactions were then ran on 1% agarose gel and DNA fragments purified from the gel were assembled with Gibson Assembly reaction. pZE IR pUreD sfGFP plasmid was later verified with Sanger sequencing (appendix D).

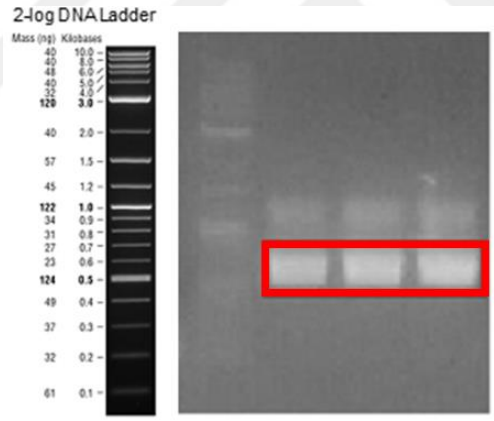

Figure 16: PCR-amplified IR region with UreD direction sized at 582 bp.

3.1.8 Characterization of Intergenic Region directed at UreR as promoter

Constructed pZE IR pUreR sfGFP plasmid was first co-transformed to *E.coli* DH5α PRO host with the pZS mproD UreR plasmid. Urea induction assay was conducted as described previously with cells in the log-phase being induced with 100 mM fresh urea solution. Signal amplification of the sensor was determined at the time points 4^{th},6^{th},8^{th} and the 16^{th} hours after the induction.

Uninduced cells carrying the pZE IR pUreR sfGFP and the pZS mproD UreR plasmids were used as control.

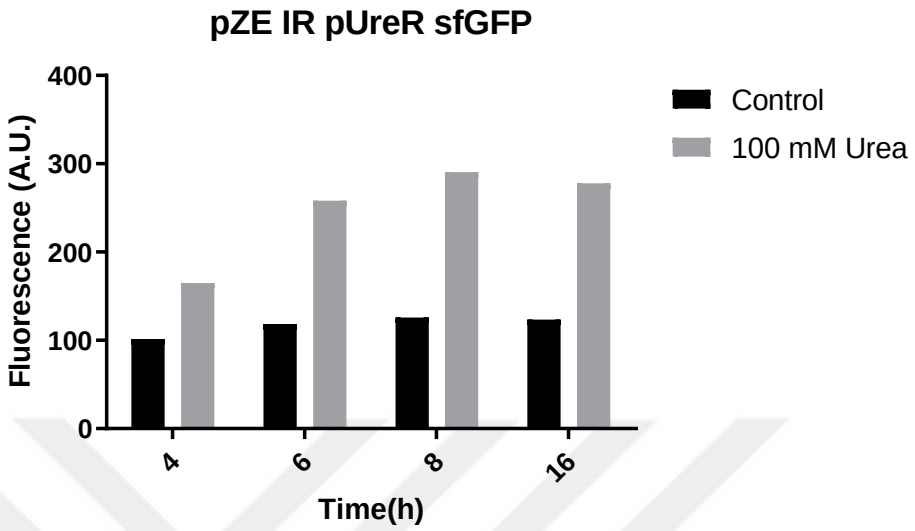

Figure 17: Characterization of the pZE IR pUreR sfGFP urea biosensor. After induction with 100 mM urea solution the response signal was measured at stated time points.

While the signal of fluorescence increased with urea presence, the levels of the signal was lower compared to experiments conducted with pZE pUreR sfGFP tranducing unit. Therefore, pZE IR pUreR sfGFP was not used in further experiments.

3.1.9 Characterization of Intergenic Region directed at UreD as promoter

Constructed pZE IR pUreD sfGFP plasmid was co-transformed to *E.coli* DH5α PRO host with the pZS mproD UreR plasmid. Urea induction assay was followed according to the description mentioned previously. Cells in the log-phase were induced with 100 mM fresh urea solution. Signal amplification of the sensor was determined at the time points 4^{th},6^{th},8^{th} and the 16^{th} hours after

the induction. Cells that have not been induced with urea solution carrying the pZE IR pUreD sfGFP and the pZS mproD UreR plasmids were used as control.

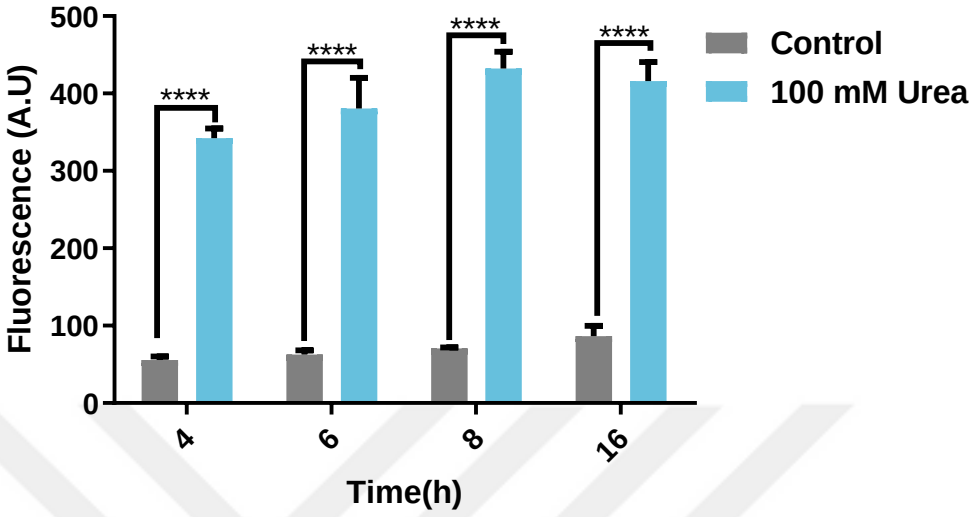

Figure 18: Characterization of the pZE pUreD sfGFP urea biosensor. After induction with 100 mM urea solution the response signal was measured with a microplate reader at the 4^{th},6^{th},8^{th} and the 16^{th} hours. Biosensing cells showed constant increase in fluorescence over time while dropping slightly after the 8^{th} hour. Experiments were conducted with three replicates and the normalized data was analyzed with two-way ANOVA ($p \leq 0.05$, $p \leq 0.01$, $p \leq 0.001$ and $p \leq 0.0001$ were shown as "*", "**", "***" and "****" respectively).

When the whole IR region directed at UreD was used in the upstream of the sfGFP gene, it was observed from the characterization experiments that the urea sensing and responding capabilities of the pZE IR pUreD sfGFP- pZS mproD UreR sensor were the most functional among others. Therefore, the this optimized promoter set up was used in following the experiments.

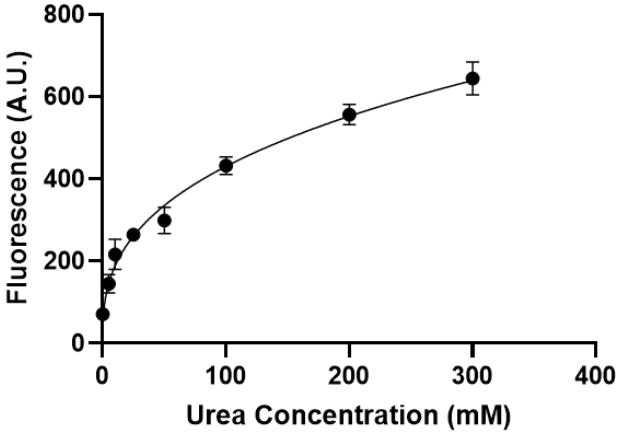

Figure 19: The dynamic range of the pZE IR pUreD sfGFP-pZS mproD UreR biosensor showing the fluorescence levels among a range of different urea concentrations (0, 5, 10, 25, 50, 100, 200 and 300 mM). Fluorescence and the optical density measurements were taken at the 8th hour of induction. Experiments had three replicates and the normalized data was fitted to one site specific binding graph with Hill Slope (Graphpad Prism8.3).

3.1.10 Signal Optimization of the Urea Biosensor with Post-Transcriptional Modifications

One of the major issues of synthetic genetic circuit construction is the context dependence resulting in unpredicted behaviours of the circuits due to the interactions of the chosen genetic parts with adjacent or nearby parts[55].Since these interactions affect the modularity of the circuits, the use of genetic insulators have been on the rise to prevent unpredictable behaviour of the constructed gene circuits[56, 57]. Regulatory regions located at the downstream of the transcription start site are some of the sources of context dependence affecting the translational properties of genetic constructs. This is due to fact that the transcription of unintended nucleotides at the 5′ end of the transcript can modify the stability and secondary structure of mRNA [58]. With

the idea that the divergent behaviour of the circuits used in previous studies for the characterization of the urease operon[53] may not only be due to the transcriptional regulations but also an effect of the RNA leaders on translation, a genetic insulator named RiboJ was decided to be used in urea biosensor. The self-cleaving RiboJ is a 75 nucleotide sequence has a ribozyme sequence derived from the satellite RNA of tobacco ringspot virus and a 23 nucleotide hairpin[58]. As an insulator, it is inserted between the promoter and the ribosome binding region fo gene of interest. This results in the removal of the RNA leaders upstream of the ribosome binding site during the post-transcriptional processes.

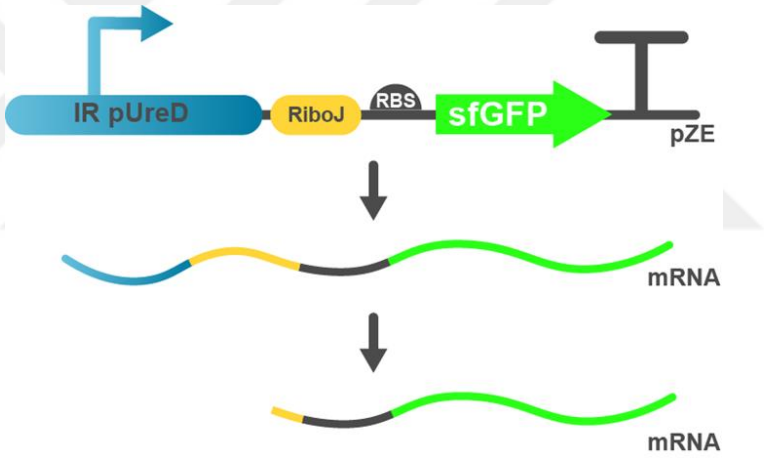

Figure 20: Schematic Representation of RiboJ-aided-RNA leader removal mechanism.

3.1.11 Construction of pZE IR pUreD RiboJ sfGFP Plasmid as the Urea Transducer Unit

For the construction of pZE IR pUreD RiboJ sfGFP plasmid the pZE vector carrying sfGFP gene was amplified with PCR from the pZE IR pUreD sfGFP template. After that, 75 bp RiboJ sequence was added the pUreD promoter

region using appropriate primers (Appendix B) with two consecutive PCR reactions.

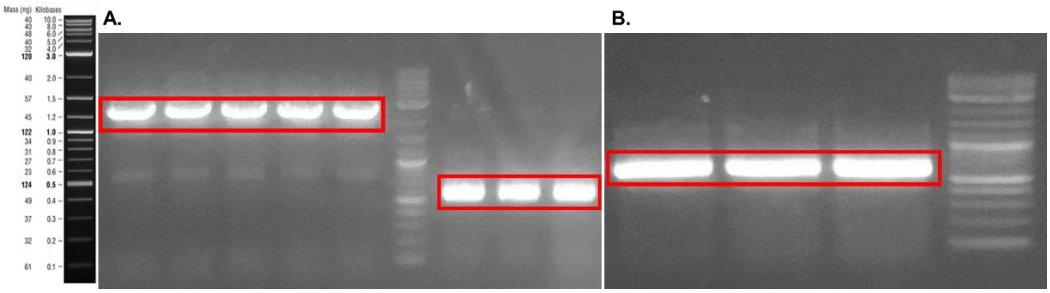

Figure 21: 1% Agarose gel images of the biological parts needed to construct pZE IR pUreD RiboJ sfGFP. A. PCR- amplified pZE backbone sized 2578 bp is on the left and the first PCR reaction of pUreD RiboJ insert that is 580 bp is on the right. B. Second PCR reaction of pUreD RiboJ amplification sized 631 bp.

The reactions were then ran on 1% agarose gel and target DNA fragments were purified from the gel. DNA fragments were then assembled with Gibson Assembly reaction. Verification of the pZE IR pUreD RiboJ sfGFP plasmid was then confirmed with Sanger sequencing (Appendix D).

3.1.12 Characterization of pZE IR pUreD RiboJ sfGFP Plasmid as the Urea Transducer Unit

Constructed pZE IR pUreD RiboJ sfGFP plasmid was co-transformed to *E.coli* DH5α PRO host with the pZS mproD UreR plasmid. Urea induction assay was followed the same protocol with other urea biosensor constructs. Cells in the log-phase were induced with 100 mM fresh urea solution. Signal amplification of the sensor was determined at the time points 0, 2, 4,6,8 and the 16 hours after the induction. Cells that have not been induced with urea solution carrying

the pZE IR pUreD RiboJ sfGFP and the pZS mproD UreR plasmids were used as control.

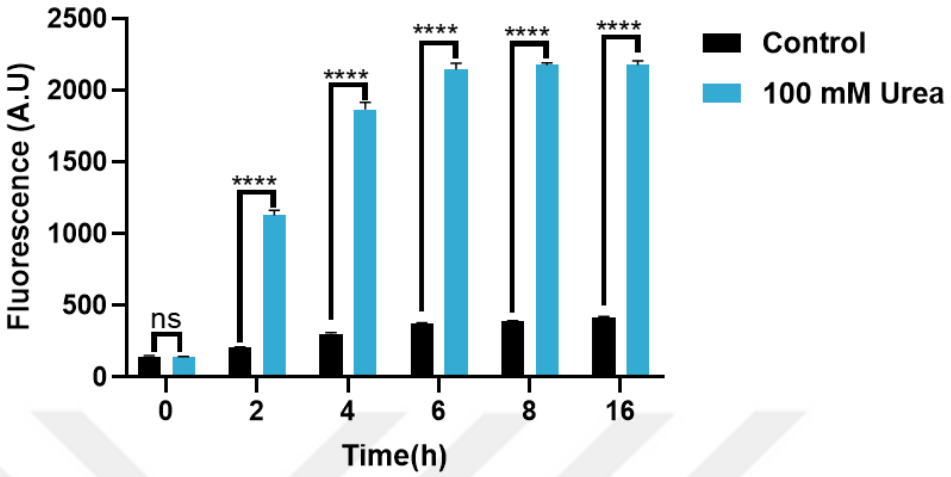

Figure 22: Characterization of the pZE pUreD RiboJ sfGFP urea biosensor. After induction with 100 mM urea solution the response signal was measured with a microplate reader at the 0^{th},2^{nd}, 4^{th},6^{th},8^{th} and the 16^{th} hours. Experiments were conducted with three replicates and the normalized data was analyzed with two-way ANOVA ($p \leq 0.05$, $p \leq 0.01$, $p \leq 0.001$ and $p \leq 0.0001$ were shown as "*", "**", "***" and "****" respectively).

When urea induction was done with pZE pUreD RiboJ sfGFP, signal amplification capability of the circuit showed a significant increase compared to all other constructed urea sensors showing how the RNA leader sequences located at the upstream of mRNAs of sfGFP was affecting its translation. Since the binding kinetics between components were not affected by the addition of the mRNA processing step, the background of the system has also increased with this signal amplification modification.

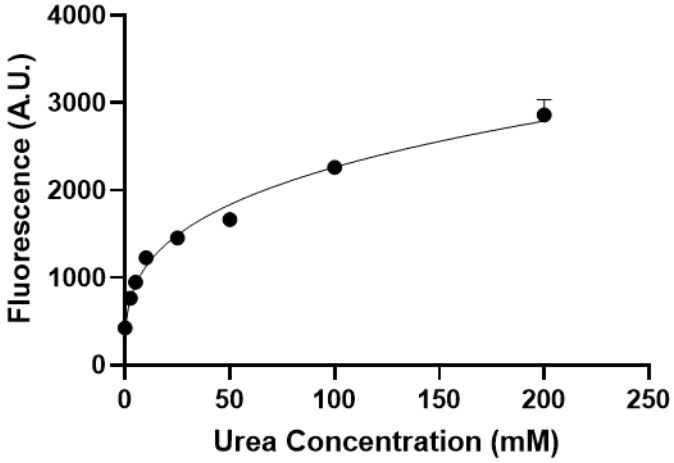

Figure 23: The dynamic range of the pZE IR pUreD RiboJ sfGFP-pZS mproD UreR biosensor showing the fluorescence levels among a range of different urea concentrations (0, 2.5, 5, 10, 25, 50, 100 and 200 mM). Fluorescence and the optical density measurements were taken at the 8th hour of induction. Experiments had three replicates and the normalized data was fitted to one site specific binding graph with Hill Slope (GraphPad Prism8.3).

3.1.13 Signal Optimization of the Urea Biosensor with Protein Engineering

In a study to identify UreR-urea binding kinetics, it was observed that some of the aminoacid mutations modified binding-kinetics of UreR lowered spontenaus UreR binding to its promoter without urea[59]. Therefore, the most mutations were analyzed and combined to reduce the noise of the urea biosensor.

3.1.15 Construction of pZS mproD mt UreR (K169A) Plasmid

For the introduction of K169A mutation, pZS mproD UreR plasmid was digested with BamHI and KpnI restriction enzymes. Reaction was then ran on 1%agarose gel comprised of pZS backbone and restricted UreR gene near the

mutation site (Figure 24.A). K169A mutation was introduced with designed primers using a PCR reaction (Figure 24.B). Later, mutation introduced part of UreR and restricted UreR part were assembled together using two-template PCR (Appendix E).

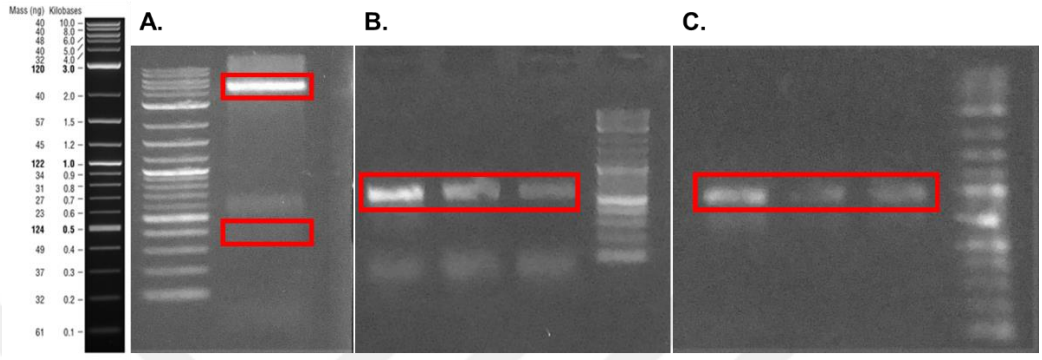

Figure 24: DNA parts needed for the construction of pZS mproD mt UreR (K169A) ran on 1% agarose gel. A. Restriction digestion of pZS mproD UreR showing pZS backbone (3567 bp) and digested UreR parts sized at 546 bp and 352 bp. B. PCR-amplified mutation introduced UreR part sized at 594 bp. C. Assembly of UreR parts with two template PCR showing the expected 957 bp band.

The complete mt UreR (K169A) part was ran on 1% agarose gel (Figure16.C) and then later assembled with isolated pZS backbone in Gibson assembly reaction. Verification of the pZS mproD mt UreR (K169A) plasmid was then confirmed with Sanger sequencing (appendix D).

3.1.16 Characterization of pZS mproD mt UreR (K169A) Plasmid as the Urea Sensor Unit

Constructed pZS mproD mt UreR (K169A) plasmid was co-transformed to *E.coli* DH5α PRO host with the pZE IR pUreD RiboJ sfGFP plasmid. The previously described urea induction assay was followed. Cells in the early

exponential phase were induced with 100 mM fresh urea solution. Fluorescence and the optical density measurements of the sensor was determined at the time points 0, 2, 4,6,8 and the 16 hours after the induction. Cells that have not been induced with urea solution carrying the pZE IR pUreD RiboJ sfGFP and the pZS mproD mt UreR (K169A) plasmids were used as control.

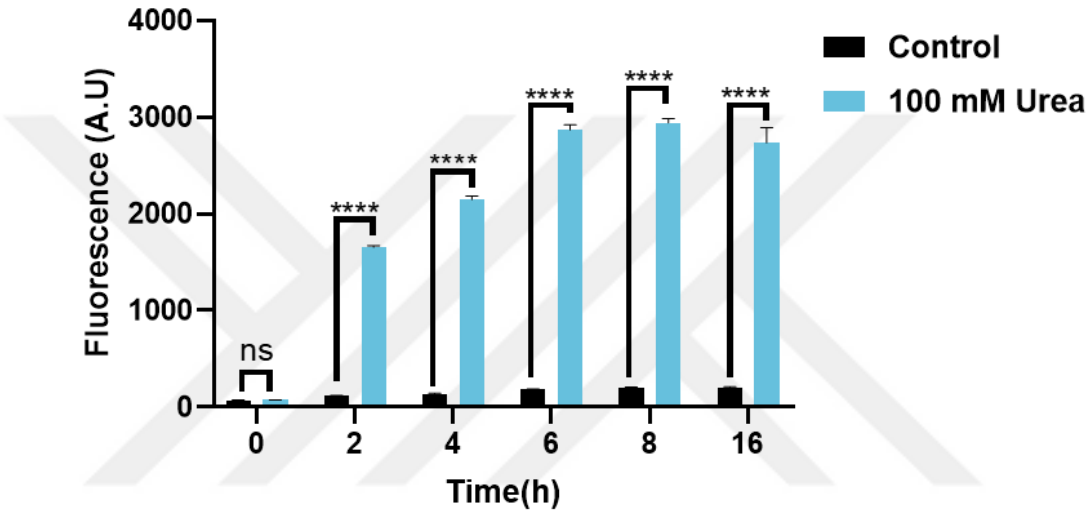

Figure 25: Characterization of the pZS mproD mt UreR (K169A) urea biosensor with pZE IR pUreD RiboJ sfGFP. After induction with 100 mM urea solution the response signal was measured with a microplate reader at the 0^{th},2^{nd}, 4^{th},6^{th},8^{th} and the 16^{th} hours. Experiments were conducted with three replicates and the normalized data was analyzed with two-way ANOVA ($p \leq 0.05$, $p \leq 0.01$, $p \leq 0.001$ and $p \leq 0.0001$ were shown as "*", "**", "***" and "****" respectively).

After the optimization of the signal amplification levels with RiboJ, the high background of the urea biosensor was reduced with engineered UreR transcription factor. The point mutation introduced to UreR modulated the binding kinetics between UreR and its target sequences on the intergenic

region, so that spontenaous UreR binding to its operator site in the absence of urea decreased, lowering the noise of the sensor.

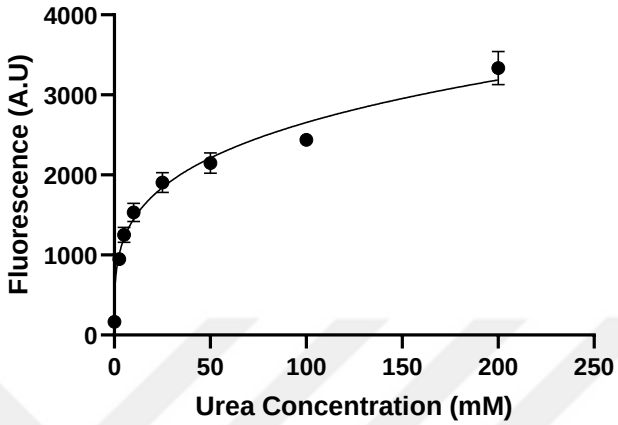

Figure 26: The dynamic range of the pZE IR pUreD RiboJ sfGFP-pZS mproD mt UreR (K169A) biosensor showing the fluorescence levels among a range of different urea concentrations (0, 2.5, 5, 10, 25, 50, 100 and 200 mM). Fluorescence and the optical density measurements were taken at the 8th hour of induction. Experiments had three replicates and the normalized data was fitted to one site specific binding graph with Hill Slope (GraphPad Prism8.3).

3.1.17 Construction of pZS mproD mt UreR (K15A-K169A) Plasmid

For the second site-directed mutation on UreR, K15A, pZS mproD mt UreR(K169A) plasmid was digested with BamHI and KpnI restriction enzymes. Reaction was then ran on 1%agarose gel comprised of pZS backbone and restricted UreR parts (Figure 19.A). K15A mutation was introduced with designed primers and the pZS mproD mt UreR(K169A) template using a PCR reaction (Figure 19.B). Later, mutation introduced part of UreR was amplified

with PCR to complete the UreR sequence and addition of the overhangs fort he Gibson assembly.

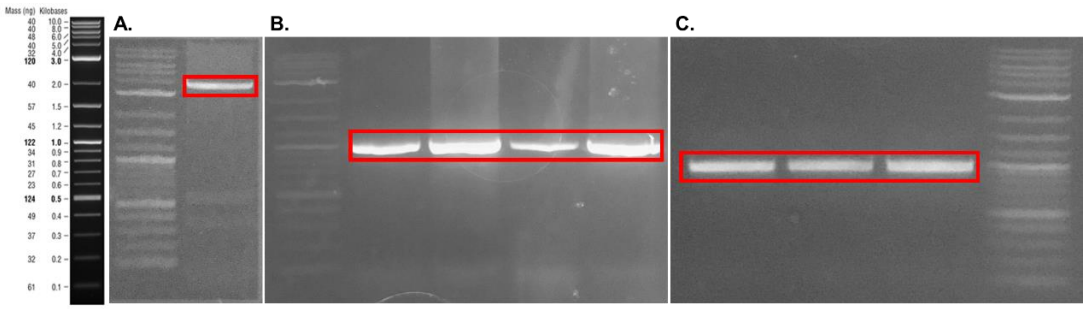

Figure 27: DNA parts needed for the construction of pZS mproD mt UreR (K15A-K169A) ran on 1% agarose gel. A. Restriction digestion of pZS mproD UreR showing pZS backbone (3567 bp) and digested UreR parts sized at 546 bp and 352 bp. B. PCR-amplified K15A mutation introduced mt UreR (K169A) part sized at 911 bp. C. Second PCR of mt UreR(K15A-K169A) at the 957 bp band.

The complete mt UreR (K15A-K169A) and restricted pZS backbone then assembled in Gibson assembly reaction. Verification of the pZS mproD mt UreR (K15A-K169A) plasmid was then confirmed with Sanger sequencing (appendix D).

3.1.18 Characterization of pZS mproD mt UreR (K15A-K169A) Plasmid as the Urea Sensor Unit

Constructed pZS mproD mt UreR (K15A-K169A) plasmid was co-transformed to *E.coli* DH5α PRO host with the pZE IR pUreD RiboJ sfGFP plasmid. The previously described urea induction assay was followed. Cells in the early exponential phase were induced with 100 mM fresh urea solution. Fluorescence and the optical density measurements of the sensor was determined at the time points 0, 1, 2, 4,6,8 and the 16 hours after the induction.

Cells that have not been induced with urea solution carrying the pZE IR pUreD RiboJ sfGFP and the pZS mproD mt UreR (K15A-K169A) plasmids were used as control.

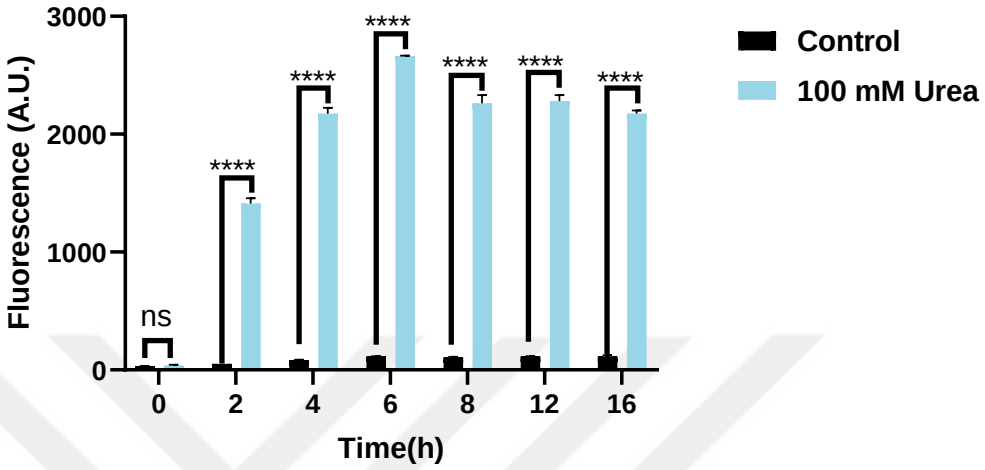

Figure 28: Characterization of the pZS mproD mt UreR (K15A-K169A) urea biosensor with pZE IR pUreD RiboJ sfGFP. After induction with 100 mM urea solution the response signal was measured with a microplate reader at the 0^{th}, 2^{nd}, 4^{th},6^{th},8^{th},12^{th} and the 16^{th} hours. Experiments were conducted with three replicates and the normalized data was analyzed with two-way ANOVA ($p \leq 0.05$, $p \leq 0.01$, $p \leq 0.001$ and $p \leq 0.0001$ were shown as "*", "**", "***" and "****" respectively).

With the introduction of another mutation on the UreR protein, the noise of the circuit was further reduced. While overall signal amplification capability of the circuit decreased slightly, the binding kinetics of the UreR and its target sequences on the intergenic region was modified in as way that binding of UreR to its operator in the absence of urea was decreased, increasing the fold-change between the induced and the uninduced states of the circuit.

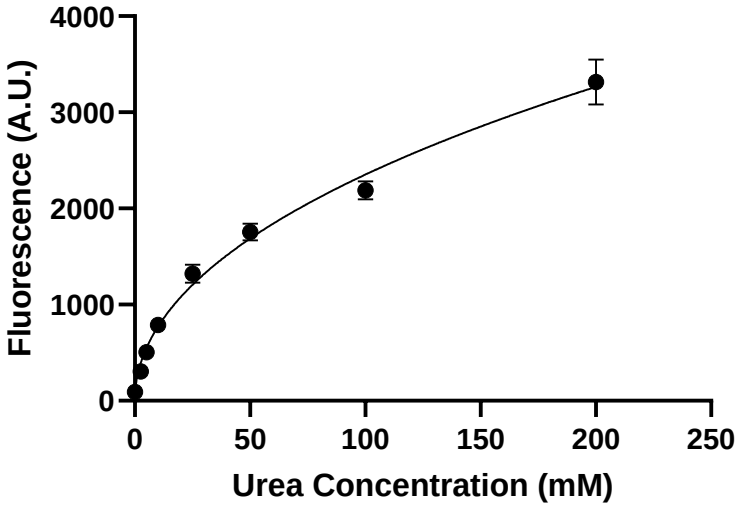

Figure 29: The dynamic range of the pZE IR pUreD RiboJ sfGFP-pZS mproD mt UreR (K15A-K169A) biosensor showing the fluorescence levels among a range of different urea concentrations (0, 2.5, 5, 10, 25, 50, 100 and 200 mM). Fluorescence and the optical density measurements were taken at the 8th hour of induction. Experiments had three replicates and the normalized data was fitted to one site specific binding graph with Hill Slope (GraphPad Prism8.3).

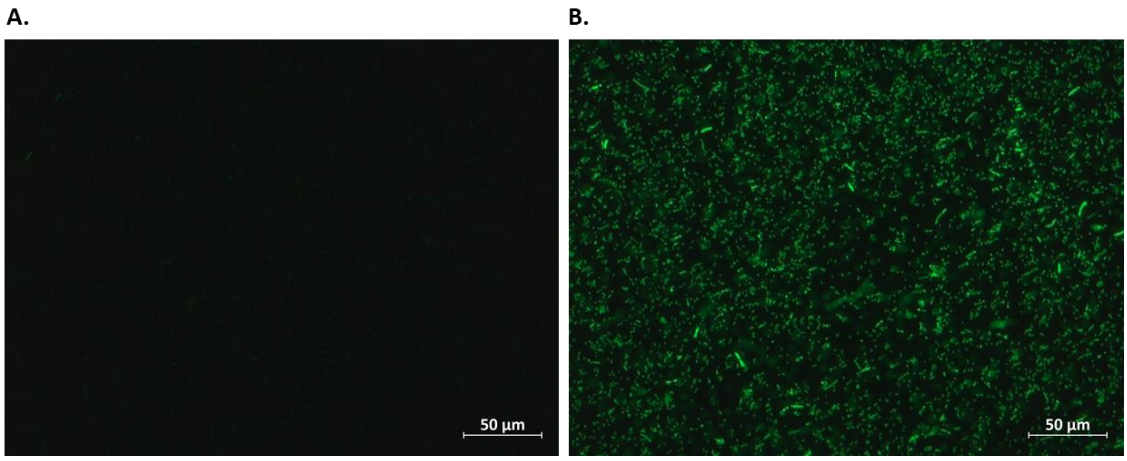

Figure 30: Fluorescence microscopy images of the samples 8 hours after the induction. A. Uninduced cells carrying pZE IR pUreD RiboJ sfGFP-pZS mproD mt UreR (K15A-K169A) and pZS mproD UreR plasmids. B. 100 mM urea

induced cells carrying pZE IR pUreD RiboJ sfGFP-pZS mproD mt UreR (K15A-K169A) and pZS mproD UreR plasmids.

3.2 Development and Signal Optimization of Uric Acid Biosensor

3.2.1 Construction of the Initial Uric Acid Biosensor

The construction of synthetic gene circiuts for the uric acid biosensors, the genetic parts from the organism *Deinococcus radiodurans* was used. The uric acid detection system derived from this organism consisted of the homodimer transcriptional repressor HucR and its promoter pHucO. In additiona, a uric acid transporter named UACT was used to permit uric acid flux into the cell. The repressor HucR binds to its operator region in the absence of uric acid and prevents RNA polymerase from initiating transcription. When uric acid is present inside the cell, it binds to and changes the conformation of HucR blocking its dimerization. Consequently, the repressor can not associate with its binding site on the promoter and transcription by RNA polymerase is initiated[60].

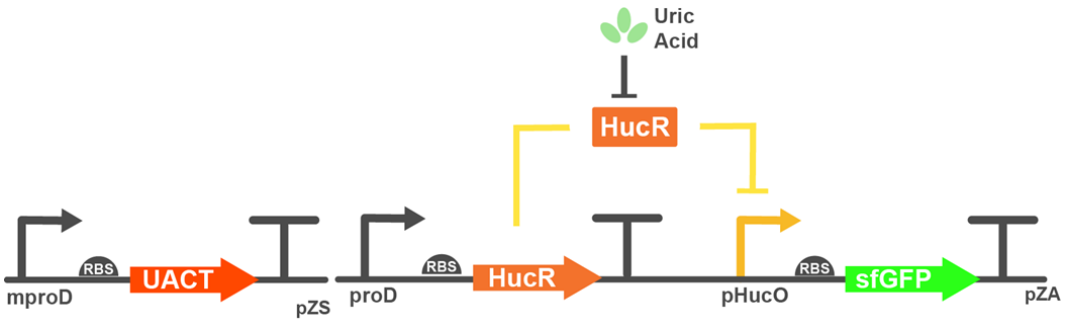

Figure 31: The biological parts and the mechanism used in the uric acid biosensor. Uric acid sensitive HucR repressor is constituvely expressed via proD promoter and represses the transcription of signal protein by binding to HucO operator site on its promoter. When uric acid is tranported inside cells

via UACT, HucR binds to uric acid and detaches from the promoter which activates the transcription of sfGFP.

To enable uric acid flux into the host, constitutive expression of UACTw as established by cloning UACT into the low copy pZS vector downstream of a low-strength promoter mproD. To prevent unnecessary metabolic burden to the host, a weak constitutive promoter was chosen to express the uric acid transporter.

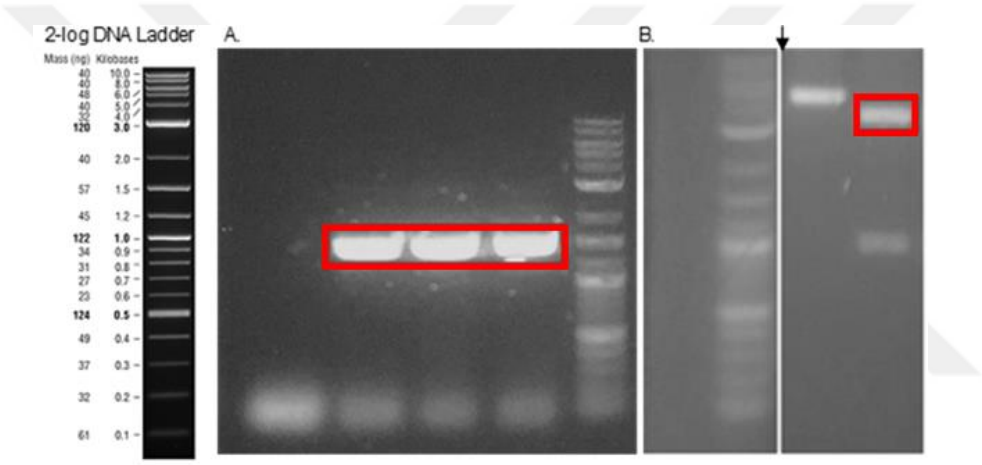

Figure 32: Agarose gel images of the biological parts needed to construct pZS mproD UACT plasmid. A. PCR- amplified UACT insert sized at 1517 bp. B. HindIII and KpnI digested pZS vector with mproD promoter, 3573 bp.

For the cloning of pZS mproD UACT, the pZS mproD UreR was digested with BamHI and HindIII restriction enzymes and the UACT gene was amplified with PCR using gibson primers. After running the first PCR reaction and the restriction digestion reaction on 1%agarose gel, the bands on the correct size were isolated using MN-gel extraction kit according to manufacturer's instructions (Figure 32). The isolated pZS backbone and the UACT insert were

then assembled using the Gibson Assembly method. The success of the cloning was then determined with Sanger sequencing (Appendix D).

To generate a fluorescent signal in response the uric acid, a minimal version of the pHuco promoter consisting of the native -35 and -10 regions as well as the HucO binding site in the middle was cloned upstream of the sfGFP reporter protein. The designed synthetic promoter was added to sfGFP gene with primers over the coarse of four consequetive PCRs (Figure 33).

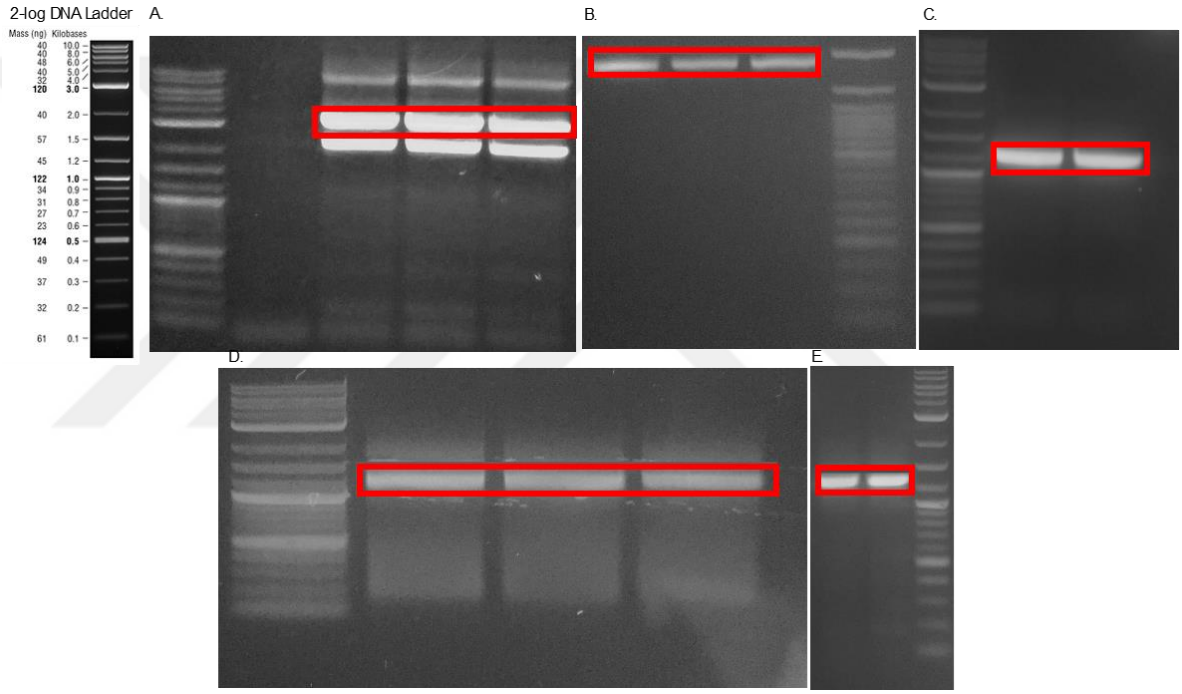

Figure 33: DNA parts needed for the construction of pZA syn pHucO sfGFP ran on 1% agarose gel. A. PCR amplified pZA vector showing (3339 bp) B. First PCR of syn pHucO sfGFP region. C. Second PCR of syn pHucO sfGFP sized at 1254 bp. D. Third PCR of syn pHucO sfGFP sized at 1282 bp. E. Fourth PCR of syn pHucO sfGFP sized at 1312 bp.

After isolating the final PCR product of syn pHucO sfGFP and pZA vector from 1% agarose gel, DNA parts were assembled using the Gibson Assembly

method. The success of the cloning was then determined with Sanger sequencing (Appendix D).

After confirming the cloning of pZA syn pHucO sfGFP, the transcriptional repressor HucR was cloned downstream of constitutively active promoter proD on the plasmid. To do so, HucR was amplified from synthesized DNA order using PCR with appropriate gibson primers. Also the proD promoter was amplifed with designed primers using PCR.

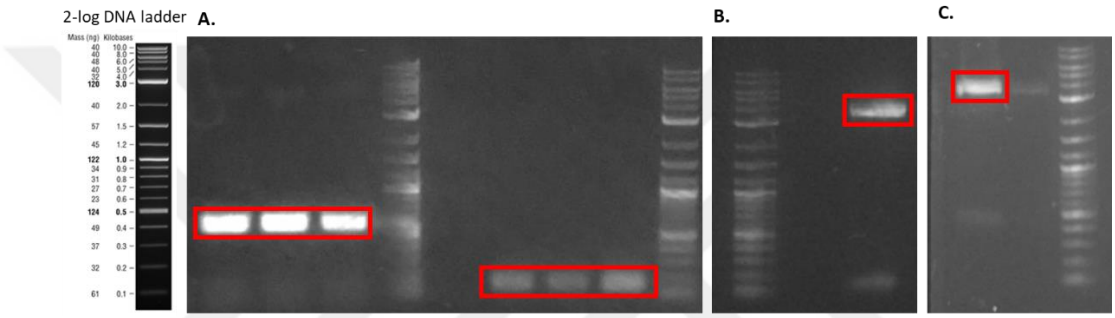

Figure 34: DNA parts needed for the construction of pZA syn pHucO sfGFP proD HucR ran on 1% agarose gel. A. PCR-amplified HucR transcription factor sized at 616 bp (left) and proD promoter region sized at 174 bp (right). B.PCR-amplified pZA backbone with expected size at 3374 bp. C.AatII restriction enzyme digested pZA syn pHucO sfGFP vector (expected size at 2970 bp).

After isolating the final PCR product of syn pHucO sfGFP and initially PCR-amplified and then AatII digested pZA vector from 1% agarose gel, DNA parts were assembled using the Gibson Assembly method. The success of the cloning was then determined with Sanger sequencing (Appendix D).

3.2.2 Characterization of the Initial Uric Acid Biosensor

The sensivity and response capability of the constructed genetic gates were initially assayed with uric acid induction experiments. Firstly, uric acid

transportation plasmid pZS mproD UACT and the uric acid biosensor plasmid pZA syn pHucO sfGFP proD HucR were co-transformed to *E.coli* DH5α PRO host. Uric acid induction assay was done on cells prepared as described previously. For the initial screening, uric acid was dissolved in dH2O 10 mM NaOH and directly added to appropriately grown cells to have a final concentration of 50 µM. Uninduced cells carrying pZA syn pHucO sfGFP proD HucR and pZS mproD UACT were used as control.

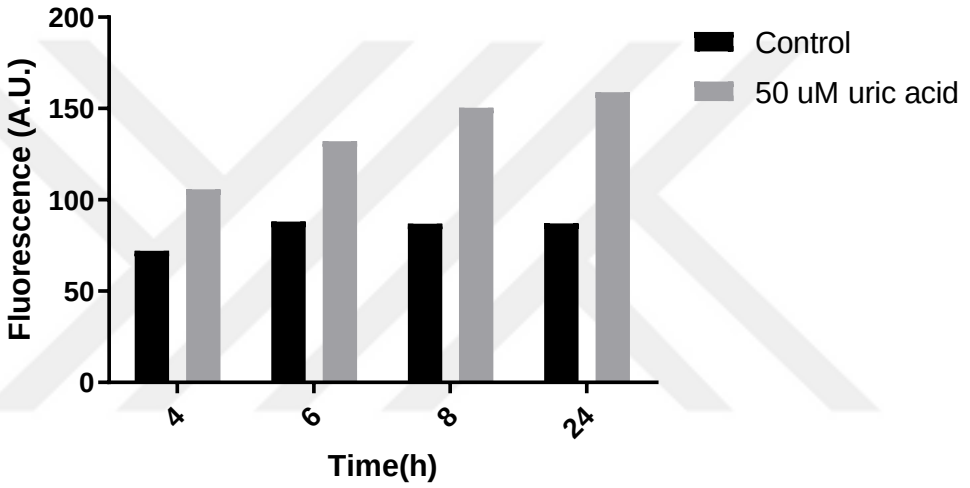

Figure 35: Characterization of pZA syn pHucO sfGFP proD after induction with 50 µM uric acid solution. The fluorescence and the optical density of the samples were measured at the 4^{th},6^{th},8^{th} and the 24^{th} hours. The data shows the normalized values of single samples.

Uric acid induced cells have shown moderate fluorescence increase in response.Therefore, it was decided to continue optimization of the dose-response curve using synthetic biology approaches.

3.2.3 Signal Optimization of the Uric Acid Biosensor with Promoter Engineering and High Copy Plasmid

The generated pZA syn pHucO sfGFP proD HucR uric acid sensor system was transferred to the high copy plasmid pET22b-(+) vector system to increase the sensor efficiency and the amount of response signal. Furthermore, the native -35 -10 regions of pHucO were replaced by PCR reactions with the -35-10 regions of the pL promoter, a strong viral promoter. With this design, it was aimed that when there is no uric acid in the environment, the HucR protein would bind to the HucO region with the same dynamics and the noise of the uninduced system would remain the same, while a significant increase in the signal when induced with uric acid due to the strong pL promoter.

3.2.4 Construction of pET-22b(+) synpHucO v2 sfGFP proD HucR plasmid

For the construction of pET 22b(+) synpHucO v2 sfGFP proD HucR, syn pHucO sfGFP was amplified with two consecutive PCRs. With the designed primers also the -35 and -10 regions on the promoter was changed from the native ones to pL viral vector's. The pET22b (+) plasmid was subjected to restriction digestion to have the high copy vector (Figure 27).

After the PCR and restriction digestion, products were run in 1% Agarose gel, they were isolated combined by Gibson Assembly method. The plasmids assembled by Gibson Assembly method were transformed into *E.coli* DH5α PRO cells, plasmid isolation was done on selected colonies and were verified later by Sanger sequencing. The DNA sequencing result of the confirmed samples is shown in Appendix D.

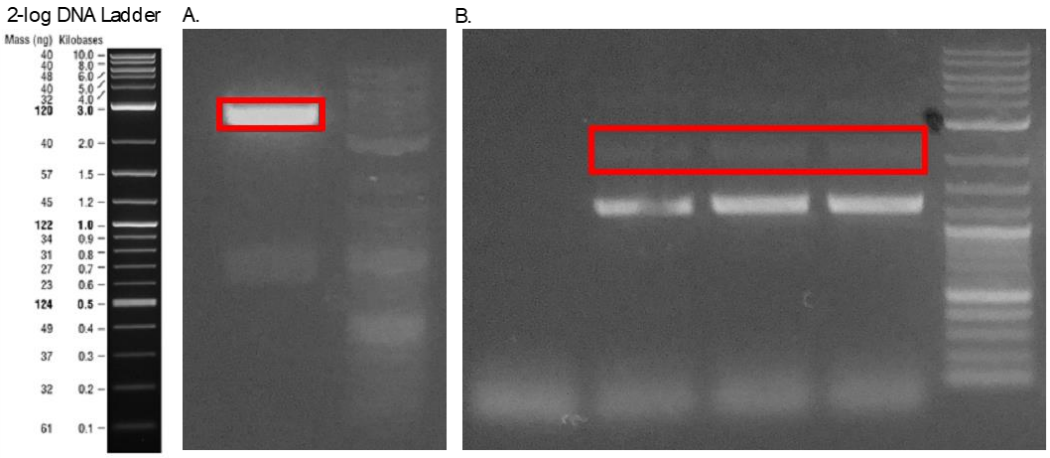

Figure 36: DNA parts needed for the construction of pET 22b(+) synpHucO v2 sfGFP proD HucR ran on 1% agarose gel. A. MluI and XhoI digested pET22-b(+) vector expected size at 4537 bp B. PCR- amplified pL-pHucO sfGFP proD HucR region sized at 2068 bp

3.2.5 Characterization of the Uric Acid Biosensor with Engineered in a High Copy Plasmid

Constructed pET-22b(+) synpHucO v2 sfGFP proD HucR plasmid was co-transformed to *E.coli* DH5α PRO host with the pZS mproD UACT plasmid. The previously described uric acid induction assay was followed. Cells in the early exponential phase were induced with 50 μM fresh uric acid solution. Fluorescence and the optical density measurements of the sensor was determined at the time points 4,6,8 and the 24 hours after the induction. Cells that have not been induced with uric acid solution carrying the pET-22b(+) synpHucO v2 sfGFP proD HucR and the pZS mproD UACT plasmids were used as control.

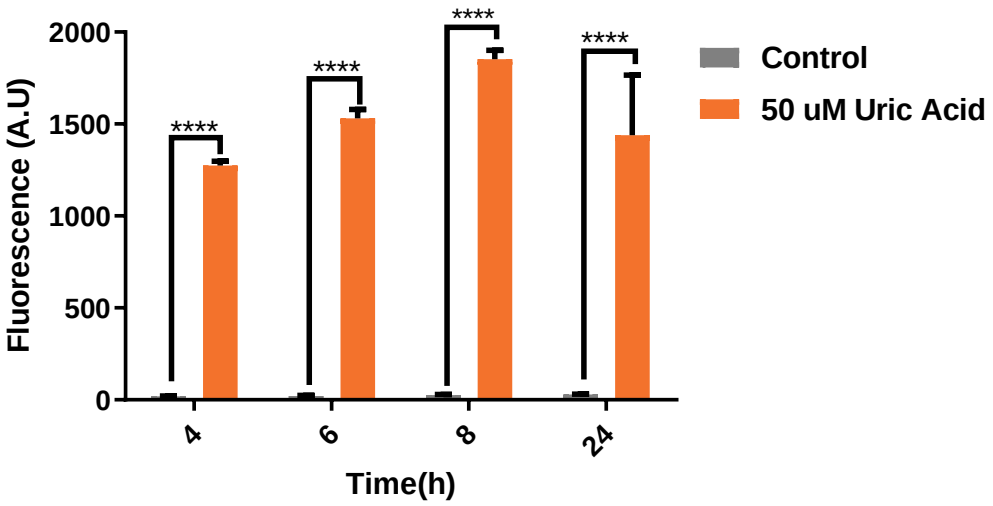

Figure 37: Characterization of the uric acid biosensor co-transformed with pET-22b(+) synpHucO v2 sfGFP proD HucR and pZS mproD UACT plasmids. After induction with 50 μM uric acid solution the response signal was measured with a microplate reader at the 4th,6th,8th and the 24th hours. Experiments were conducted with three replicates and the normalized data was analyzed with two-way ANOVA ($p \leq 0.05$, $p \leq 0.01$, $p \leq 0.001$ and $p \leq 0.0001$ were shown as “*”, “**”, “***” and “****” respectively).

Uric acid induction with pET-22b(+) synpHucO v2 sfGFP proD HucR, signal amplification capability of the circuit showed a significant increase compared to pET-22b(+) synpHucO sfGFP proD HucR uric acid with native -35 and -10 regions of the pHucO plasmid. Addition of -35 and -10 regions from the strong viral promoter did not change the background signal but risen the levels of fluorescent response signal to uric acid to a considerable extent. Dynamic range assays has shown that our modified uric acid sensor forms a digital like response to uric acid working in an ON and OFF manner (Figure 38).

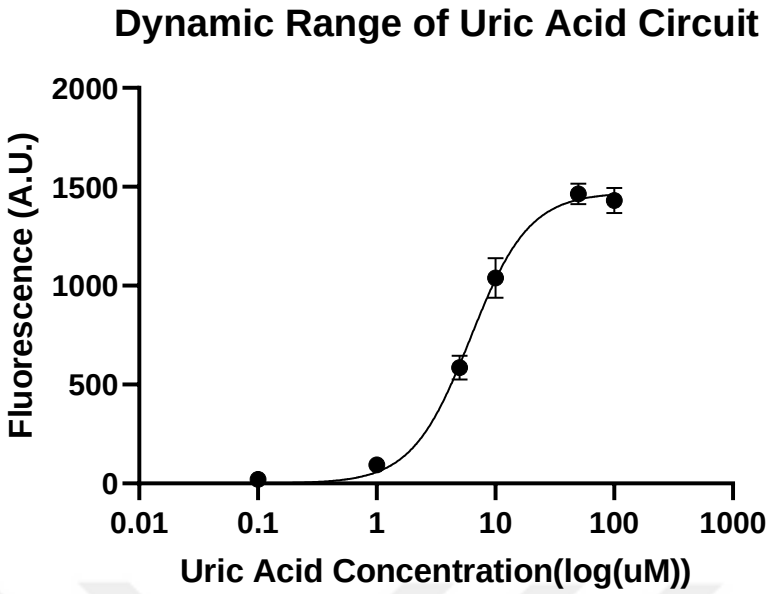

Figure 38: The dynamic range of the uric acid biosensor co-transformed with pET-22b(+) synpHucO v2 sfGFP proD HucR and pZS mproD UACT plasmids showing the fluorescence levels among a range of different uric acid concentrations (0, 0.1,1,5,10 and 50μM). Fluorescence and the optical density measurements were taken at the 8th hour of induction. Experiments had three replicates and the normalized data was fitted to one site specific binding graph with Hill Slope (GraphPad Prism8.3).

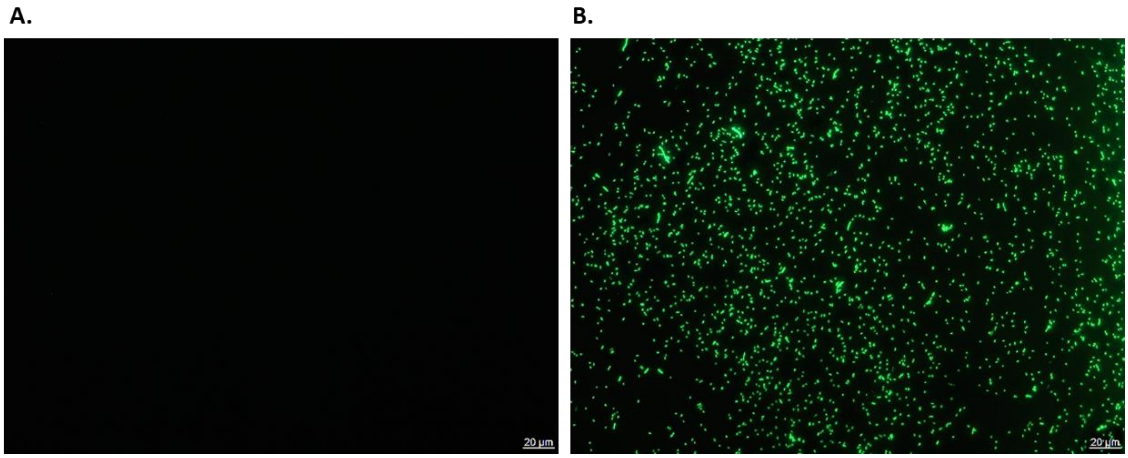

Figure 39: Fluorescence microscopy images of the samples 8 hours after the induction. A. Uninduced cells carrying pET-22b(+) synpHucO v2 sfGFP proD

HucR and pZS mproD UACT plasmids. B. 50 μM uric acid induced cells carrying pET-22b(+) synpHucO v2 sfGFP proD HucR and pZS mproD UACT plasmids. (White bars represent 20μm)

3.3 Development and Signal Optimization of Multiplexed Biosensors

3.3.1 Development of Urea-Uric Acid AND-Gate Biosensor

In the next phase of the project, we focused on combining the urea and uric acid sensors with the AND-logic mimicking system. Reprogramming of urea and uric acid biosensors into a signal processing AND operation system has the potential for integrating medical knowledge and overcoming clinical constraints of diagnosing heterogenous kidney related diseases

To do so, the essential biological elements of both systems were first incorporated into a single biosensing module and a synthetic promoter was designed by cloning the HucO binding site between the -35 -10 regions of one of the urea promoters inside the pUreD directed Intergenic Region. The expected behaviour of this design was that the system would not be activated in the absence of analytes or the with presence of only one of the analytes. The HucR would prevent the transcription in the absence of uric acid, and the transcription would not start in the absence of urea since the pUreD promoters require activated UreR to start transcription.

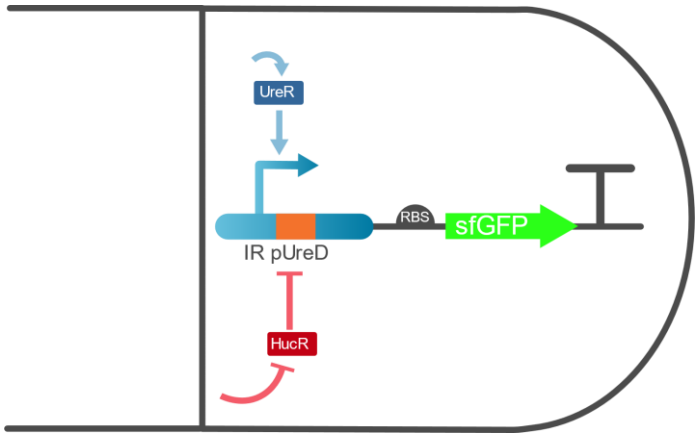

Figure 40: Schematic representation of AND-logic mimicking Multi-Input System. Both of the transcription factors are needed to be activated before RNAP can bind freely bind to the promoter site and initiate transcription. Therefore system mimick AND-logic, in the absence of any input or presence of only one input is not strong enough to generate an output.

3.3.2 Construction of pZS mproD UreR mproD UACT

In order to establish the AND-logic gated biosensor for urea and uric acid, first it was planned to carry the uric acid transporter UACT and the urea transcription factor UreR gene onto the same plasmid. Since both elements were already positioned on the same low-copy plasmid unlike the other elements included in the systems, these two elements were moved to the pZS vector, while the other elements were moved to the pZE vector. To construct the pZS mproD UreR mproD UACT plasmid, after restricting the pZS mproD UreR plasmid with proper enzymes, a double terminator site and the mproD UACT gene segment were amplified with PCR.

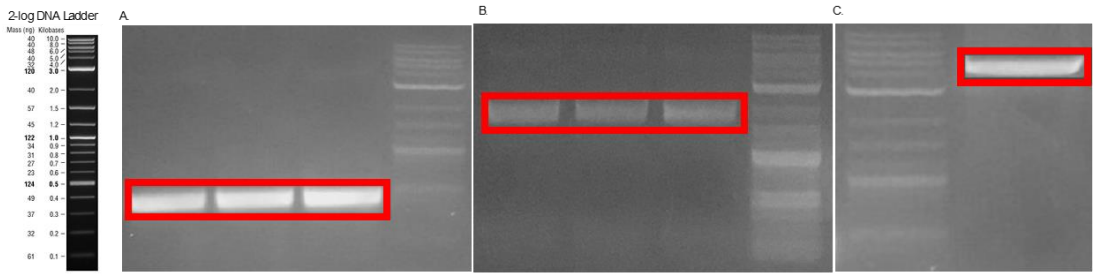

Figure 41: DNA parts needed for the construction of pZS mproD ureR mproD UACT ran on 1% agarose gel. A. PCR-amplified double terminator region sized at 438 bp. B. PCR-amplified mproD UACT DNA region sized at 1568 bp. C. Restriction digested pZS mproD UreR vector with NotI enzyme sized at 4257 bp.

After running the PCR and the restriction digestion reactions on 1%agarose gel, the bands on the correct size were isolated using MN-gel extraction kit according to manufacturer's instructions (Figure 41). The isolated pZS mproD UreR backbone, the double termianor region and the mproD UACT inserts were then assembled using the Gibson Assembly method. The success of the cloning was then determined with Sanger sequencing (Appendix D).

3.2.3 Construction of pZE pUreD sfGFP proD HucR plasmid

As mentioned above, to unite other elements of urea and uric acid biosensors, the proD-HucR and a double terminator DNA region were transferred to the pZE vector. To do so, the proD HucR DNA region, dual terminator region and pZE IR pUreD sfGFP vector were amplified using the PZR reaction with primers suitable for Gibson Assembly method.

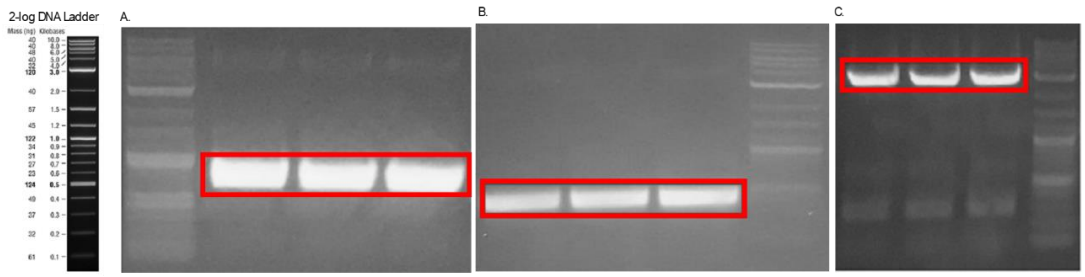

Figure 42: DNA parts needed for the construction of pZE IR pUreD sfGFP proD HucR ran on 1% agarose gel. A. PCR-amplified proD HucR DNA region sized at 765bp. B. PCR-amplified double terminator DNA region sized at 438 bp. C. PCR-amplified pZE IR pUreD sfGFP vector sized at 2991 bp.

The reactions were then ran on 1% agarose gel and target DNA fragments were purified from the gel. DNA fragments were assembled with Gibson Assembly reaction. Verification of the pZE IR pUreD sfGFP proD HucR plasmid was then confirmed with Sanger sequencing (appendix D).

3.2.4 Construction of pZE pUreD-HucO sfGFP proD HucR plasmid

To engineer a promoter region that is regulated by both UreR transcriptional activator and the HucR transcriptional repressor, the HucO binding site was inserted into the urea promoter (between -35 and -10 regions). For this, primers suitable for the Gibson Assembly method were used to amplify pZE sfGFP proD HucR vector. Using PCR and suitable primers, HucO binding region was added between the -35 -10 regions of one of the pUreD promoters.

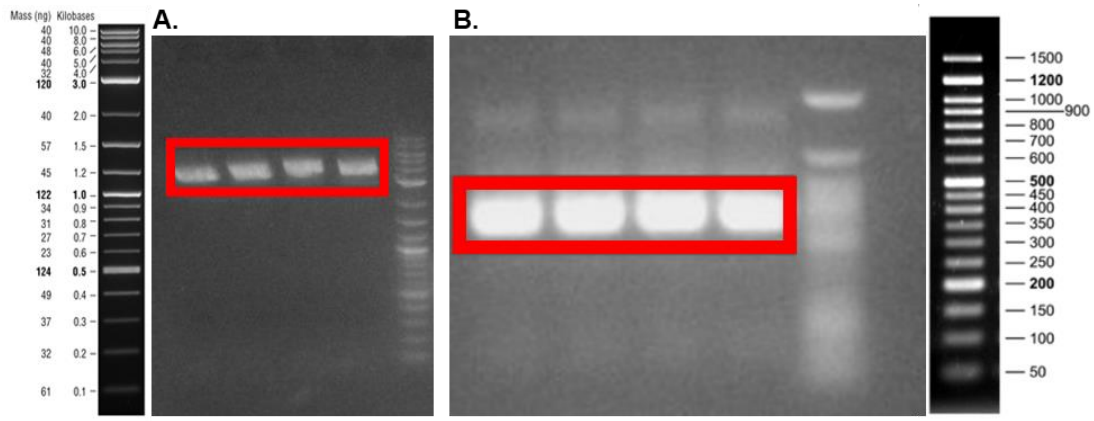

Figure 43: DNA parts needed for the construction of pZE IR pUreD-HucO sfGFP proD HucR ran on 1% agarose gel. A. PCR-amplified pZE sfGFP proD HucR vector sized at 3689 bp. B. PCR-amplified pUreD-HucO DNA region sized at 575 bp.

The reactions were then ran on 1% agarose gel and target DNA fragments were purified from the gel. DNA fragments were assembled with Gibson Assembly reaction. Verification of the pZE IR pUreD-HucO sfGFP proD HucR plasmid was then confirmed with Sanger sequencing (appendix D).

3.3.5 Orthogonality Tests of Urea and Uric Acid Biosensing Modules

Before characterization of multi-input biosensors, optimized urea and uric acid whole-cell biosensors were subjected to cross-reactivity tests to show analytes did not initiate a response except from their respective biosensing modules. Therefore, experiments were set up with necessary biosensing elements to test cross-analytes. For testing of urea biosensor tests with uric acid pZE pUreD sfGFP and pZS mproD UreR mproD UACT plasmids were co-transformed to enable uric acid flux into the cell. For testing of uric acid biosensor with urea such set up was not necessary since urea can readily diffuse into the cells, thus pET-22b(+) synpHucO v2 sfGFP proD HucR and

pZS mproD UACT biosensing modules were used in the tests. Orthogonality tests of urea and uric acid biosensors shown that biosensors were sensitive to their respective analytes and responded to their own analytes with the significant signal level differences. They also did not produce a visible response to the opposite analyte. The working principles of multiplexed sensors were designed in line with urea and uric acid biosensing modules being orthogonal to each other.

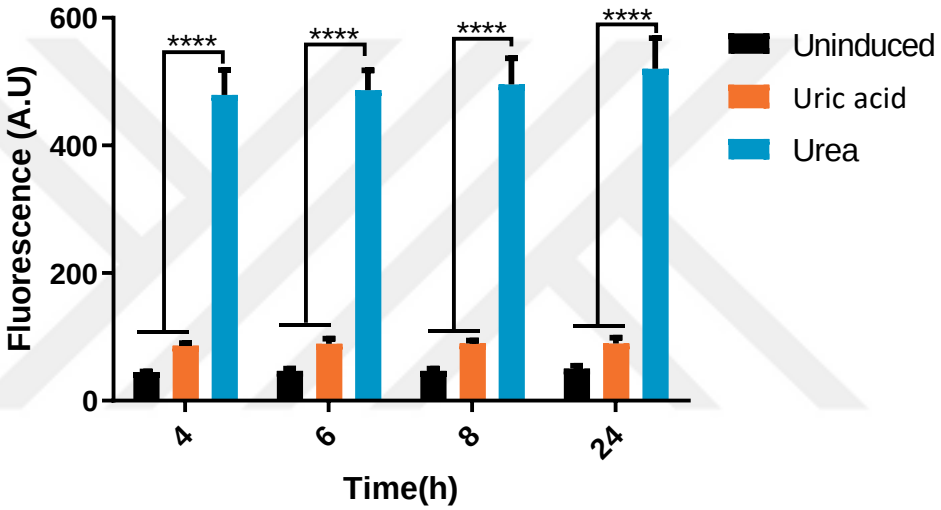

Figure 44: Cross reactivity tests of urea biosensor. pZE pUreD sfGFP and pZS mproD UreR mproD UACT tranformed *E.coli* cells were induced with 50 µM uric acid solution and 100 mM urea. After induction the response signal from uninduced, uric acid-induced and urea-induced samples was measured with a microplate reader at the 4th,6th,8th and the 24th hours. Experiments were conducted with three replicates and the normalized data was analyzed with two-way ANOVA ($p \leq 0.05$, $p \leq 0.01$, $p \leq 0.001$ and $p \leq 0.0001$ were shown as "*", "**", "***" and "****" respectively).

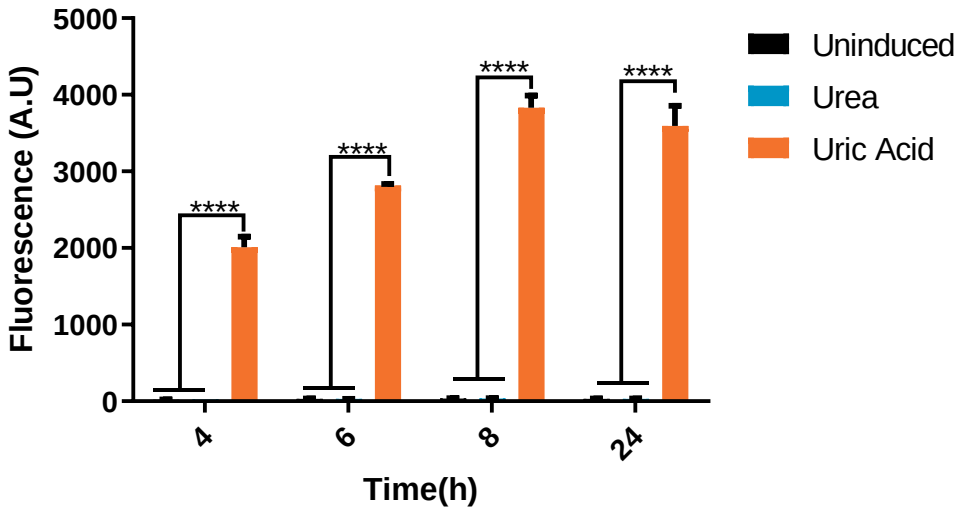

Figure 45: Cross reactivity tests of uric acid biosensor. pET-22b(+) synpHucO v2 sfGFP proD HucR and pZS mproD HucR transformed *E.coli* cells were induced with 50 µM uric acid solution and 100 mM urea. After induction the response signal from uninduced, uric acid-induced and urea-induced samples was measured with a microplate reader at the 4th,6th,8th and the 24th hours. Experiments were conducted with three replicates and the normalized data was analyzed with two-way ANOVA ($p \leq 0.05$, $p \leq 0.01$, $p \leq 0.001$ and $p \leq 0.0001$ were shown as "*", "**", "***" and "****" respectively).

3.3.6 Characterization of Multi-Input AND-Logic Gated System

Constructed pZE IR pUreD-HucO sfGFP proD HucR plasmid was co-transformed to *E.coli* DH5α PRO host with the pZS mproD UreR mproD UACT plasmid. Similar to previously described induction assays, cells were induced with 100 mM fresh urea solution and 50 µM fresh uric acid solution. Here four groups were prepared for induction; no analyte added cells, only urea added cells, only uric acid added cells and simultenaously induced cells with urea and uric acid solutions.

Fluorescence and the optical density measurements of the AND-Gate sensor was determined at the time points 8 hours after the induction. Cells that have not been induced or induced with only one of the analytes but carrying the pZE IR pUreD-HucO sfGFP proD HucR and the pZS mproD UreR mproD UACT plasmids were used as control.

Inputs		Output
Urea	Uric Acid	sfGFP
0	0	0
1	0	0
0	1	0
1	1	1

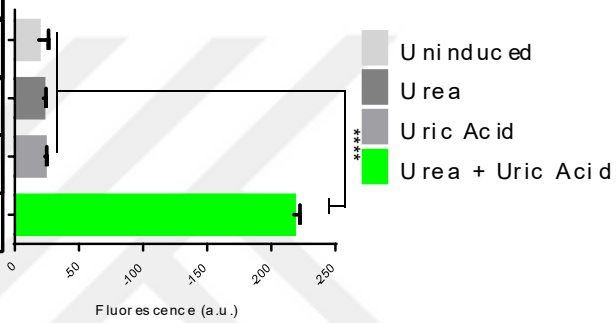

Figure 46: The truth table of AND-Logic Gate and the characterization assay of the multi-input AND-Logic Gated Urea-Uric Acid sensor carrying pZE IR pUreD-HucO sfGFP proD HucR and the pZS mproD UreR mproD UACT plasmids. After induction with 100 mM urea and/or 50 μM uric acid solution the response signal was measured with a microplate reader at the 8th hour. The expected outcomes and the experimental signal levels of the four conditions were matched. Experiments were conducted with three replicates and the normalized data was analyzed with two-way ANOVA ($p \leq 0.05$, $p \leq 0.01$, $p \leq 0.001$ and $p \leq 0.0001$ were shown as “*”, “**”, “***” and “****” respectively).

To measure the dynamic range of the AND-Gate biosensor, individual urea and uric acid cross-tested with each other. Fluorescence and optical density measurements were taken at the 8th hour after the induction.

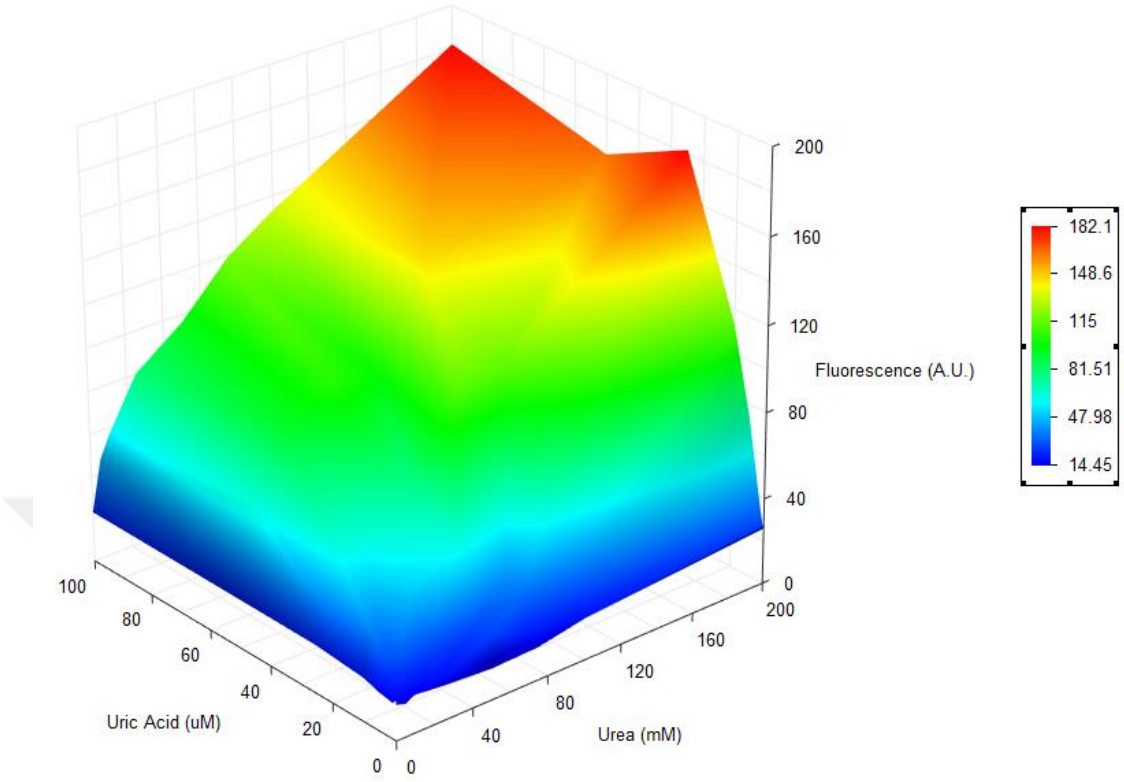

Figure 47: The dynamic range of multi-input AND-Logic Gated Urea-Uric Acid sensor carrying pZE IR pUreD-HucO sfGFP proD HucR and the pZS mproD UreR mproD UACT plasmids. 0, 0.1, 1, 5, 10,25, 50,100 μM of uric acid concentrations were tested against 0, 5, 10, 25, 50,75, 100, 200 mM urea concentrations. Experiments were conducted without replicates, each data point were used to draw the 3D plot with TeraPlot 1.4.06.

3.3.7 Construction of Dual Reporter Urea-Uric Acid Biosensor

In the next step a second fluorescent protein mScarlet-I was incorporated into the multiplexed detection system. Here, individual biosensor modules were designed to operate in a single cell. In the urea sensing module, sfGFP was used as the reporter molecule and in the uric acid module mScarlet-I fluorescent protein was used as reporter allowing simultenous detection of the

both pathological markers. This system is especially important for conditions that require monitoring and quantification of pathological biomarkers levels at the same time.

3.3.8 Construction of pZE pUreD sfGFP syn pHucO v2 mScarlet-I proD HucR plasmid

The sfGFP and mScarlet I fluorescent proteins were selected as the reporters for the urea and uric acid sensitive dual reporter system. For this, the mScarlet I gene and the rrntb1 terminator were amplified with the appropriate primers from the pEB2-mScarlet-I (Addgene, #104007) plasmid. Using consecutive PCR reactions, synpHucO v2 promoter was added to to mScarlet-I rrntb1 DNA region.

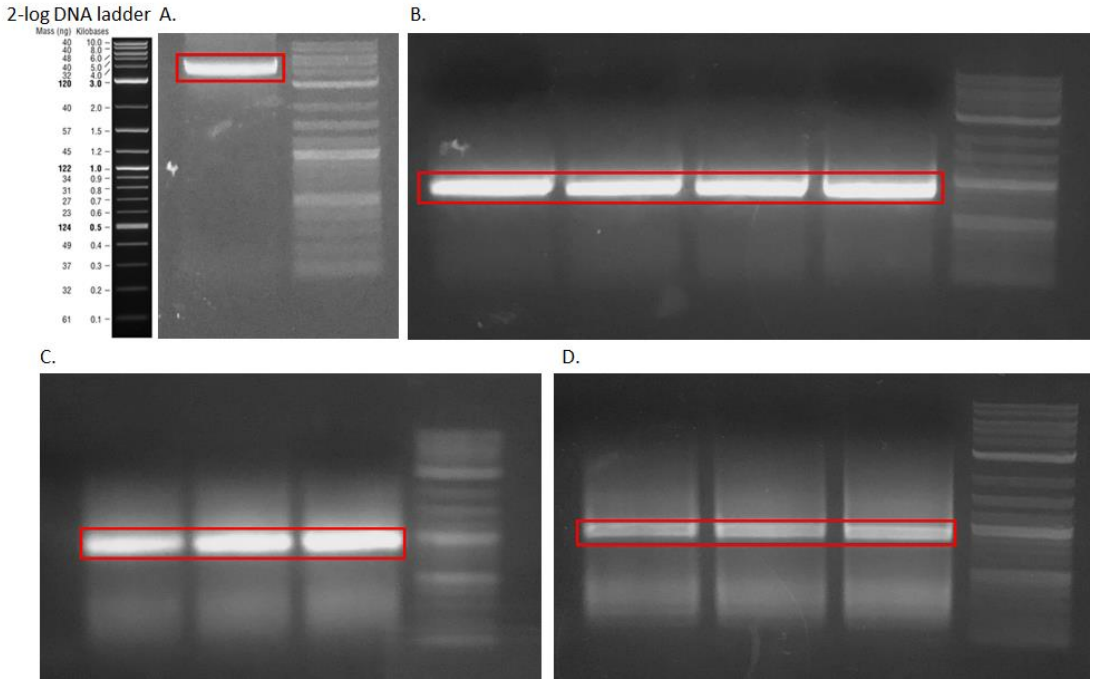

Figure 48: DNA parts needed for the construction pZE proD HucR IR pUreD sfGFP synpHucO mScarlet I ran on 1% agarose gel. A. SpeI and SacI digested pZE proD HucR IR pUreD sfGFP vector, expected size at 3988 bp. B. First PCR of synpHucO mScarlet I DNA region, expected size at 861 bp. C. Second

PCR of synpHucO mScarlet I DNA region, expected size at 901 bp. D. Third PCR of synpHucO mScarlet I DNA region, expected size at 946 bp.

The reactions were then ran on 1% agarose gel and target DNA fragments were purified from the gel. In consecutive PCR reactions, previous PCR reaction's isolated DNA was used as template. DNA fragment of the final PCR and the digested backbone were assembled with Gibson Assembly reaction. Verification of the pZE pUreD sfGFP syn pHucO v2 mScarlet-I proD HucR plasmid was then confirmed with Sanger sequencing (appendix D).

3.3.8 Characterization of pZE pUreD sfGFP syn pHucO v2 mScarlet-I proD HucR Dual Reporter Urea-Uric Acid Biosensor

Constructed pZE pUreD sfGFP syn pHucO v2 mScarlet-I proD HucR plasmid was co-transformed to E.coli DH5α PRO host with the pZS mproD UreR mproD UACT plasmid. Similar to previously described induction assays, cells were induced with 100 mM fresh urea solution and 50 µM fresh uric acid solution. Here three groups were prepared for induction; no analyte added cells, urea added cells and uric acid added cells.

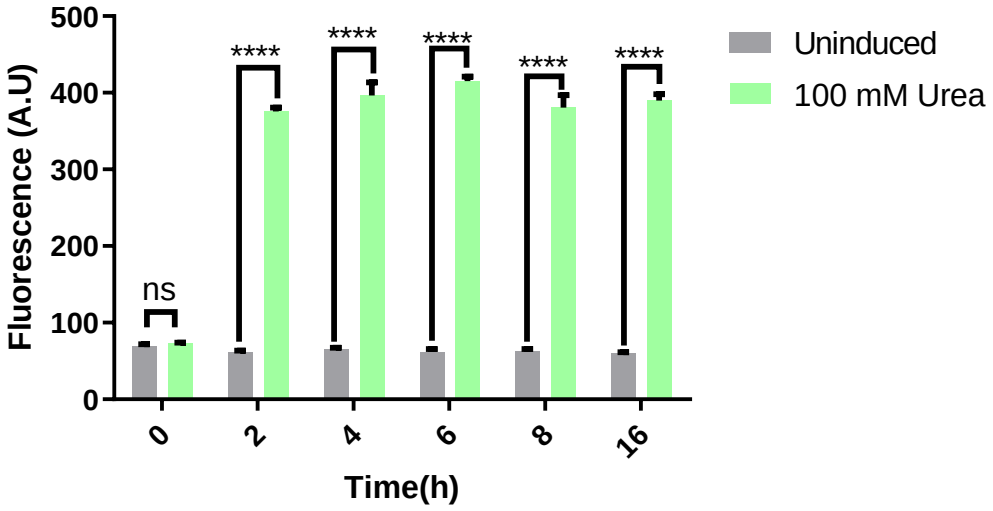

Figure 49: Characterization of the dual reporter urea uric acid biosensors with pZE pUreD sfGFP syn pHucO v2 mScarlet-I proD HucR and pZS mproD UreR mproD UACT plasmids. After induction with 100 mM urea solution the GFP fluorescence response signal samples was measured with a microplate reader 0,2,4,6,8 and 16 hours after induction at 485 nm excitation and 538 nm emission. Experiments were conducted with three replicates and the normalized data was analyzed with two-way ANOVA ($p \leq 0.05$, $p \leq 0.01$, $p \leq 0.001$ and $p \leq 0.0001$ were shown as “*”, “**”, “***” and “****” respectively).

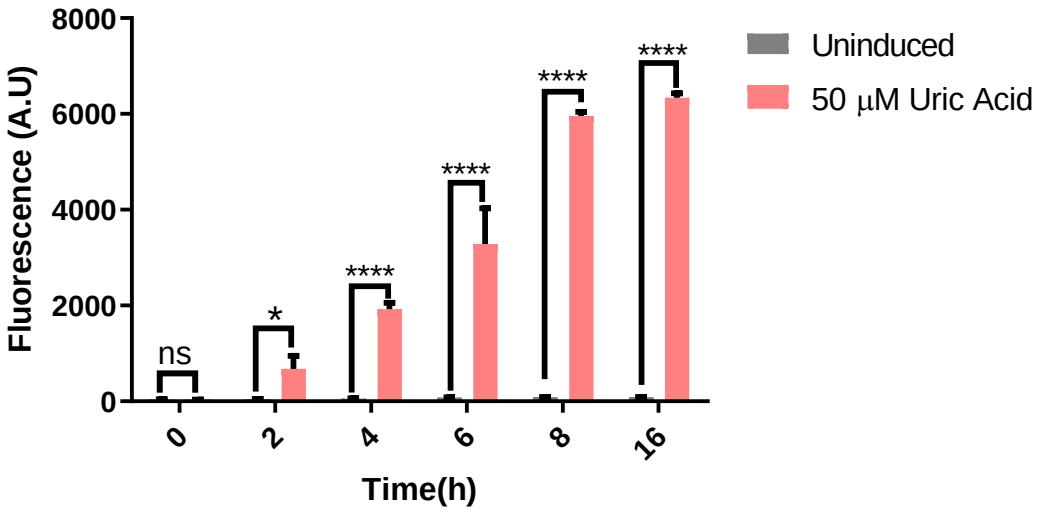

Figure 50: Characterization of the dual reporter urea uric acid biosensors with pZE pUreD sfGFP syn pHucO v2 mScarlet-I proD HucR and pZS mproD UreR mproD UACT plasmids. After induction with 50 μM uric acid solution the RFP fluorescence response signal samples was measured with a microplate reader 0,2,4,6,8 and 16 hours after induction at 544 nm excitation and 612 nm emission. Experiments were conducted with three replicates and the normalized data was analyzed with two-way ANOVA ($p \leq 0.05$, $p \leq 0.01$, $p \leq 0.001$ and $p \leq 0.0001$ were shown as "*", "**", "***" and "****" respectively).

3.3.9 Construction of pZE pUreD-RiboJ sfGFP syn pHucO v2 mScarlet-I proD HucR plasmid

For the construction of pZE pUreD-RiboJ sfGFP syn pHucO v2 mScarlet-I proD HucR, pZE vector carrying all the necessary components was amplified with PCR with primers that have RiboJ overhangs with two consecutive PCR reactions.

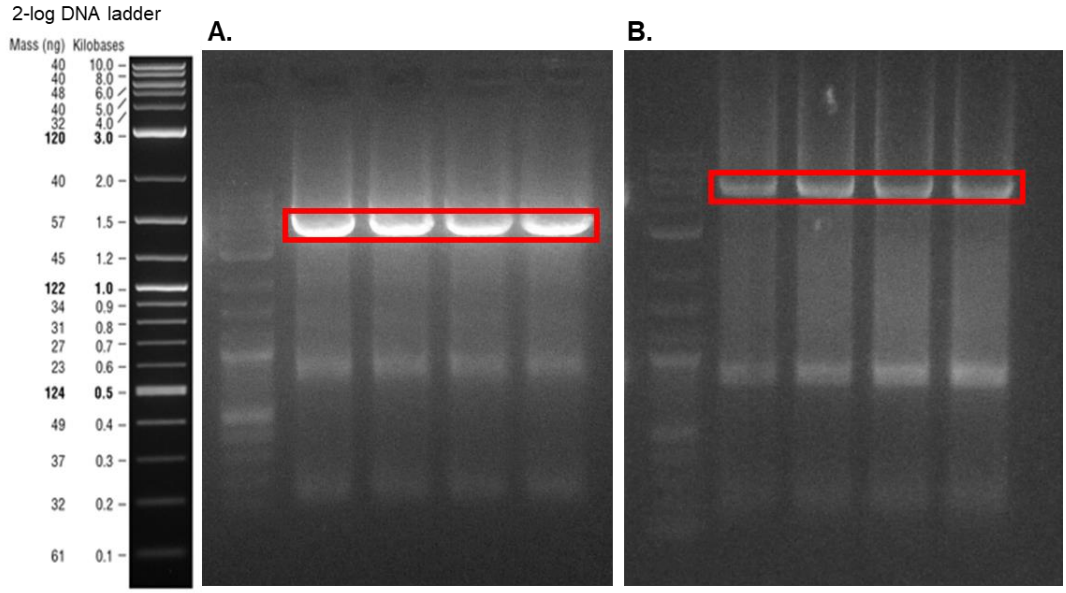

Figure 51: 1% Agarose gel images of the biological parts needed to construct pZE pUreD-RiboJ sfGFP syn pHucO v2 mScarlet-I proD HucR. A. PCR-amplified pZE backbone with part of RiboJ overhang sized 4914 bp B. Second PCR reaction of completing RiboJ part addition, expected size 4965 bp.

The second PCR reaction were then ran on 1% agarose gel and target DNA fragment was purified from the gel. Vector was self-ligated with Gibson Assembly reaction. Verification of the pZE IR pUreD-HucO RiboJ sfGFP plasmid was then confirmed with Sanger sequencing (appendix D).

3.3.10 Characterization of of pZE pUreD-RiboJ sfGFP syn pHucO v2 mScarlet-I proD HucR Dual Reporter Urea-Uric Acid Biosensor

Constructed pZE pUreD-RiboJ sfGFP syn pHucO v2 mScarlet-I proD HucR plasmid was co-transformed to E.coli DH5α PRO host with the pZS mproD UreR mproD UACT plasmid. Similar to previously described induction assays, cells were induced with 100 mM fresh urea solution and 50 µM fresh uric acid solution. Here, four groups were prepared for induction; no analyte added

cells, urea added cells, uric acid added cells and urea and uric acid added cells.

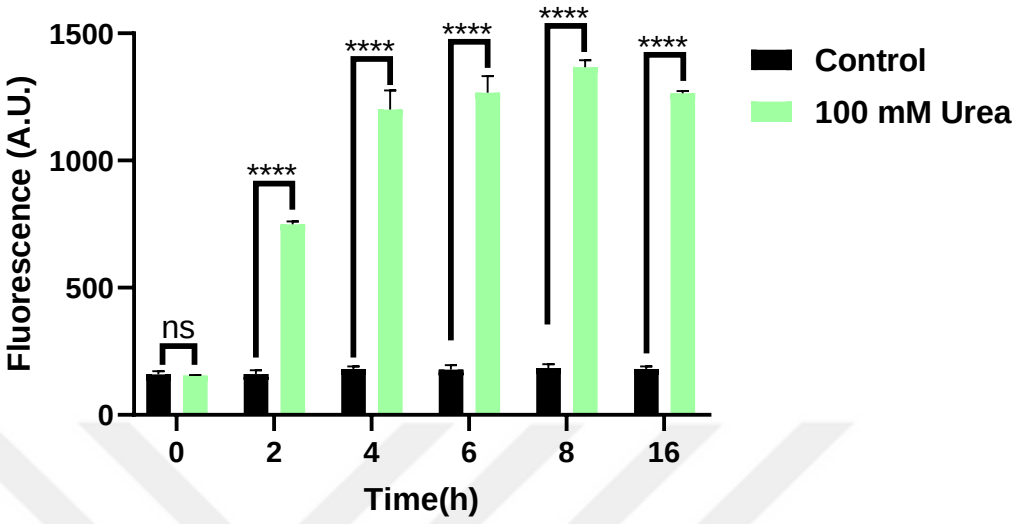

Figure 52: Characterization of the dual reporter urea uric acid biosensors with pZE pUreD-RiboJ sfGFP syn pHucO v2 mScarlet-I proD HucR and pZS mproD UreR mproD UACT plasmids. After induction with 100 mM urea solution the GFP fluorescence response signal samples was measured with a microplate reader 0,2,4,6,8 and 16 hours after induction at 485 nm excitation and 538 nm emission. Experiments were conducted with three replicates and the normalized data was analyzed with two-way ANOVA ($p \leq 0.05$, $p \leq 0.01$, $p \leq 0.001$ and $p \leq 0.0001$ were shown as “*”, “**”, “***” and “****” respectively).

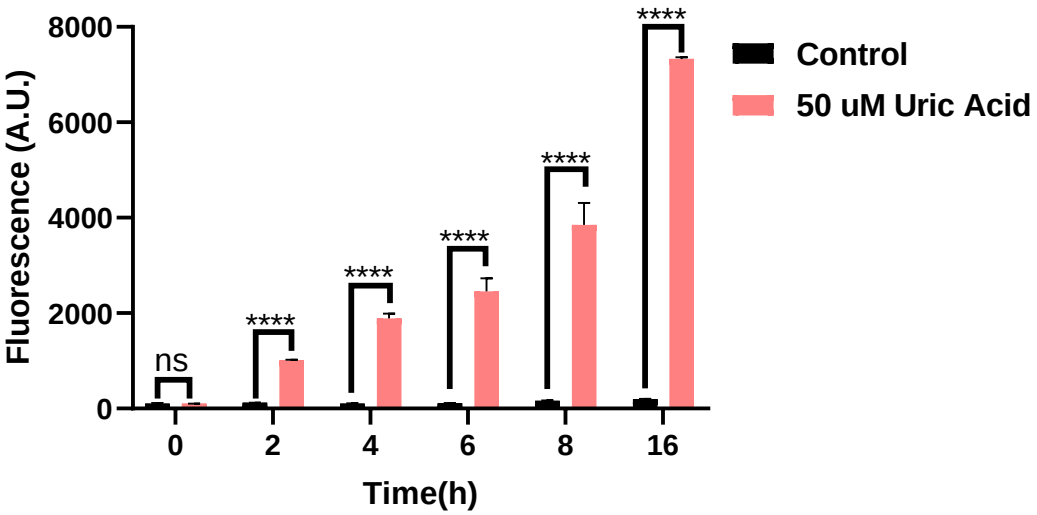

Figure 53: Characterization of the dual reporter urea uric acid biosensors with pZE pUreD-RiboJ sfGFP syn pHucO v2 mScarlet-I proD HucR and pZS mproD UreR mproD UACT plasmids. After induction with 50 µM uric acid solution the RFP fluorescence response signal samples was measured with a microplate reader 0,2,4,6,8 and 16 hours after induction at 544 nm excitation and 612 nm emission. Experiments were conducted with three replicates and the normalized data was analyzed with two-way ANOVA ($p \leq 0.05$, $p \leq 0.01$, $p \leq 0.001$ and $p \leq 0.0001$ were shown as “*”, “**”, “***” and “****” respectively).

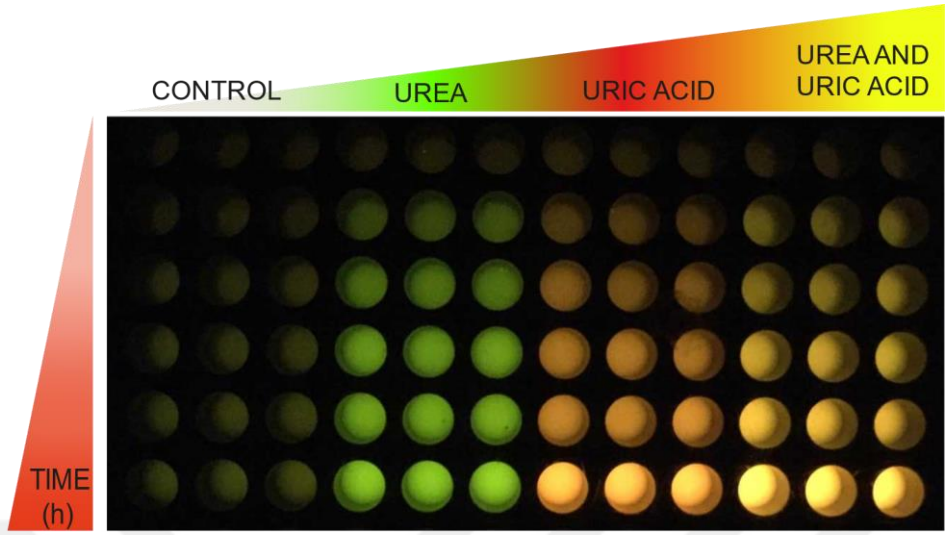

Figure 54: Image of the optimized dual reporter urea-uric acid biosensor taken under transilluminator. Three replicates of uninduced, urea-induced, uric acid-induced and urea and uric acid-induced were positioned next to each other from left to right at each time point. Images was taken before the 16th hour microplate measurements. 96-well plate was kept at 4°C between measurements to preserve fluorescent proteins from degredation.

3.4 Biofilm Aided Cell Immobilization on Paper

Functional materials gain more and more importance over the recent years with properties such as embedded sensing, energy generation and storage, self-repair, and mobility. In nature, such functionality can be observed by the cells part of the structural scaffold [61]. Cells intrinsically have complex regulatory networks that aid organization and differentiation patterns as the material grows into a macroscopic 3D form[62]. For example, bacterial cells use biofilms, microbial community structures that are composed of polysaccharides, proteins, and extracellular DNA, to adhere onto surfaces or to form pellicles at the air–liquid interface [63]. To develop point of care devices

from living biosensors inside biocompatible, biodegradable and low-cost portable paper discs, we utilized biofilm aided adhesion of functionalized cells onto paper through biofilm-cellulose interactions while keeping the ability of the cells sensing and responding to changes in the environment.

In enterobacteria, curli proteins are the main components that form amyloid fibers anchored to the cell wall[64]. The major structural subunit of this protein-based polymer is the CsgA protein which is nucleated by the CsgB protein[65]. Since, bacterial cellulose is part of biofilm structure with probable implications in elasticity, reinforcement and promoting adhesion[66, 67], it is thought that these interactions may also occur with plant sourced cellulose (paper discs) and biofilms resulting in immobilizing cells on paper during biofilm formation. For the initial tests, biofilm deficient *E. coli* ΔcsgA cells (provided by Ebru Şahin Kehribar) were transformed with pZA pBAD csgA plasmid (provided by Ebru Şahin Kehribar) for controllable biofilm production. Biofilm production in cells was re-established through arabinose induction.

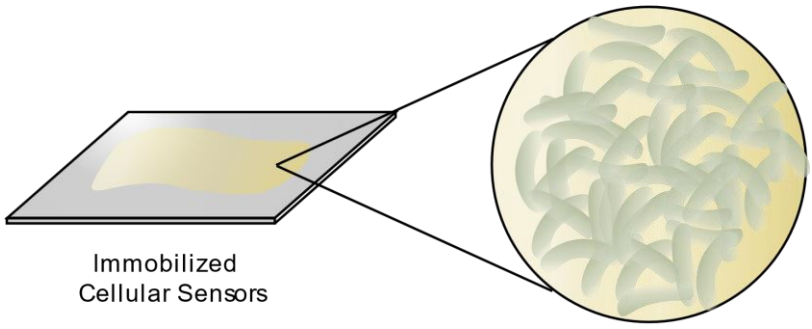

Figure 55: Schematic Representation of immobilized cellular biosensors on paper surface.

3.4.1 Construction of pZA pBAD csgA-CBDcex plasmid

Previously, specific adhesion of cells with surface-exposed cellulose-binding domain (CBD) on cellulose-based materials has shown successful implementations[68, 69]. To amplify cellulose-biofilm interactions and reinforce the adhesion of cells on paper a cellulose binding domain of an exoglucanase from *Cellulomonas fimi* (CBDcex)[70] was fused to CsgA protein. To do so, CBDcex was amplified with appropriate primers from Bba_K1321342 (2019 IGEM DNA distribution kit). To maintain its function, CBDcex was fused to C-terminal of CsgA protein [71] which also maintains the function of CsgA[72].

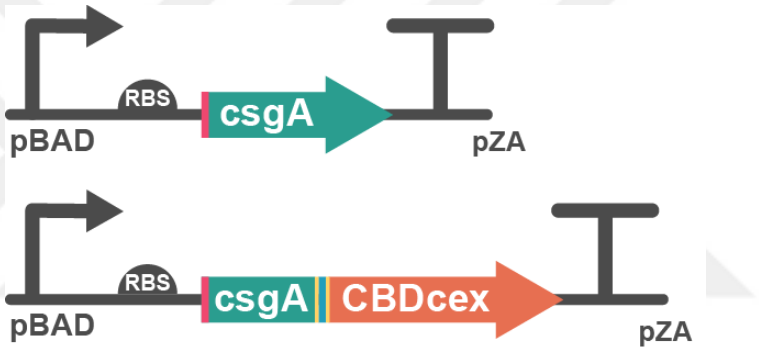

Figure 56: Constructs used in biofilm-aided cell immobilization. On the top; pZA pBAD csgA plasmid was kindly provided by Ebru Şahin Kehribar. On the bottom pZA plasmid carrying CsgA gene sequence fused with CBDcex on the C-terminal (Endegenous localization signal peptide of CsgA is shown in red, GS linkers are shown in yellow and His-Tag is shown in blue.).

For the construction of pZA pBAD csgA-CBDcex plasmid, pZA pBAD csgA plasmid was digested with KpnI and XhoI restriction enzymes(Figure 57.A). pZA pBAD spycatcher-csgA plasmid was digested with KpnI and BamHI restriction enzymes to acquire csgA (Figure 57.B). CBDcex peptide was amplified from Bba_K1321342 (2019 IGEM DNA distribution kit) with

appropriate primers (Figure 57.C). Isolated csgA and CBDcex were then assembled together using two-template PCR (Figure 57.D) (Appendix E).

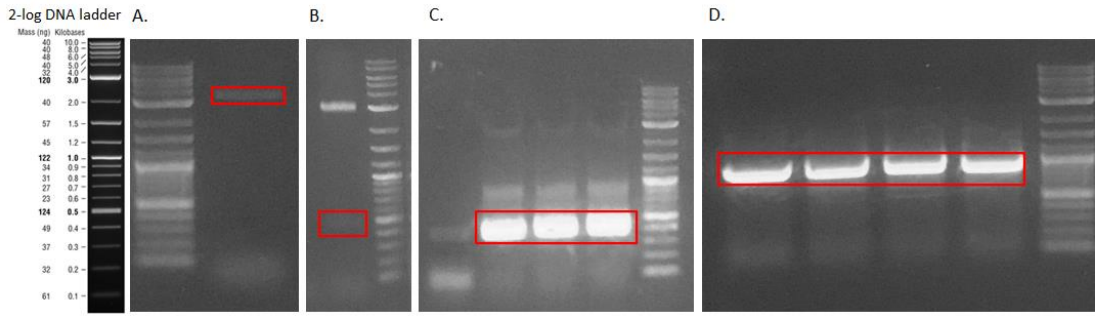

Figure 57: DNA parts needed for the construction of pZA pBAD csgA-CBDcex ran on 1% agarose gel. A. Restriction digestion of pZA pBAD csgA showing pZA backbone (3211 bp). B. Restriction digestion of pZA pBAD spycatcher-csgA showing csgA insert (485 bp). C.PCR amplification of CBDcex gene sequence expected size at 396 bp. D.PCR assembly of csgA and CBDcex parts with two template PCR showing the expected 885 bp band.

The PCR of csgA-CBDcex fusion and the digestion of pZA backbone were then ran on 1% agarose gel and target DNA fragments were purified from the gel. DNA fragments were then assembled with Gibson Assembly reaction. Verification of the pZA pBAD csgA-CBDcex plasmid was then confirmed with Sanger sequencing (appendix D).

3.4.2 Adhesion of Biofilm Producing Cells on Paper

To examine the surface adhesion activity of biofilm producing cells consisted of cells were grown stationarily on paper in with liquid minimal M63 medium on top (Materials and Methods) for 9 days. After washing with 1x PBS media 3 times, results were observed in ESEM. Since paper also has a fibrillious structure, unmodified paper samples were used as reference to differentiate biofilm formation from cellulose fibrils on paper.

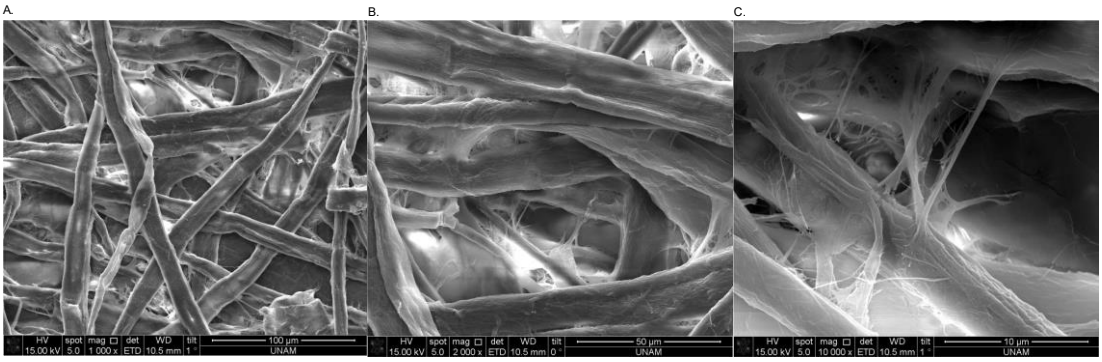

Figure 58: Images of Whatman Paper to be used as reference, taken with Scanning Electron Microscope. A. Image of Whatman Paper taken with x1000 magnification. B. Image of Whatman Paper taken with x2000 magnification C. Image of Whatman Paper taken with x10.000 magnification.

	E. coli ΔcsgA induced	*E. coli* ΔcsgA carrying pZA pBAD csgA uninduced	*E. coli* ΔcsgA carrying pZA pBAD csgA induced
OD 0.5	Group 1	Group 2	Group 3
OD 0.01	Group 4	Group 5	Group 6

Table 1: Experimental set up of the initial adhesion assay. Cells were grouped according to their phenotype, optical densities and induction status.

First, three sets of cells were tested for biofilm production and subsequent adhesion on surface; *E. coli* ΔcsgA cells induced with 0.2% arabinose, *E. coli* ΔcsgA carrying pZA pBAD csgA cells that were not induced and ΔcsgA carrying pZA pBAD csgA cells that were induced with 0.2% arabinose. The groups *E. coli* ΔcsgA cells induced and *E. coli* ΔcsgA carrying pZA pBAD csgA cells that were not induced were used as control.

To test the effects of the initial number of cells added onto paper two sets of cell suspensions were added onto paper. One set had initial OD 0.5 while in

the other set on grown cells were directly diluted(1.200) into minimal medium. Cells that have initial OD 0.5 has shown less adhesion on paper(Figure 59).

For the groups that had optical density 0.5, number of cells remaining on the paper discs did not vary to a considerable extent. This shows that either the level of biofilm production was not efficient enough or the process of biofilm production did not initiate interactions with the surface to immobilize cells onto the paper surface.

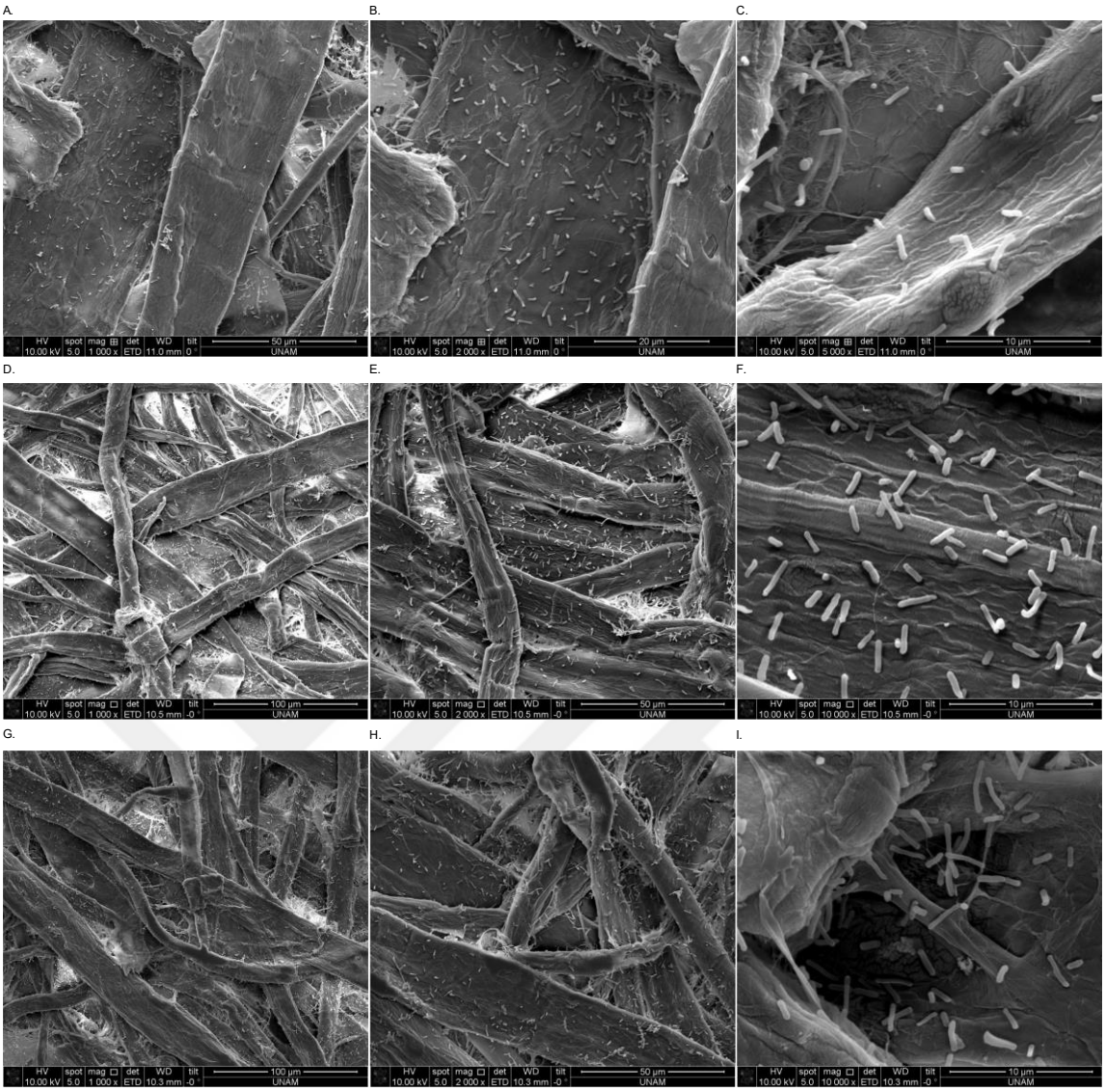

Figure 59: Biofilm adhesion assays of group 1,2 and 3 under ESEM. The ESEM pictures of group 1, *E. coli* ΔcsgA with an optical density of 0.5 that were induced with 0,2% arabinose under x1000 magnification (A.), x2000 magnification (B.) and x10.000 magnification (C.). The ESEM pictures of group 2, *E. coli* ΔcsgA carrying pZA pBAD csgA with an optical density of 0.5 that were not induced under x1000 magnification (D.), x2000 magnification (E.) and x10.000 magnification (F.). The ESEM pictures of group 3, *E. coli* ΔcsgA carrying pZA pBAD csgA with an optical density of 0.5 that were induced with

0,2% arabinose under x1000 magnification (G.), x2000 magnification (H.) and x10.000 magnification (I.).

However, the groups that had optical density 0.01, number of cells remaining on the paper discs did change to a considerable extent. This shows that the process of biofilm production is initiating certain interactions with the surface which results in cells remaining attached on paper surface after consecutive wash cycles.

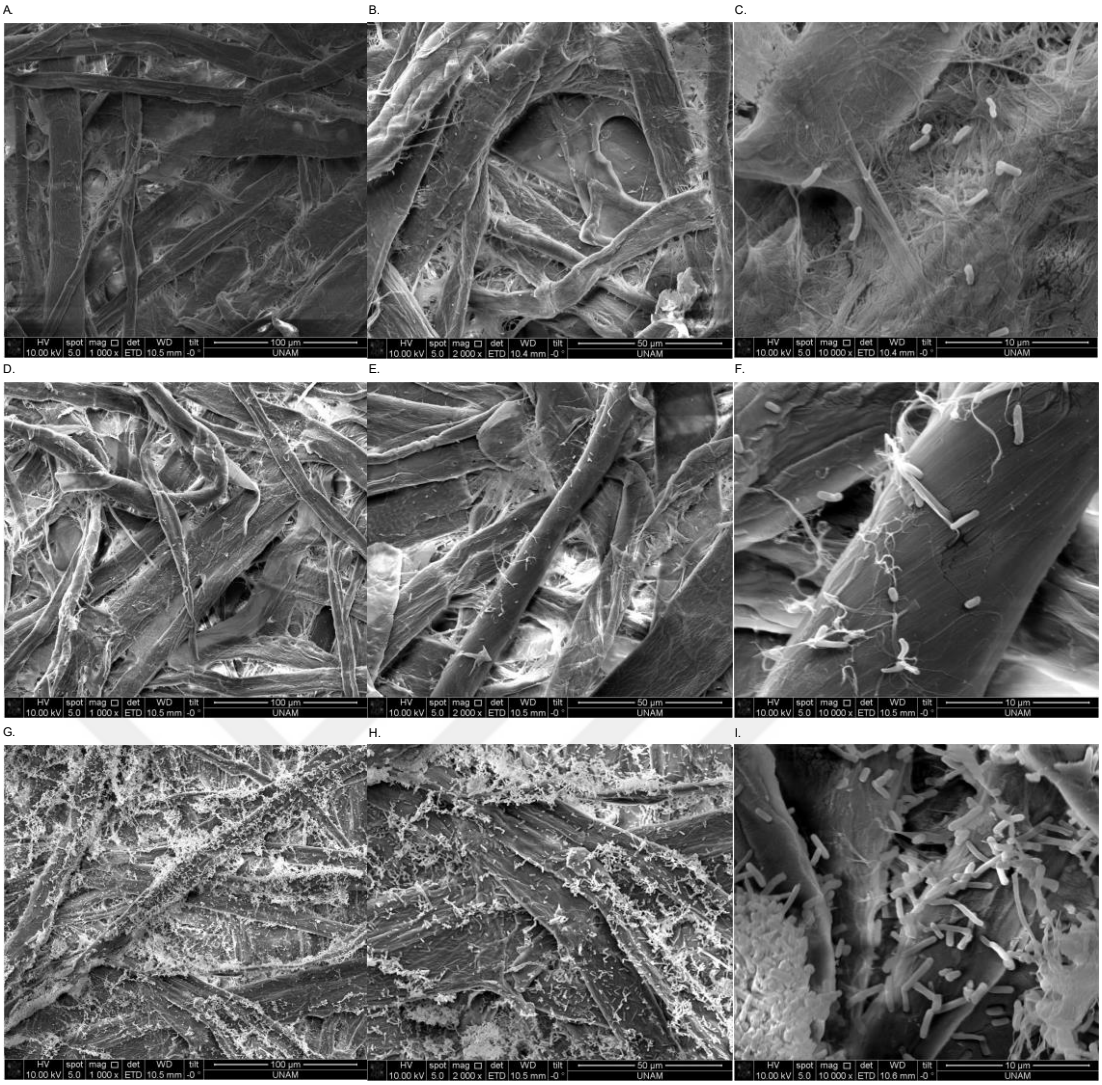

Figure 60: Biofilm adhesion assays of group 4,5 and 6 under ESEM. The ESEM pictures of group 4, *E. coli* ΔcsgA with an optical density of 0.01 that were induced with 0,2% arabinose under x1000 magnification (A.), x2000 magnification (B.) and x10.000 magnification (C.). The ESEM pictures of group 5, *E. coli* ΔcsgA carrying pZA pBAD csgA with an optical density of 0.01 that were not induced under x1000 magnification (D.), x2000 magnification (E.) and x10.000 magnification (F.). The ESEM pictures of group 6, *E. coli* ΔcsgA carrying pZA pBAD csgA with an optical density of 0.01 that were induced with 0,2% arabinose under x1000 magnification (G.), x2000 magnification (H.) and x10.000 magnification (I.).

3.4.3 Testing the Maintanence of Biofilm Production in the CsgA-CBDcex Fusion Protein

Since the β-sheet-rich amyloid protein CsgA is the primary structural component of the curli fibers forming biofilms, curli formation in bacterial cells can be quantified with classic amyloid dyes such as Congo red (CR). CR binding to β-amyloid causes a detectable fluorescence change which can be used for comparatively quantify whole-cell curliation[73, 74].

To test if the biofilm formation was affected by the size or the chemical properties of CsgA-CBDcex fusion protein, on cultures of *E. coli* ΔcsgA and *E. coli* ΔcsgA carrying pZA pBAD csgA-CBDcex plasmid were diluted into M63 medium supplemented with 0.2% glycerol, suitable antibiotics and 0.2% arabinose and grown stationarily at 30°C for 6 days. At the end of the 3rd day cells were re-induced with and 0.2% arabinose solution. At the end of the 6th day 1 mL of cell culture was centrifuged at 8000 rpm for 6 minutes and and resuspended in same volume of 1x PBS solution. 100 µL of cells were taken for the cell density measurement. Remaining cells were centrifuged at 8000 rpm and resuspended in 1x CR solution. Cells were kept in the solution for 20 minutes at room temperature. Cells were centrifuged one more time before taking the 100 µL supernatant for optical density measurements at 480 nm. Normalization was done by dividing the negative OD480 values to OD600 values.

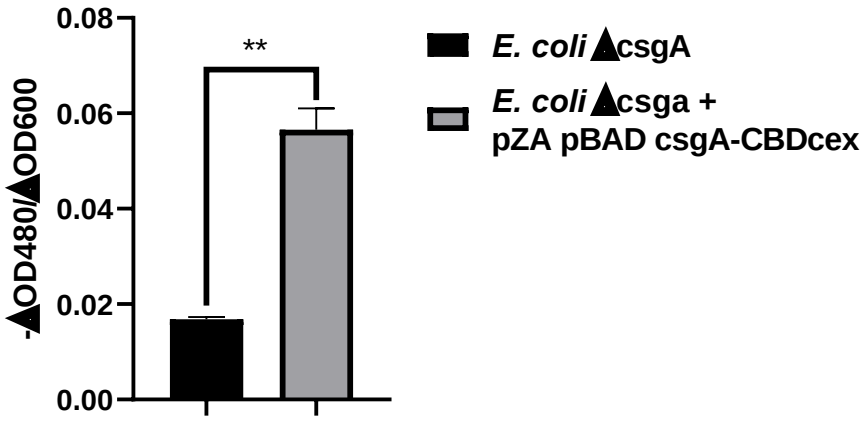

Figure 61: Congo Red assay of *E. coli* ΔcsgA carrying pZA pBAD csgA-CBDcex .CR binding to *E. coli* ΔcsgA cells carrying pZA pBAD csgA-CBDcex was significantly more than the *E. coli* ΔcsgA cells. The data shows the normalized values of double samples. Statistical significance was determined with t-test. (**: $p < 0.01$)

3.4.4 Adhesion of Modified Biofilm Producing Cells on Paper

To examine the surface adhesion activity of biofilm producing cells modified with cellulose binding domain a similar experiment set up was done for *E. coli* ΔcsgA cells carrying pZA pBAD csgA-CBDcex. Cells were grown until their OD reached 0.5 and then diluted to liquid minimal M63 medium on top of paper discs to grow stationarily for 6 days(Materials and Methods). After washing with 1x PBS media 3 times results were observed in ESEM.

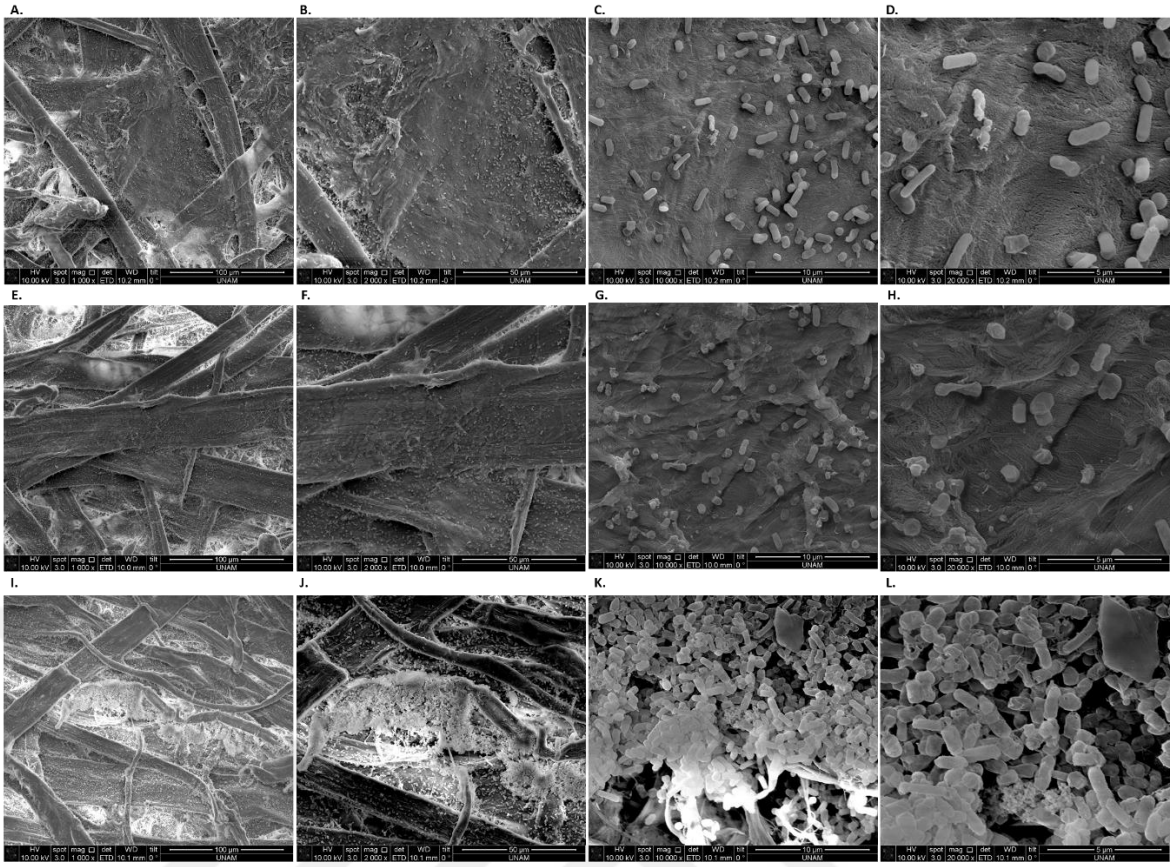

Figure 62: Biofilm adhesion assays of *E. coli* ΔcsgA cells carrying pZA pBAD csgA-CBDcex under ESEM. The ESEM pictures of group *E. coli* ΔcsgA that were induced with 0,2% arabinose under x1000 magnification (A.), x2000 magnification (B.), x10.000 magnification (C.) x20.000 magnification (D.). The ESEM pictures of, *E. coli* ΔcsgA cells carrying pZA pBAD csgA-CBDcex that were not induced under x1000 magnification (E.), x2000 magnification (F.), x10.000 magnification (G.) and x20.000 magnification (H.). The ESEM pictures of *E. coli* ΔcsgA cells carrying pZA pBAD csgA-CBDcex that were induced with 0,2% arabinose under x1000 magnification (I.), x2000 magnification (J.), x10.000 magnification (K.) and x20.000 magnification (L.).

In *E. coli* ΔcsgA cells carrying pZA pBAD csgA-CBDcex plasmid, the number of cells remaining on the paper discs has shown a significant increase in a shorter amount of time. This shows that the process of biofilm production

combined with exposed cellulose binding domain is also interacts with cellulose surface which results in cells remaining immobilized on paper after consecutive wash cycles.

3.5 Cell Entrapment inside Gelatin Hydrogel Beads

Hydrogels are attractive biomaterials for encapsulating living cells with desirable properties such as high water content, permeability to various chemical and biological molecules, low cell toxicity also being enviromentally friendly[75]. Therefore, they have high potential in three-dimensional cell culture and tissue engineering applications[76]. Even though, cell-based synthetic biology inspired technologies hold great promise, a bottleneck for their real life applications is their safe containment to prevent environmental escape[77, 78]. To solve physical containment issues of engineered cellular biosensors for real-world applications, a hydrogel-based encapsulation system was developed. The two main concerns of this system was to keep functionality of the cellular biosensors as well as prevent cellular escape. Gelatin is a partial hydrolysis product of native collagen and has many attractive properties for being used as source of many composite biomaterials including non-toxicity, non-carcinogenicity, biocompatibility, and biodegradability [79]. Since pure gelatin is soluble in water, improving its mechanical and thermal properties by crosslinking agents is necessary for its application as scaffold for 3D cell growth applications. Gelatin can be crosslinked via physical treatments, UV irradiation, chemical crosslinking agents such as glutaraldehyde, carbodiimide, genipin or enzymatical crosslinking agents such as transglutaminase. Transglutaminase is an advantageous crosslinking agent compared to its counterparts which may

have handicaps such as degeneration of gelatin during treatment, incomplete crosslinking due to lack of full penetration of thick materials or cytotoxicity effects of residual crosslinking agents[80]. Transglutaminase induces crosslinking by catalyzing acyl-transfer reactions between λ-carboxyamide groups of glutamine residues and ε-amino groups of lysine residues, forming ε-(λ-glutaminyl) lysine intra- and intermolecular crosslinked proteins[81].

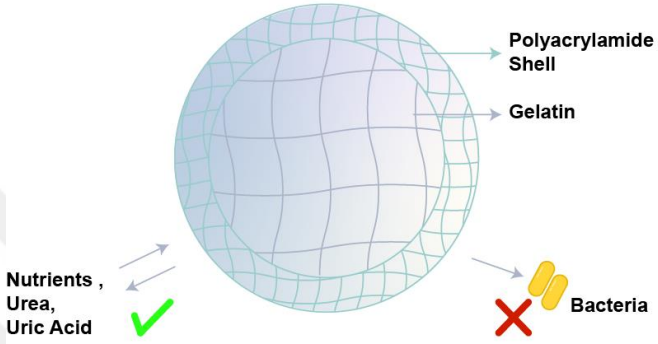

Figure 63: Strategy for genetically modified bacteria entrapment for real life applications

3.5.1 Hydrogel Bead Formation Assay

Before entrapment of cells, physically durable gelatin bead formation experiments were optimized while keeping in mind that the process of bead formation should not be toxic to cells and should support cell growth. To do so, edible gelatin was dissolved to be 10%w/v in 1xPBS buffer at 40°C. To enable bead formation and prevent cluster formation, gelatin-PBS admixture was dripped in liquid phase to a still cold cooking oil on ice. After that, to maintain their form and remove oil from the beads, they were quickly washed with ice-cold 70% ethanol and distilled water on top of a sieve. Beads were than transferred to transglutaminase-LB mixture and kept inside 4°C for 24 hours. It was observed that only after 24 hours, chemically crosslinked beads were

able to support their structure at 37°C, the temperature they are going to be kept in during the induction process.

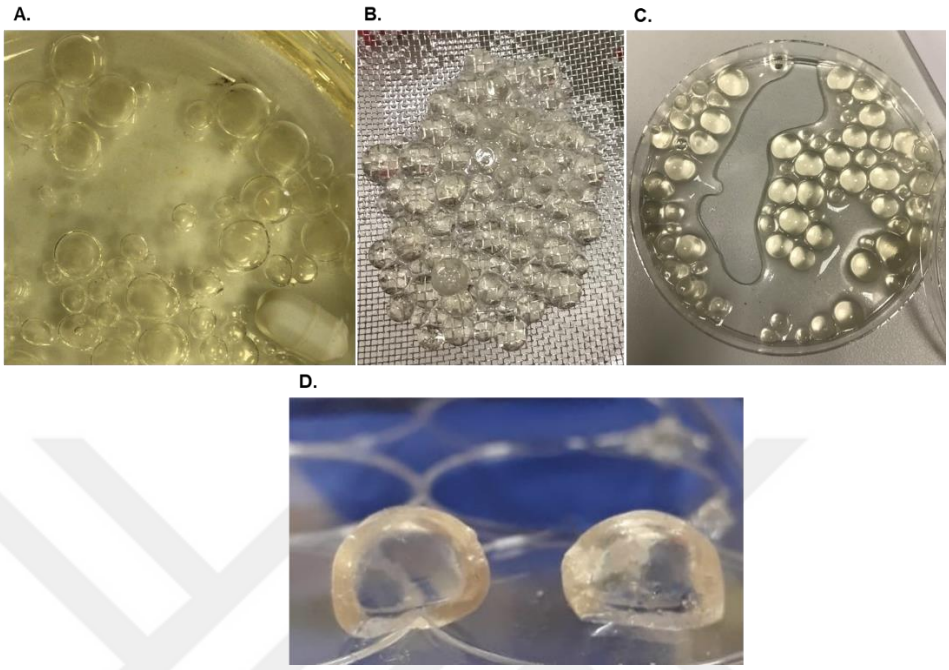

Figure 64: Pictures of gelatin beads during the bead formation process. A. Initial bead formation by dripping method. Since dripping was made by hand, various sized beads were formed. B. Beads were washed with ice-cold 70% ethanol and distilled water and excess liquids were strained with a sieve. C. For chemical-crosslinking, gelatin beads were kept transglutaminase-LB mixture for 24 hours. D. Cross-section of the chemically crosslinked gelatin beads after testing them at 37°C.

3.5.2 Cell Entrapment Assay inside Gelatin Beads

Even though gelatin meets the requirements for cell growth and maintaining sensing and responding capability, the formed gelatin beads pore size of gelatin beads is larger for the safe containment genetically modified bacterial cells and prevent their environmental escape[80, 82]. Therefore,a tough polyacrylamide shell layer was incorporated into the system to provide

mechanical protection and as an confining barrier with compatible pore size for cellular escape[83].

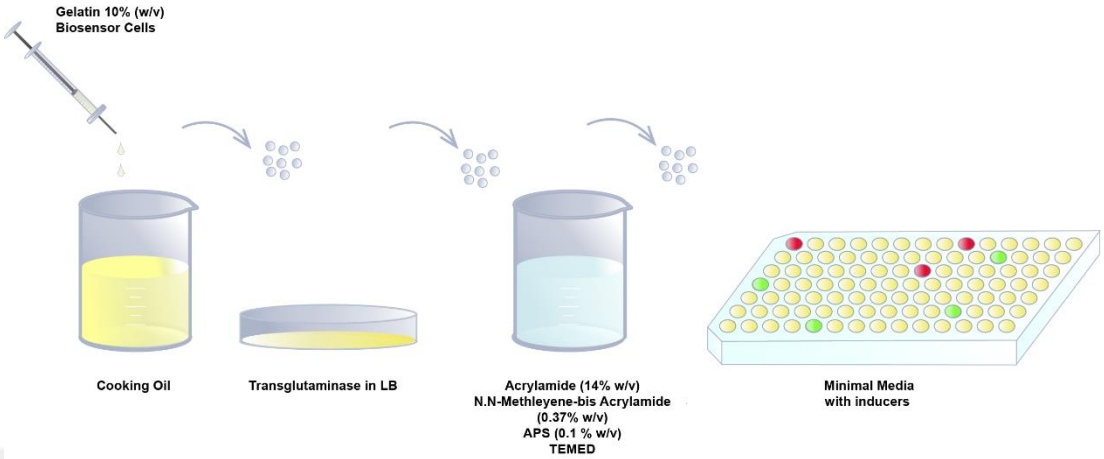

Figure 65: The schematic representation of transglutaminase crosslinked gelatin bead formation for cellular biosensor containment.

In the next step, on grown cellular biosensor suspension was diluted (1.100) in the gelatin-PBS mixture before droplet formation. In this trial much more efficient oil removal was achieved by replacing 70% ethanol with 100% acetone during the washing step. The nutrients needed to support growth were incorporated via diffusion during the crosslinking treatment. Gelatin beads containing cells were then coated the though polyacrylamide hydrogel with by swirling inside a precursor solution composed of 14% w/v acrylamide, 0.37% w/v N,N-Methylene-bis Acrylamide, 0.1 w/v ammonium persulphate (APS) mixed with the with the accelerator N,N,N',N'-tetramethylenediamine(TEMED) right before the addition of beads. After keeping them in the fast curable precursor solution for 10 minutes, beads were washed with 1xPBS buffer to remove residual monomers for 10 minutes. After that beads were kept 2 mL minimal medium with appropriate antibiotics in a 24-well plate at 37°C for 3

hours before addition of 100 mM urea to the medium. Induced beads were checked after 24 hours under a transilluminator.

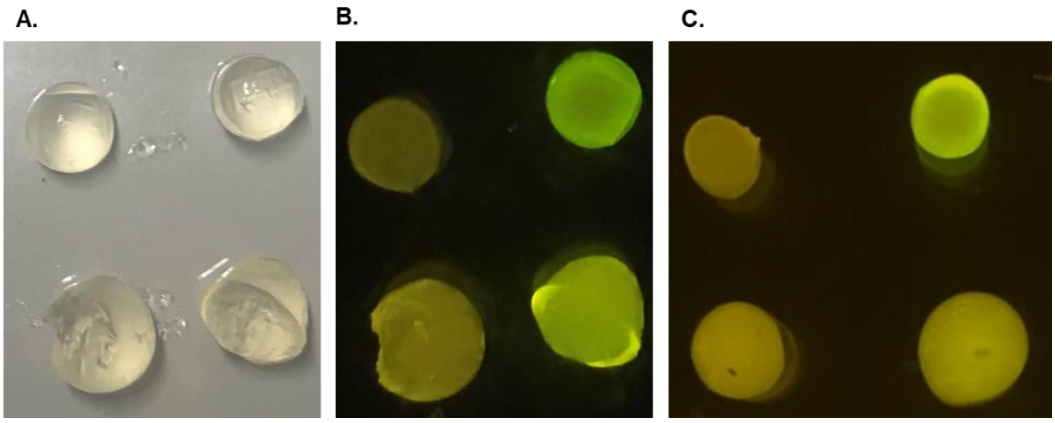

Figure 66: Pictures taken after inducing cellular biosensor containing beads with 100 mM urea. A. Pictures of beads under white light, on the top gelatin beads not coated with polyacrylamide layer were shown. On the bottom polyacrylamide coated gelatin beads were shown. For both cases, uninduced beads were positioned on the left and the induced beads were positioned at the right. B. Pictures of beads under the transilllumunator, 24 hours after induction. Beads were positioned as described in A.. Pictures of beads under the transilllumunator, 48 hours after the induction. Beads were positioned as described in A..

To asses toxicity from the residual acrylamide monomers, gelatin beads were not coated was also subjected same induction. In both coated and noncoated beads, a fluorescence respond to urea were observed with noncoated beads showing a slightly higher signal. Polyacrylamide coated beads swelled more under the same conditions. In both cases, medium samples that beads were kept in was inoculated in liquid media with appropriate antibiotics and grown overnight. In both cases cell growth was observed (data not shown.) This might

signify failing to prevent cell leakage from hydrogel beads or contamination during the bead preparation process.

3.6 Detection of Pathological Biomarkers in Human Clinical Samples

In the final step of this study, it was aimed to asses the relevance of the developed cellular biosensors by doing direct measurements from a common biofluid; human blood serum samples. To optimize the response fluorescence signal according to disease states, as well as prevent intereference of bacterial growth by the passive immune factors present in human serum such as the complement system[12]. Therefore, serum samples and minimal M63 medium mixtures were prepared with differing percentages to asses the most suitable testing conditions for preliminary validation of detection with urea and uric acid biosensors.

For initial urea screening with clinical samples, urea biosensor pZE IR pUreD RiboJ sfGFP-pZS mproD mt UreR (K169A) was grown as described in Materials and Methods. Testing conditions were arranged to be 50% and 25% serum sample in total in induction medium. Urea levels in the samples were determined previously by conventional laboratory tests (Table 2).

Urea Level	Assesed Urea Level in Sample	Urea Level in 50% Serum	Urea Level in 25% Serum	Urea Level in 10% Serum	Urea Level in 5% Serum
Low, in-range	3,571428571 mM	1,785714286 mM	0,892857 mM	0,357143 mM	0,178571 mM
High, in-range	6,428571429 mM	3,214286 mM	1,607143 mM	0,642857 mM	0,321429 mM
High, out-of-range	9,642857143 mM	4,821428571 mM	2,410714 mM	0,964286 mM	0,482143mM

Table 2: The table showing respective urea concentrations of tested clinical samples. Urea concentrations were determined with conventional laboratory

tests previously. Then urea concentrations in tested conditions were calculated by the dilution factor.

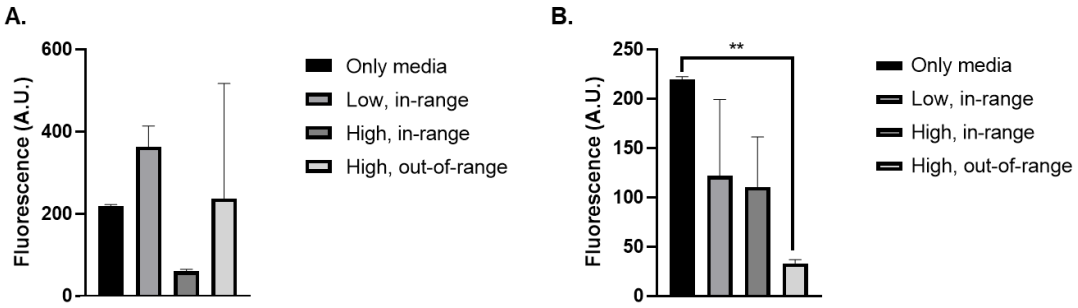

Figure 67: Validation of urea biosensor with human serum samples. A. Urea detection with samples that have 50% serum of the total volume. B. Urea detection with samples that have 25% serum of the total volume.After cells reached the optimal optical density for induction, respective serum samples were added to cells. The fluorescence response signals of the samples were measured with a microplate reader 8 hours after induction at 485 nm excitation and 538 nm emission. Experiments were conducted with three replicates and the normalized data was analyzed with one-way ANOVA ($p \leq 0.05$, $p \leq 0.01$, $p \leq 0.001$ and $p \leq 0.0001$ were shown as “*”, “**”, “***” and “****” respectively). The tested conditions have not shown a coherent response to varying urea levels. Furthermore, a significant decrease in the fluorescence signal was observed for the samples with the highest urea levels compared to no serum added samples, possibly due to the drop in cell survival inside human serum added medium (data not shown).

In the next set-up, serum concentrations were dropped to be 10%, 5% serum sample of the total in induction medium. Urea levels in the samples were determined previously by conventional laboratory tests (Table ..).

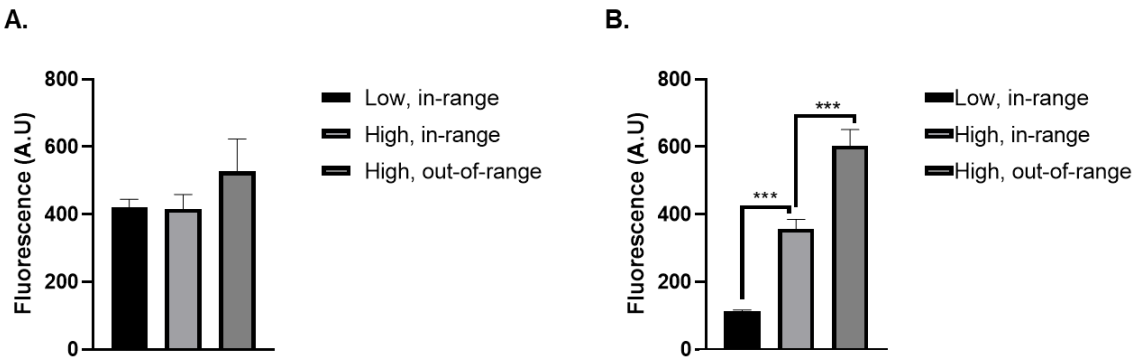

Figure 68: Validation of urea biosensor with human serum samples. A. Urea detection with samples that have 10% serum of the total volume. B. Urea detection with samples that have 5% serum of the total volume.After cells reached the optimal optical density for induction, respective serum samples were added to cells. The fluorescence response signals of the samples were measured with a microplate reader 8 hours after induction at 485 nm excitation and 538 nm emission. Experiments were conducted with three replicates and the normalized data was analyzed with one-way ANOVA ($p \leq 0.05$, $p \leq 0.01$, $p \leq 0.001$ and $p \leq 0.0001$ were shown as “*”, “**”, “***” and “****” respectively).

The higher dilution factors resulted in conditions to show a coherent response to varying urea levels. For the 10% serum samples there was no statistical significance. However, a gradually increasing significant response for 5% serum samples was observed with varying urea levels.

For uric acid screening with clinical specimens, uric acid biosensor pET-22b(+) synpHucO v2 sfGFP proD HucR-pZS mproD UACT was grown as described in Materials and Methods. Testing conditions were arranged to be 1% and 0.5% serum sample in total in induction medium(Table ..).. Uric Acid levels in the samples were determined previously by conventional laboratory tests (Table ..).

Uric Acid Level	Assesed Uric Acid Level in Sample	Uric Acid Level in 1% Serum	Uric Acid Level in 0.5% Serum
Low, in-range	398 µM	3,98 µM	1,99 µM
Mid-High, out-of-range	578 µM	5,78 µM	2,89 µM
High, out-of-range	859 µM	8,59 µM	4,295 µM

Table 3: The table showing respective uric concentrations of tested clinical samples. Uric acid concentrations were determined with conventional laboratory tests previously. Then uric acid concentrations in the test conditions were calculated by the dilution factor.

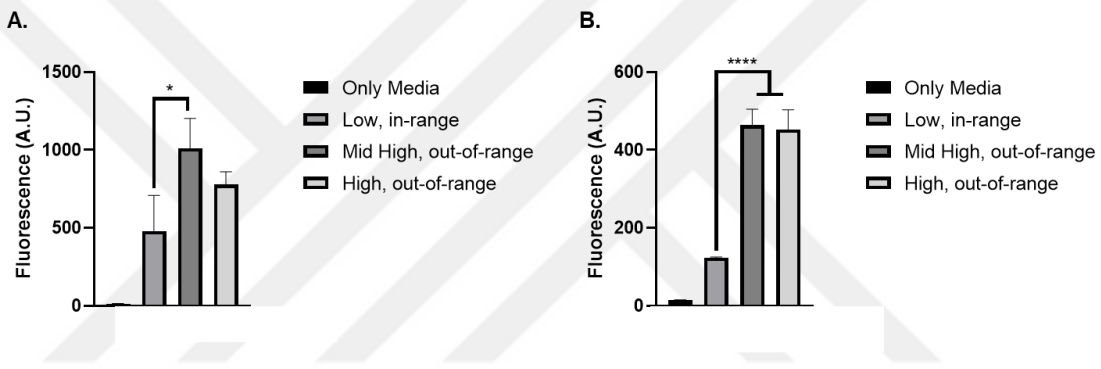

Figure 69: Validation of uric acid biosensor with human serum samples. A. Uric acid detection with samples that have 1% serum of the total volume. B. Uric acid detection with samples that have 0.5% serum of the total volume.After cells reached the optimal optical density for induction, respective serum samples were added to cells. The fluorescence response signals of the samples were measured with a microplate reader 8 hours after induction at 485 nm excitation and 538 nm emission. Experiments were conducted with three replicates and the normalized data was analyzed with one-way ANOVA. Statistical significance was shown only for samples that were tested with clinical specimens. ($p \leq 0.05$, $p \leq 0.01$, $p \leq 0.001$ and $p \leq 0.0001$ were shown as "*", "**", "***" and "****" respectively).

While the biosensors tested with 1% serum samples of total volume did not show a coherent response, the tested 0.5 % serum condition showed a

coherent response to varying uric acid levels signifying the digital response of the circuit.

CHAPTER 4

Conclusion

Overall, with the goal of reliable, inexpensive and fast-screening biodevice development; cellular biosensors for pathological biomarkers were developed and optimized. For urea biosensor, transcriptional activator UreR and its native promoter was used in a gene circuit suitable for the detection of urea with fluorescent response. The most impactful manipulations on the urea gene circuit have expectedly shown the importance of binding dynamics between the transcription factor to its promoter and the inducer as well as the effect of the number of operating units inside the cell on the response curve. An unexpected outcome was observed with the post-transcriptional modification, removal of the RNA leader sequence before the ribosome binding site, which signifies the substantial role of post-transcriptional dynamics on gene expression. Uric acid responsive biosensors signal optimizations were more straightforward than the urea biosensor since the system was based on a transcriptional repressor. Since the transcriptional repressor prevents transcription by steric hindrance, promoter modifications on the -35 -10 regions did not affect the binding the dynamics between the operator and the TF. Even though, there is still need for standardized biological parts for the development of modular cell-based biosensors responsive to vast number of analytes, the cell based biosensors for clinically relevant biosensors is a considerable progress for the synthetic biology inspired biodevice actuation in real-life applications. Furthermore, multi-input versions of the biosensors for simultenaous detection were developed and optimized. The multi-input biosensing modules are considered valuable since they can be integrated into

medical algorhythms to be used in the detection of more complex and heteregenous diseases. The framework for immobilization of biosensors on low-cost portable paper discs tested here presents a biocompatible production methods for living biodevices. However, the stability of the biofilm-paper interactions and the cell functionality have to be further tested for validation. The entrapment method for the bacterial biosensors proposed here also holds a great promise for remote detection of the pathological biomarkers. However, this method should be optimized with reagents that have higher purity for replicable results. Finally, the robustness of the urea and uric acid biosensors was validated with human clinical samples. With the correct concentration adjustments, a coherent and significant response was observed with clinical samples that have out of range levels of urea and uric acid. Further optimizations on survival of bacterial cells can improve the response functions of biosensors.

APPENDIX A

DNA sequences used in this study

Table A. 1: Sequences of genetic parts used in this study

Name	Type	Sequence 5'-to-3'
proD	Promoter	CACAGCTAACACCACGTCGTCCCTATCTG CTGCCCTAGGTCTATGAGTGGTTGCTGGA TAACTTTACGGGCATGCATAAGGCTCGTAT AATATATTCAGGGAGACCACAACGGTTTC CCTCTACAAATAATTTTGTTTAACTTT
mproD	Promoter	TCTAGATTTACAGCTAGCTCAGTCCTAGGT ATAATGCTAGCTACTAGAG
min-pHucO	Promoter	AAGACACGACCCGGTGCCGCCGCCAGAT ACTTAGATGTCT
pL-HucO	Promoter	TTGACATAGGTAGACATCTAAGTAGATACT
pUreR	Promoter	CTCGAGAAAAAATAACAATGGTAAAAAGAA AAAATGAAAAAGATCTACAGATATCGATAT TGTTATTGCTCAGCAACAAGATTATATTCT GAGCCAGAAAGAGGAGAAAATGTACAGGT ACC
Intergenic Region pUreD direction	Promoter	TGTCTTAGATATACCACAGGCAAGTTCAAA ATGAACATGGGTTAAAATAAACAAAGCTTA AAGTTAACCACTTAATTTGTGAACTTATAA GCAGTAAGCATGGGTTTTATTATCACAATA TTCCTATTGCGAAACCGCGTCGTTATACC GAATAGTATAAGAGTGGCTCAGAATATAAT CTTGTTGCTGAGCAATAACAATATCGATAT CTGTTCATTTTTTACTTTTATTTTTACCATT GTTATTTTTTCTAAACAAATTGCTGTTTATT TAAAACGCATTTTTTGAAACTCGGTGTAAA ATCGCGCGGCATTGATGGAGCGCTTTATC CTGTTTGAGGAAAATGCAATTTATCTTTATT CACACCCTACCCAACATTCATTTCATTATT TTCTCGGTGATTTTGAATGACATAATCTGA TGGGTAGTGCGGTATATATTCGTCTATTTC CTGATTTATTTGATCAATTTTGCCAAGTTG GCAGGAGTGGGT
IR pUreD (-80 +180)	Promoter	TACTTTTATTTTTACCATTGTTATTTTTTCTA AACAAATTGCTGTTTATTTAAAACGCATTTT TTGAAACTCGGTGTAAAATCGCGCGGCAT TGATGGAGCGCTTTATCCTGTTTGAGGAA AATGCAATTTATCTTTATTCACACCCTACC CAACATTCATTTCATTATTTTCTCGGTGATT

		TTGAATGACATAATCTGATGGGTAGTGCG GTATATATTCGTCTATTTCCTGATTTATTTG ATCAATTTTGCCAAGTTGGCAGGAGTGGG T
IR pUreD (-80 +80)	Promoter	TACTTTTATTTTTACCATTGTTATTTTTTCTA AACAAATTGCTGTTTATTTAAAACGCATTTT TTGAAACTCGGTGTAAAATCGCGCGGCAT TGATGGAGCGCTTTATCCTGTTTGAGGAA AATGCAATTTATCTTTATTCACACCCTACC CAACATTCATTTCATTA
rrnB T1	Terminator	GCATCAAATAAAACGAAAGGCTCAGTCGA AAGACTGGGCCTTTCGTTTTATCTGTTGTT TGTCGGTGAACGCTCTCCTGAGTAGGACA AATCCGCCGCCCTAGA
T7 Terminator	Terminator	CTAGCATAACCCCTTGGGGCCTCTAAACG GGTCTTGAGGGGTTTTTTG
UreR	Transcription Factor	ATGGAATATAAACATATTCTGAGCTCTAAC CAGATCAGCCTGAAAACCTTCTACATCGAA AACCCGATGATCGCAATGGTTTACGGCGC TAAAGGTGAAATTTGCATCAACGGCCAGA CCATTACGGTCACCACGAATCTGACCCTG ATTATCCCGAAATACAGTCAAGTCTCCTGT GATGTGACCAACTTTTTCCCGACGAAACC GATCGAACTGCACACCCTGGTGCTGAGCG AAACGGAACTGCAGTCAGTTTTCTCGCTG CTGAAACCGCTGATTAAAAGCGGTGCACC GATCACCCGTCATCTGCCGGATTATCACC TGTCTACCCCGGAAGTGGTTAAAACCAAC TTTACGCTGCTGCAGCAATGCCTGCCGCT GGAACATGGCACCCCGTCACAGGAAACG CTGTTCATGCAGCAATCGCTGTTTTTCATT CTGCTGGCGGTTTATCACGAAGGTGTCGA TATTCTGAACATCTTTCGTTTCAATTACGA CGAACCGAAAAATCAGGCGATTACCCATC TGATCACGCAGGATCCGCAACGCAAATGG CACCTGGAAGACGTGGCCAAAACCCTGTA TACCACGCCGAGTACGCTGCGTCGCCATC TGAGTAAAGAAGGCGTCTCCTTTTGTCAG CTGCTGCTGGATGTGCGCATGGGTATTGC GCTGAACTATCTGACCTTTAGCAATTACTC TGTTTTCCAAATCAGTCACCGTTGCGGCTT TGGTTCCAATGCGTATTTTTGTGACGCCTT CAAACGCAAATACGGCATGACCCCGAGCC AGTTCCGTACGCAGTCTCGCCAAGCAAAC GATCCGAATGCGATTGCCACCATGGCTTC ACAAAATGACGAATCGATTAAGAAAGTGTT TTAA
UreR (K169A)	Engineered Transcription Factor	ATGGAATATAAACATATTCTGAGCTCTAAC CAGATCAGCCTGAAAACCTTCTACATCGAA AACCCGATGATCGCAATGGTTTACGGCGC

		TAAAGGTGAAATTTGCATCAACGGCCAGA CCATTACGGTCACCACGAATCTGACCCTG ATTATCCCGAAATACAGTCAAGTCTCCTGT GATGTGACCAACTTTTTCCCGACGAAACC GATCGAACTGCACACCCTGGTGCTGAGCG AAACGGAACTGCAGTCAGTTTTCTCGCTG CTGAAACCGCTGATTAAAAGCGGTGCACC GATCACCCGTCATCTGCCGGATTATCACC TGTCTACCCCGGAAGTGGTTAAAACCAAC TTTACGCTGCTGCAGCAATGCCTGCCGCT GGAACATGGCACCCCGTCACAGGAAACG CTGTTCATGCAGCAATCGCTGTTTTTCATT CTGCTGGCGGTTTATCACGAAGGTGTCGA TATTCTGAACATCTTTCGTTTCAATTACGA CGAACCGGCGAATCAGGCGATTACCCATC TGATCACGCAGGATCCGCAACGCAAATGG CACCTGGAAGACGTGGCCAAAACCCTGTA TACCACGCCGAGTACGCTGCGTCGCCATC TGAGTAAAGAAGGCGTCTCCTTTTGTCAG CTGCTGCTGGATGTGCGCATGGGTATTGC GCTGAACTATCTGACCTTTAGCAATTACTC TGTTTTCCAAATCAGTCACCGTTGCGGCTT TGGTTCCAATGCGTATTTTTGTGACGCCTT CAAACGCAAATACGGCATGACCCCGAGCC AGTTCCGTACGCAGTCTCGCCAAGCAAAC GATCCGAATGCGATTGCCACCATGGCTTC ACAAAATGACGAATCGATTAAGAAAGTGTT TTAA
UreR (K15A-K169A)	Engineered Transcription Factor	ATGGAATATAAACATATTCTGAGCTCTAAC CAGATCAGCCTGGCGACCTTCTACATCGA AAACCCGATGATCGCAATGGTTTACGGCG CTAAAGGTGAAATTTGCATCAACGGCCAG ACCATTACGGTCACCACGAATCTGACCCT GATTATCCCGAAATACAGTCAAGTCTCCTG TGATGTGACCAACTTTTTCCCGACGAAACC GATCGAACTGCACACCCTGGTGCTGAGCG AAACGGAACTGCAGTCAGTTTTCTCGCTG CTGAAACCGCTGATTAAAAGCGGTGCACC GATCACCCGTCATCTGCCGGATTATCACC TGTCTACCCCGGAAGTGGTTAAAACCAAC TTTACGCTGCTGCAGCAATGCCTGCCGCT GGAACATGGCACCCCGTCACAGGAAACG CTGTTCATGCAGCAATCGCTGTTTTTCATT CTGCTGGCGGTTTATCACGAAGGTGTCGA TATTCTGAACATCTTTCGTTTCAATTACGA CGAACCGGCGAATCAGGCGATTACCCATC TGATCACGCAGGATCCGCAACGCAAATGG CACCTGGAAGACGTGGCCAAAACCCTGTA TACCACGCCGAGTACGCTGCGTCGCCATC TGAGTAAAGAAGGCGTCTCCTTTTGTCAG

		CTGCTGCTGGATGTGCGCATGGGTATTGC GCTGAACTATCTGACCTTTAGCAATTACTC TGTTTTCCAAATCAGTCACCGTTGCGGCTT TGGTTCCAATGCGTATTTTTGTGACGCCTT CAAACGCAAATACGGCATGACCCCGAGCC AGTTCCGTACGCAGTCTCGCCAAGCAAAC GATCCGAATGCGATTGCCACCATGGCTTC ACAAAATGACGAATCGATTAAGAAAGTGTT TTAA
HucR	Transcription Factor	ATGTCAGCCCGCATGGACAACGACACGGC AGCCCTTCTGGAGCGGATTCGGAGCGACT GGGCGAGGCTCAATCACGGTCAGGGACC AGACTCGGACGGTCTGACCCCCAGCGCC GGGCCGATGCTGACCCTGCTGCTGCTCG AGCGGCTGCACGCGGCTCTGGGGCGTGA AATCGAGCGGACCTACGCCGCTTCGGGG CTGAACGCGGCGGGCTGGGACCTGCTGC TCACGCTTTACCGCTCGGCGCCGCCCGA GGGCCTGCGGCCCACCGAACTCAGCGCC CTGGCCGCCATTTCCGGGCCTTCGACGAG CAACCGGATCGTGCGGCTGCTCGAAAAG GGCCTGATCGAGCGCCGCGAGGACGAAC GTGACCGCCGCTCGGCGAGTATTCGCCT GACGCCGCAGGGCCGCGCCCTGGTCACG CACCTGCTGCCCGCACATCTGGCGACCAC GCAGCGGGTGCTTGCTCCGCTGTCGGCG CAGGAGCAGCGCACCCTGGAGGAGCTGG CGGGGCGAATGCTGGCGGGGCTGGAGCA GGGGGTATAA
UACT	Uric Acid Transporter	ATGAGCGCCATAGATTCCCAACTTCCCTC ATCTTCTGGGCAAGACCGCCCAACTGATG AGGTTGACCGCATATTATCACCAGGAAAG CTGATCATACTCGGTCTGCAACACGTCCTT GTCATGTACGCAGGTGCAGTCGCTGTTCC TCTTATGATTGGTGACCGACTGGGCCTCT CAAAAGAAGCTATTGCGATGCTCATTAGCT CGGATCTCTTTTGCTGCGGGATCGTCACA TTATTGCAATGTATCGGTATCGGCCGCTTT ATGGGGATCCGCCTGCCGGTGATTATGTC GGTGACCTTTGCTGCTGTAACACCAATGA TAGCCATTGGGATGAACCCGGATATCGGC CTGCTGGGGATATTTGGTGCCACTATCGC CGCGGGTTTTATCACCACATTATTAGCGC CACTTATCGGTCGCTTGATGCCTTTATTCC CGCCACTGGTTACCGGTGTGGTTATTACT TCTATCGGGCTTAGCATCATTCAGGTGGG TATTGACTGGGCCGCCGGAGGTAAAGGG AATCCGCAATATGGTAATCCCGTTTATTTA GGTATCTCCTTTGCCGTCTTAATTTTTATCT TGCTCATTACTCGCTATGCGAAAGGATTTA

		TGTCCAACGTCGCCGTATTACTGGGGATT GTATTTGGCTTTTTACTTTCGTGGATGATG AATGAAGTCAATTTATCCGGGCTACATGAT GCTTCATGGTTTGCGATTGTTACGCCGAT GTCGTTTGGTATGCCGATTTTCGATCCCGT TTCCATTCTGACCATGACTGCCGTGTTAAT CATCGTGTTTATCGAGTCAATGGGGATGTT CCTGGCACTGGGTGAAATAGTCGGTCGTA AACTCTCTTCGCACGATATTATTCGCGGG CTGCGTGTCGATGGCGTAGGGACAATGAT AGGCGGCACGTTTAACAGCTTCCCCCACA CGTCATTTTCTCAAAACGTTGGCCTGGTTA GCGTGACGCGCGTTCATAGCCGCTGGGT GTGTATTTCTTCGGGAATTATATTAATCCT GTTTGGCATGGTGCCAAAAATGGCGGTGC TGGTAGCCTCCATTCCGCAATTTGTGCTG GGCGGCGCTGGTCTAGTGATGTTCGGCAT GGTACTGGCGACAGGGATTCGAATTCTGT CGCGCTGTAACTACACCACCAACCGTTAC AACCTCTATATTGTGGCGATCAGTCTCGG CGTTGGCATGACTCCGACGCTCTCTCACG ATTTCTTTTCTAAGTTACCGGCCGTACTGC AACCGCTGCTACATAGCGGCATTATGCTC GCAACCCTTAGCGCCGTTGTGCTGAACGT CTTCTTTAATGGCTATCAGCATCATGCTGA CCTGGTGAAGGAATCCGTCTCTGATAAAG ATTTAAAAGTCAGGACAGTACGTATGTGG CTTCTGATGCGCAAGCTGAAGAAAAATGA GCATGGAGAATAA
sfGFP	Protein	ATGCGTAAAGGCGAAGAGCTGTTCACTGG TGTCGTCCCTATTCTGGTGGAACTGGATG GTGATGTCAACGGTCATAAGTTTTCCGTG CGTGGCGAGGGTGAAGGTGACGCAACTA ATGGTAAACTGACGCTGAAGTTCATCTGTA CTACTGGTAAACTGCCGGTACCTTGGCCG ACTCTGGTAACGACGCTGACTTATGGTGT TCAGTGCTTTGCTCGTTATCCGGACCATAT GAAGCAGCATGACTTCTTCAAGTCCGCCA TGCCGGAAGGCTATGTGCAGGAACGCAC GATTTCCTTTAAGGATGACGGCACGTACA AAACGCGTGCGGAAGTGAAATTTGAAGGC GATACCCTGGTAAACCGCATTGAGCTGAA AGGCATTGACTTTAAAGAAGACGGCAATAT CCTGGGCCATAAGCTGGAATACAATTTTAA CAGCCACAATGTTTACATCACCGCCGATA AACAAAAAAATGGCATTAAAGCGAATTTTA AAATTCGCCACAACGTGGAGGATGGCAGC GTGCAGCTGGCTGATCACTACCAGCAAAA CACTCCAATCGGTGATGGTCCTGTTCTGC TGCCAGACAATCACTATCTGAGCACGCAA

		AGCGTTCTGTCTAAAGATCCGAACGAGAA ACGCGATCATATGGTTCTGCTGGAGTTCG TAACCGCAGCGGGCATCACGCATGGTATG GATGAACTGTACAAA
mScarlet I	Protein	ATGAGTAAAGGAGAAGCTGTGATTAAAGA GTTCATGCGCTTCAAAGTTCACATGGAGG GTTCTATGAACGGTCACGAGTTCGAGATC GAAGGCGAAGGCGAGGGCCGTCCGTATG AAGGCACCCAGACCGCCAAACTGAAAGTG ACTAAAGGCGGCCCGCTGCCTTTTTCCTG GGACATCCTGAGCCCGCAATTTATGTACG GTTCTAGGGCGTTCATCAAACACCCAGCG GATATCCCGGACTATTATAAGCAGTCTTTT CCGGAAGGTTTCAAGTGGGAACGCGTAAT GAATTTTGAAGATGGTGGTGCCGTGACCG TCACTCAGGACACCTCCCTGGAGGATGGC ACCCTGATCTATAAAGTTAAACTGCGTGGT ACTAATTTTCCACCTGATGGCCCGGTGAT GCAGAAAAAGACGATGGGTTGGGAGGCG TCTACCGAACGCTTGTATCCGGAAGATGG TGTGCTGAAAGGCGACATTAAAATGGCCC TGCGCCTGAAAGATGGCGGCCGCTATCTG GCTGACTTCAAAACCACGTACAAAGCCAA GAAACCTGTGCAGATGCCTGGCGCGTACA ATGTGGACCGCAAACTGGACATCACCTCT CATAATGAAGATTATACGGTGGTAGAGCA ATATGAGCGCTCCGAGGGTCGTCATTCTA CCGGTGGCATGGATGAACTATACAAATAA
IR pUreD double-HucO	Promoter	TGTCTTAGATATACCACAGGCAAGTTCAAA ATGAACATGGGTTAAAATAAACAAAGCTTA AAGTTAACCACTTAATTTGTGAACTTATAA GCAGTAAGCATGGGTTTTATTATCACAATA TTCCTATTGCGAAACCGCGTCGTTATACC GAATAGTATAAGAGTGGCTCAGAATATAAT CTTGTTGCTGAGCAATAACAATATCGATAT CTGTTCATTTTTTACTTTTATTTTTACCATT GTTATTTTTTCTAAACAAATTGCTGTTTATT TAAAACGCATTTTTTGAAACTCGGTGTAAA ATCGCGCGGCATTGATGGAGCGCTTTATC CTGTTTGAGGAAAATGCAATTTATCTTTATT CACACCCTACCCAACATTCATTTCATTATT TTCTCGGTGATTTTGAATGACATAATCTGA TGGGTAGTGCGGTATATATTCGTCTATTTC CTGATTTATTTGATCAATTTTGCCAAGTTG GCAGGAGTGGGTTAGGTAGACATCTAAGT ACTGGACTAGGTAGACATCTAAGTA
IR pUreD mid-HucO	Promoter	TGTCTTAGATATACCACAGGCAAGTTCAAA ATGAACATGGGTTAAAATAAACAAAGCTTA AAGTTAACCACTTAATTTGTGAACTTATAA GCAGTAAGCATGGGTTTTATTATCACAATA

		TTCCTATTGCGAAACCGCGTCGTTATACC GAATAGTATAAGAGTGGCTCAGAATATAAT CTTGTTGCTGAGCAATAACAATATCGATAT CTGTTCATTTTTTACTTTTATTTTTACCATT GTTATTTTTTCTAAACAAATTGCTGTTTATT TAAAACGCTAGGTAGACATCTAAGTATAAA ATCGCGCGGCATTGATGGAGCGCTTTATC CTGTTTGAGGAAAATGCAATTTATCTTTATT CACACCCTACCCAACATTCATTTCATTATT TTCTCGGTGATTTTGAATGACATAATCTGA TGGGTAGTGCGGTATATATTCGTCTATTTC CTGATTTATTTGATCAATTTTGCCAAGTTG GCAGGAGTGGGT
IR -86+80 pUreD-HucO	Promoter	TACTTTTATTTTTACCATTGTTATTTTTTCTA AACAAATTGCTGTTTATTTAAAACGCATTTT TTGAAACTCGGTGTAAAATCGCGCGGCAT TGATGGAGCGCTTTATCCTGTTTGAGGAA AATGCAATTTATCTTTATTCACACCCTACC CAACATTCATTTCATTATAGGTAGACATCT AAGTA
IR -86 +80 pUreD mid-HucO	Promoter	TACTTTTATTTTTACCATTGTTATTTTTTCTA AACAAATTGCTGTTTATTTAAAACGCTAGG TAGACATCTAAGTATAAAATCGCGCGGCAT TGATGGAGCGCTTTATCCTGTTTGAGGAA AATGCAATTTATCTTTATTCACACCCTACC CAACATTCATTTCATTA
IR -86 +180 pUreD mid-HucO	Promoter	TACTTTTATTTTTACCATTGTTATTTTTTCTA AACAAATTGCTGTTTATTTAAAACGCTAGG TAGACATCTAAGTATAAAATCGCGCGGCAT TGATGGAGCGCTTTATCCTGTTTGAGGAA AATGCAATTTATCTTTATTCACACCCTACC CAACATTCATTTCATTATTTTCTCGGTGATT TTGAATGACATAATCTGATGGGTAGTGCG GTATATATTCGTCTATTTCCTGATTTATTTG ATCAATTTTGCCAAGTTGGCAGGAGTGGG T
RiboJ	Ribozyme	AGCTGTCACCGGATGTGCTTTCCGGTCTG ATGAGTCCGTGAGGACGAAACAGCCTCTA CAAATAATTTTGTTTAA
CBDcex	Cellulose Binding Domain	GGTCCGGCCGGGTGCCAGGTGCTGTGGG GCGTCAACCAGTGGAACACCGGCTTCACC GCGAACGTCACCGTGAAGAACACGTCCTC CGCTCCGGTAGACGGCTGGACGCTCACG TTCAGCTTCCCGTCCGGCCAGCAGGTCAC CCAGGCGTGGAGCTCGACGGTCACGCAG TCCGGCTCGGCCGTGACGGTCCGCAACG CCCCGTGGAACGGCTCGATCCCGGCGGG CGGCACCGCGCAGTTCGGCTTCAACGGC TCGCACACGGGCACCAACGCCGCGCCGA

		CGGCGTTCTCGCTCAACGGCACGCCCTG CACGGTCGGC
		ATGAAACTTTTAAAAGTAGCAGCAATTGCA GCAATCGTATTCTCCGGTAGCGCTCTGGC AGGTGTTGTTCCTCAGTACGGCGGCGGC GGTAACCACGGTGGTGGCGGTAATAATAG CGGCCCAAATTCTGAGCTGAACATTTACC AGTACGGTGGCGGTAACTCTGCACTTGCT CTGCAAACTGATGCCCGTAACTCTGACTT GACTATTACCCAGCATGGCGGCGGTAATG GTGCAGATGTTGGTCAGGGCTCAGATGAC AGCTCAATCGATCTGACCCAACGTGGCTT CGGTAACAGCGCTACTCTTGATCAGTGGA ACGGCAAAAATTCTGAAATGACGGTTAAAC AGTTCGGTGGTGGCAACGGTGCTGCAGTT GACCAGACTGCATCTAACTCCTCCGTCAA CGTGACTCAGGTTGGCTTTGGTAACAACG CGACCGCTCATCAGTAC
csgA	Protein	ATGAAACTTTTAAAAGTAGCAGCAATTGCA GCAATCGTATTCTCCGGTAGCGCTCTGGC AGGTGTTGTTCCTCAGTACGGCGGCGGC GGTGGCAACCACGGTGGTGGCGGTAATA ACAGCGGTCCGAATTCAGAGCTGAATATT TACCAGTACGGTGGCGGTAACTCTGCTCT TGCTCTGCAAGCTGACGCCCGTAACTCTG ATCTGACCATTACCCAGCACGGCGGCGGT AATGGCGCAGATGTGGGCCAAGGTTCTGA TGACAGCTCAATCGATCTGACTCAGCGTG GTTTCGGCAACAGCGCTACTCTTGATCAG TGGAATGGTAAAGATTCTACTATGACTGTT AAACAGTTCGGTGGCGGTAACGGTGCTGC TGTTGACCAGACTGCATCTAACTCCAGCG TTAACGTCACTCAGGTTGGCTTTGGTAACA ACGCGACCGCTCATCAGTAC
pBR 322	Origin of Replication	AGATCAAAGGATCTTCTTGAGATCCTTTTT TTCTGCGCGTAATCTGCTGCTTGCAAACAA AAAAACCACCGCTACCAGCGGTGGTTTGT TTGCCGGATCAAGAGCTACCAACTCTTTTT CCGAAGGTAACTGGCTTCAGCAGAGCGCA GATACCAAATACTGTCCTTCTAGTGTAGCC GTAGTTAGGCCACCACTTCAAGAACTCTG TAGCACCGCCTACATACCTCGCTCTGCTA ATCCTGTTACCAGTGGCTGCTGCCAGTGG CGATAAGTCGTGTCTTACCGGGTTGGACT CAAGACGATAGTTACCGGATAAGGCGCAG CGGTCGGGCTGAACGGGGGGTTCGTGCA CACAGCCCAGCTTGGAGCGAACGACCTAC ACCGAACTGAGATACCTACAGCGTGAGCA TTGAGAAAGCGCCACGCTTCCCGAAGGGA GAAAGGCGGACAGGTATCCGGTAAGCGG

		CAGGGTCGGAACAGGAGAGCGCACGAGG GAGCTTCCAGGGGGAAACGCCTGGTATCT TTATAGTCCTGTCGGGTTTCGCCACCTCT GACTTGAGCGTCGATTTTTGTGATGCTCGT CAGGGGGGCGGAGCCTATGGAAAAACGC CAGCAACGCG
p15A	Origin of Replication	GGATATATTCCGCTTCCTCGCTCACTGACT CGCTACGCTCGGTCGTTCGACTGCGGCG AGCGGAAATGGCTTACGAACGGGGCGGA GATTTCCTGGAAGATGCCAGGAAGATACT TAACAGGGAAGTGAGAGGGCCGCGGCAA AGCCGTTTTTCCATAGGCTCCGCCCCCCT GACAAGCATCACGAAATCTGACGCTCAAA TCAGTGGTGGCGAAACCCGACAGGACTAT AAAGATACCAGGCGTTTCCCCCTGGCGGC TCCCTCGTGCGCTCTCCTGTTCCTGCCTTT CGGTTTACCGGTGTCATTCCGCTGTTATG GCCGCGTTTGTCTCATTCCACGCCTGACA CTCAGTTCCGGGTAGGCAGTTCGCTCCAA GCTGGACTGTATGCACGAACCCCCCGTTC AGTCCGACCGCTGCGCCTTATCCGGTAAC TATCGTCTTGAGTCCAACCCGGAAAGACA TGCAAAAGCACCACTGGCAGCAGCCACTG GTAATTGATTTAGAGGAGTTAGTCTTGAAG TCATGCGCCGGTTAAGGCTAAACTGAAAG GACAAGTTTTGGTGACTGCGCTCCTCCAA GCCAGTTACCTCGGTTCAAAGAGTTGGTA GCTCAGAGAACCTTCGAAAAACCGCCCTG CAAGGCGGTTTTTTCGTTTTCAGAGCAAGA GATTACGCGCAGACCAAAACGATCTCAAG AAGATCATCTTATTAATCAGATAAAATATTT CTAGATTTCAGTGCAATTTATCTCTTCAAAT GTAGCACCTGAAGTCAGCCCCATACGATA TAAGTTGTTA

APPENDIX B

List of primers used in this study

Table B. 1: Primers used in PCR throughout the study.

Name	Sequence (5'-to-3')	Amplification Site
S1	CGATCGGGCCCTGAGGCCTGCAGGGATCCAAGCTTTTAAAACACTTTCTTAATCGATTCG	mproD-UreR
S2	GGTATAATGCTAGCTACTAGAGAAAGAGGAGAAAGGTACCATGGAATATAAACATATTCTGAGC	
S3	CAGCTGGCAATTCCGACGTCTCTAGATTTACAGCTAGCTCAGTCCTAGGTATAATGCTAGCTACTAGA	
S4	GGATATATTCCGCTTCCTCGCTC	pZS backbone vector
S5	CTAGGGCGGCGGATTTG	
S6	AACGTCTCATTTTCGCCAGATATCGACGTCCTCGAGAAAAAATAACAATGGTA	pUre promoter
S7	TTACGCATGGATCCCTCCTTGGTACCTGTACATTTTCTCC	
S8	AAGAGGAGAAAATGTACAGGTACCAAGGAGGGATCCATGCGTAAAGGC	sfGFP- rrnb T1 terminator
S9	TTCGTTTTATTTGATGCCACGCGTCTCGAGTCATTTGTACAGTTCATCCATACCATG	
S10	TGTCTGAGCCATTAACTTTAAGAAGGAGGGATCCATGCGTAA	syn pUre promoter (-35 -10 change)
S11	CAATCACAATATCGATATCTGTTCATTTTTTACTTTTATTTTTACCATTGTTATTTTTTCTCGAG	
S12	CTTAAAGTTAATGGCTCAGACAGTAATCTTGTTGCTGAGCAATCACAATATCGATATCTGTTCATTT	
S13	AACGTCTCATTTTCGCCAGATATCGACGTCCTCGAGACCCACTCCTGCCAACTT	Intergenic Region (pUreR direction)
S14	TGAACAGCTCTTCGCCTTTACGCATGGATCCCTCCTTCTTAAAGTTAATGTCTTAGATATACCACAGGCAAG	
S15	AACGTCTCATTTTCGCCAGATATCGACGTCCTCGAGTGTCTTAGATATACCACAGGCAAG	Intergenic Region (pUreD direction)
S16	ACCAGTGAACAGCTCTTCGCCTTTACGCATGGATCCCTCCTTCTTAAAGTTAAACCCACTCCTGCCAACTT	
S17	TTTTCGCCAGATATCGACGTCCTCGAGTACTTTTATTTTTACCATTGTTATTTTTTCTAAACAAA	IR(-86 +80, pUreD direction)
S18	TACGCATGGATCCCTCCTTCTTAAAGTTAATAATGAAATGAATGTTGGGTAGGG	

S19	ACGCGTCAGTGGGCTGATCATTAA	pET 22b(+) sfGFP proD HucR vector backbone
S20	TTAACTTTAAGAAGGAGATGGTACCATGCG	
S20	GGGCCCTGAGGCCTGCAGGGATCCAAGCTTCTCGAGTTATTCTCCATGCTCATTTTTCTTC	UACT
S21	GCTAGCTACTAGAGAAAGAGGAGAAAGGTACCATGAGCGCCATAGATTCC	
S22	TCTAGGGCGGCGGATTTG	pZA backbone vector
S23	TCCTGAGTAGGACAAATCCGCCGCCCTAGACCTAGGTAAAGCACTAAATCGGAA	pL-pHucO
S24	AAGTATATGTTGTGTGGAACCGATTTAATAAAACAATTTCACACAGTCTAGAAATAATTTTGTTTAACTT	
S25	TAGTACATTGTGATTTAAAAATGACTAAATAATTTTACATAGGTAGACATCTAAGTATATGTTGTGTGGA	
S26	TAATAGATAATCTTAATTCCTGTAAGGTAGTACATTGTGATTTAAAAATG	
S27	AGTCAGTGAGCGAGGAAGCGGAATATATCCTAATAGATAATCTTAATTCCTGTAA	
S28	ACATTTCCCCGAAAAGTGCCACCTGACGTCCACAGCTAACACCACGTC	proD
S29	AAAGTTAAACAAAATTATTTGTAGAGGG	
S30	TTCCCTCTACAAATAATTTTGTTTAACTTTAAGGAGGGATCCATGTCAGCCCGCATGGACA	HucR
S31	CCTTTCGTTTTATTTGATGCCACGCGTTCATTATACCCCCTGCTCCAGCC	
S32	ATCTCAGTGGTGGTGGTGGTGGTGCTCGAGCACAGCTAACACCACGTC	pL-pHucO sfGFP proD HucR
S33	GTTAATGATCAGCCCACTGACGCGTTTGACATAGGTAGACATCTAAGTAGATACTGTGTGGAACCGATTT	
S34	AGCATGGAGAATAACTCGAGGCATCAAATAAAACGAAAGGCTCAG	rrnb T1
S35	CAGGCCTCAGGGCCCGATCGATGCGGCCGCCACCACCACCACCACCAC	
S36	AAACTAGCAACACCAGAACAGCGCGGCCGCTCTAGATTTACAGCTAGCTCAG	mproD-UACT
S37	CCTTTCGTTTTATTTGATGCCTCGAGTTATTCTCCATGCTC	
S38	GCGGCCGCATCGATCGGGCCCTGAGGCCTGTCATTATACCCCCTGCTCCA	ProD-HucR
S39	TGAACGCTCTCCTGAGTAGGACAAATCCGCTTGAGTGAGCTGATACCGCT	pZE pUreD-sfGFP vector backbone
S40	GACGTCAGGTGGCACTTTTCGGGGAAATGTAGGCGGTAATACGGTTATCC	
S41	TTAACTTTAAGAAGGAGGGATCCATGCG	pZE proD-HucR sfGFP vector backbone
S42	CTCGAGGACGTCGATATCTGGCGAAAA	

S43	CGCATGGATCCCTCCTTCTTAAAGTTAATACTTAGATGTCTACCTATAATGAAATGAATGTTGGGTAGG	
S44	TGTCTACCTAGTCCAGTACTTAGATGTCTACCTAACCCACTCCTGCCAACTT	IR pUreD double-HucO
S45	TACGCATGGATCCCTCCTTCTTAAAGTTAATACTTAGATGTCTACCTAGTCCAGTACTTAGA	
S46	CGCGCGATTTTATACTTAGATGTCTACCTAGCGTTTTAAATAAACAGCAATTTG	IR pUreD mid-HucO
S47	TATTTAAAACGCTAGGTAGACATCTAAGTATAAAATCGCGCGGCATTGAT	
S48	CGCATGGATCCCTCCTTCTTAAAGTTAATACTTAGATGTCTACCTAACCCACTCCTGCCAACTT	
S49	CATTTGCGTTGCGGATCCTGCGTGATCAGATGGGTAATCGCCTGATTCGCCGGTTCGTCG	mproD-UreR (K169A)
S50	TATAAACATATTCTGAGCTCTAACCAGATCAGCCTGGCGACCTT	mproD-UreR (K15A-K169A)
S51	GTGAACAGCTCTTCGCCTTTACGCATGGATCCCTCCTTCTTAAAGTTAA	pZE pUreD-sfGFP vector backbone
S52	GACGTCGATATCTGGCGAAAATGAGACGTTGATCGGCACGTAAGAGGTTCC	
S53	TGTTTCGTCCTCACGGACTCATCAGACCGGAAAGCACATCCGGTGACAGCTACCCACTCCTGCCAACTT	pUreD-RiboJ
S54	GCATGGATCCCTCCTTCTTAAAGTTAATTAAACAAAATTATTTGTAGAGGCTGTTTCGTCCTCACGGAC	
S55	ACCTACTAGATTAAAGAGGAGAAAGGTACCATGAAACTTTTAAAAGTAGCAGCAATTGCAG	csgA-CBDcex
S56	GGTAGCCACCACCACCACCACCACGGATCCCCGACGTCCGGTCCGGCCGGGTGCCAG	
S57	TTCGTTTTATTTGATGCCACGCGTCTCGAGTTATTAGCCGACCGTGCAGGGCGT	

APPENDIX C

Plasmid maps used in this study

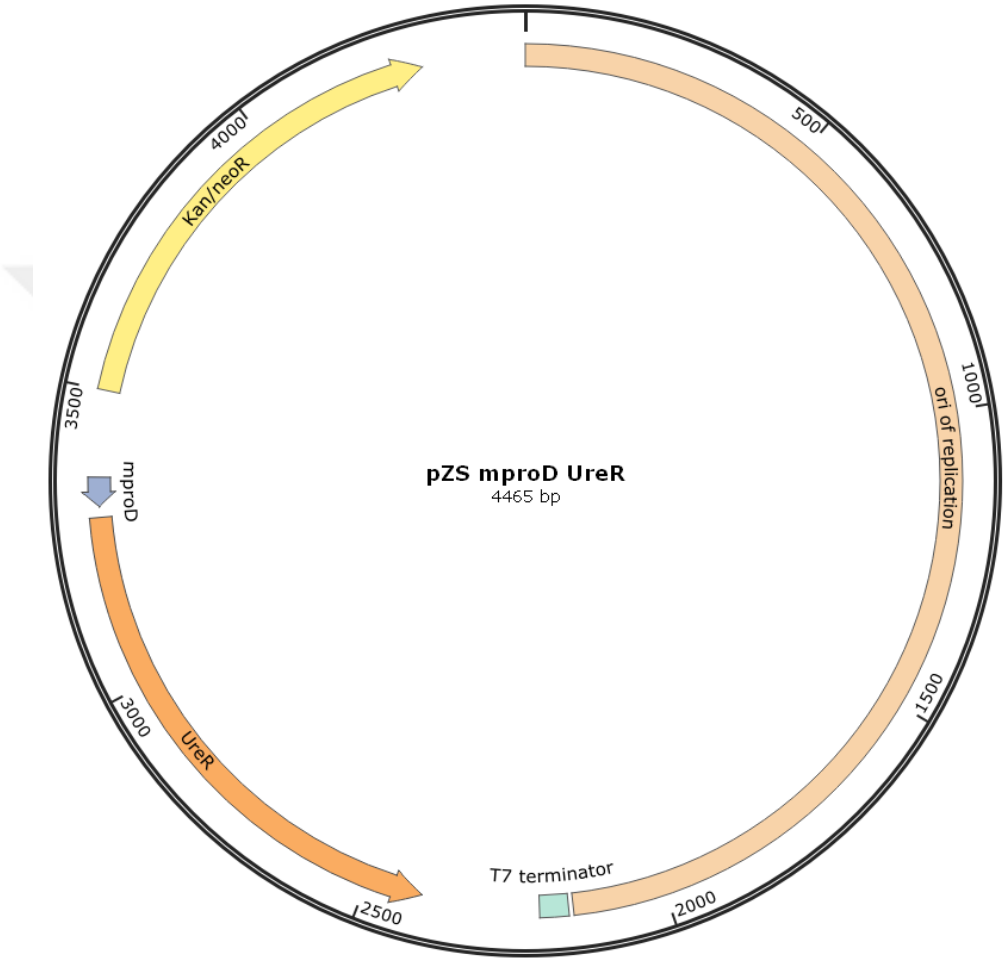

Figure C.1: Schematic representation of pZS mproD UreR vector.

Figure C. 2: Schematic representation of pZA pUreR sfGFP vector.

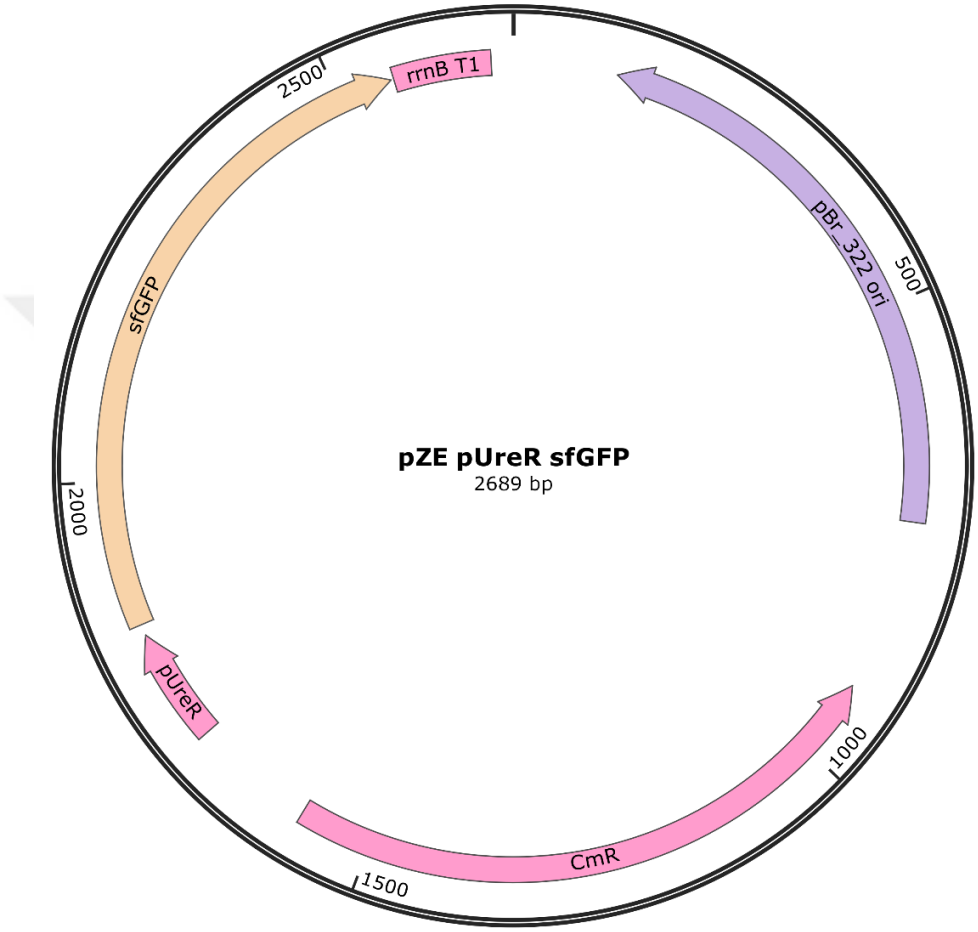

Figure C. 3: Schematic representation of pZE pUreR sfGFP vector.

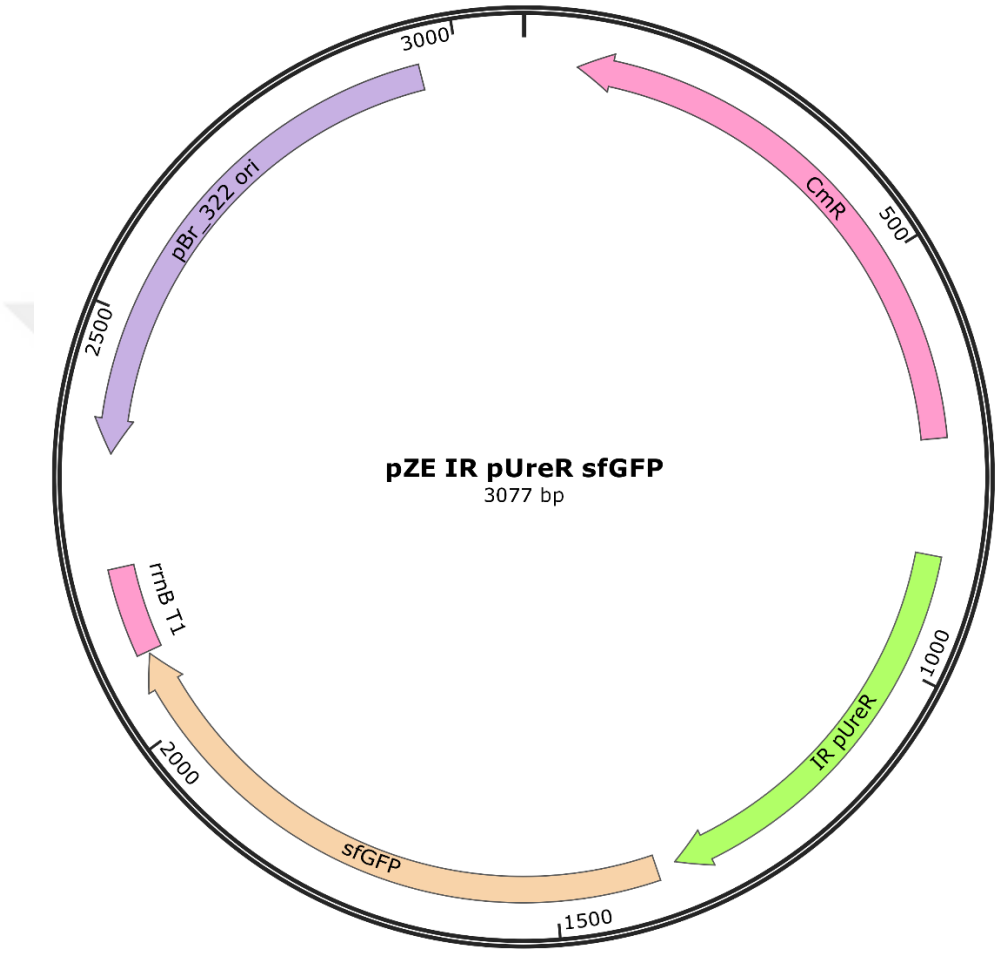

Figure C. 4: Schematic representation of pZE IR pUreR sfGFP vector.

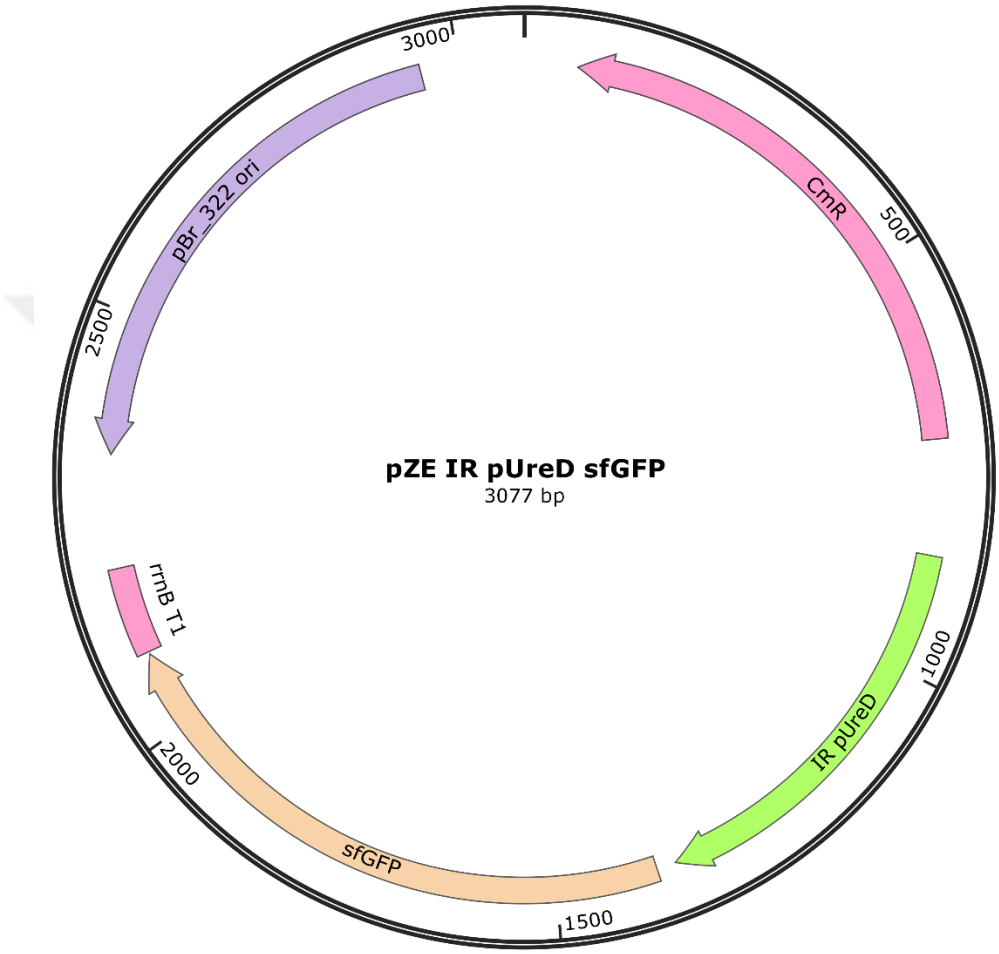

Figure C. 5: Schematic representation of pZE IR pUreD sfGFP vector.

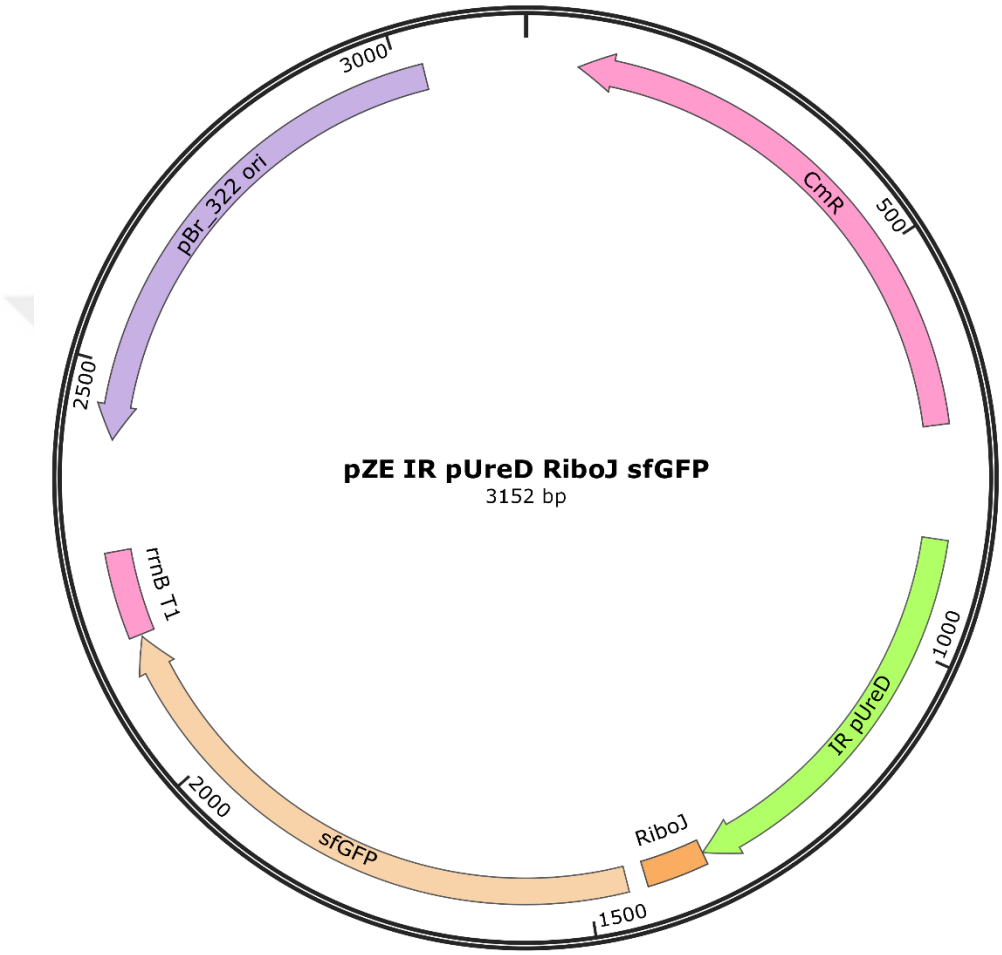

Figure C. 6: Schematic representation of pZE IR pUreD RiboJ sfGFP vector.

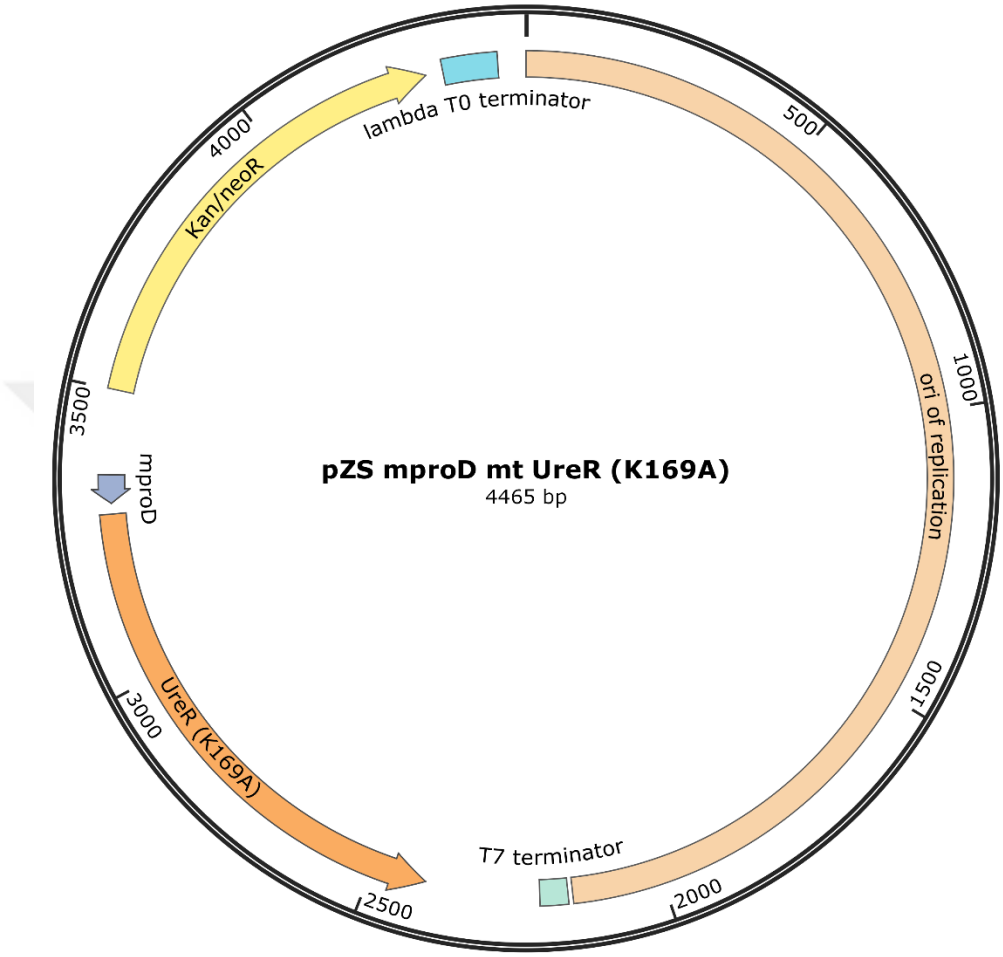

Figure C. 7: Schematic representation of pZS mproD mt UreR (K16A) vector.

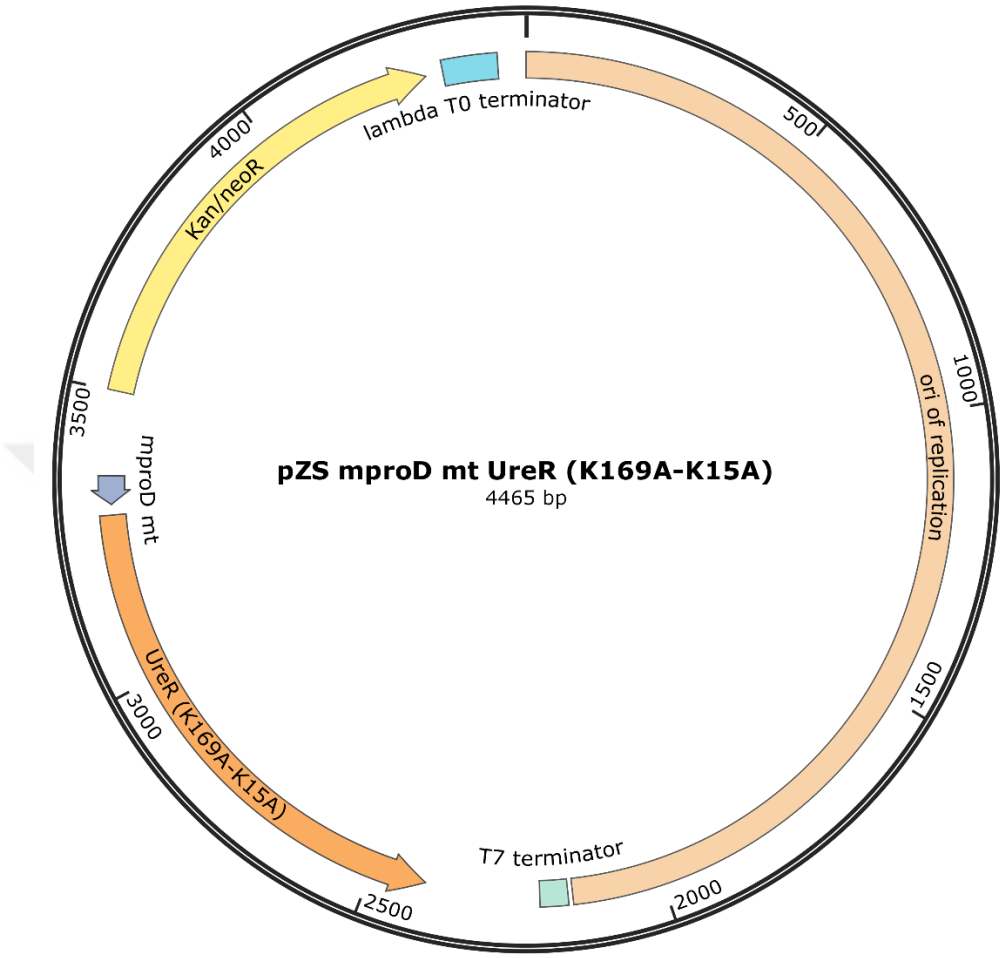

Figure C. 8: Schematic representation of pZS mproD mt UreR (K15A-K16A) vector.

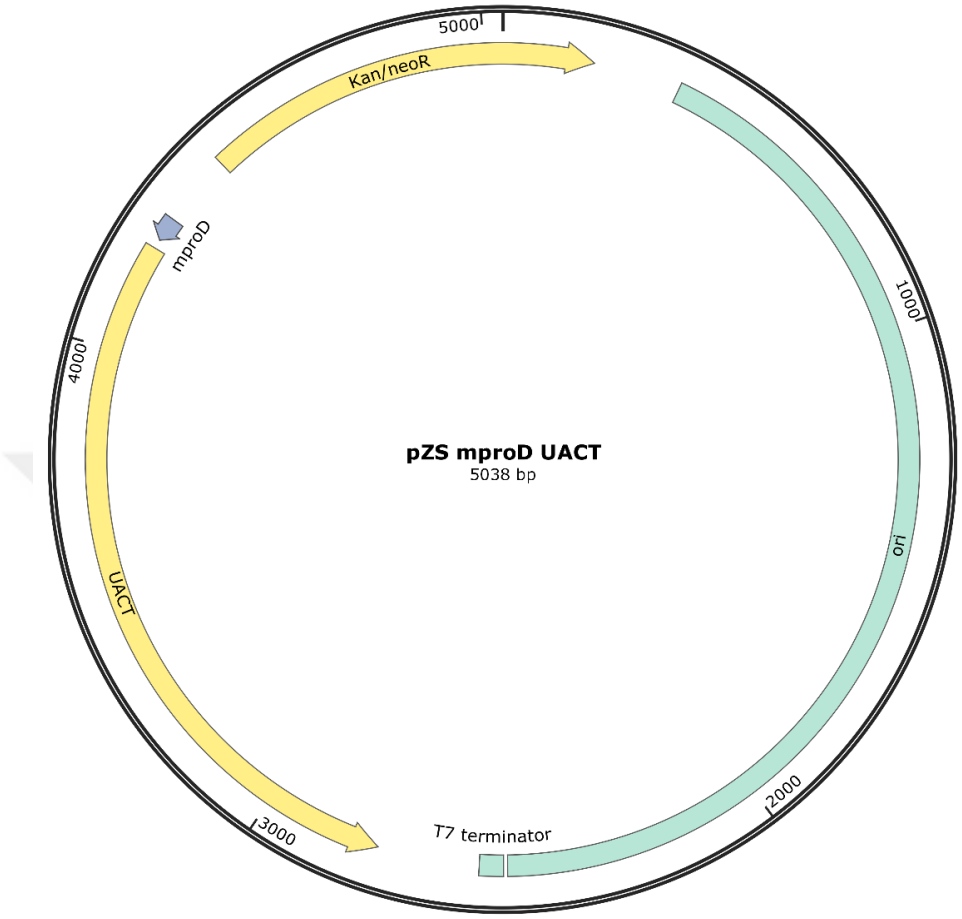

Figure C. 9: Schematic representation of pZS mproD UACT vector.

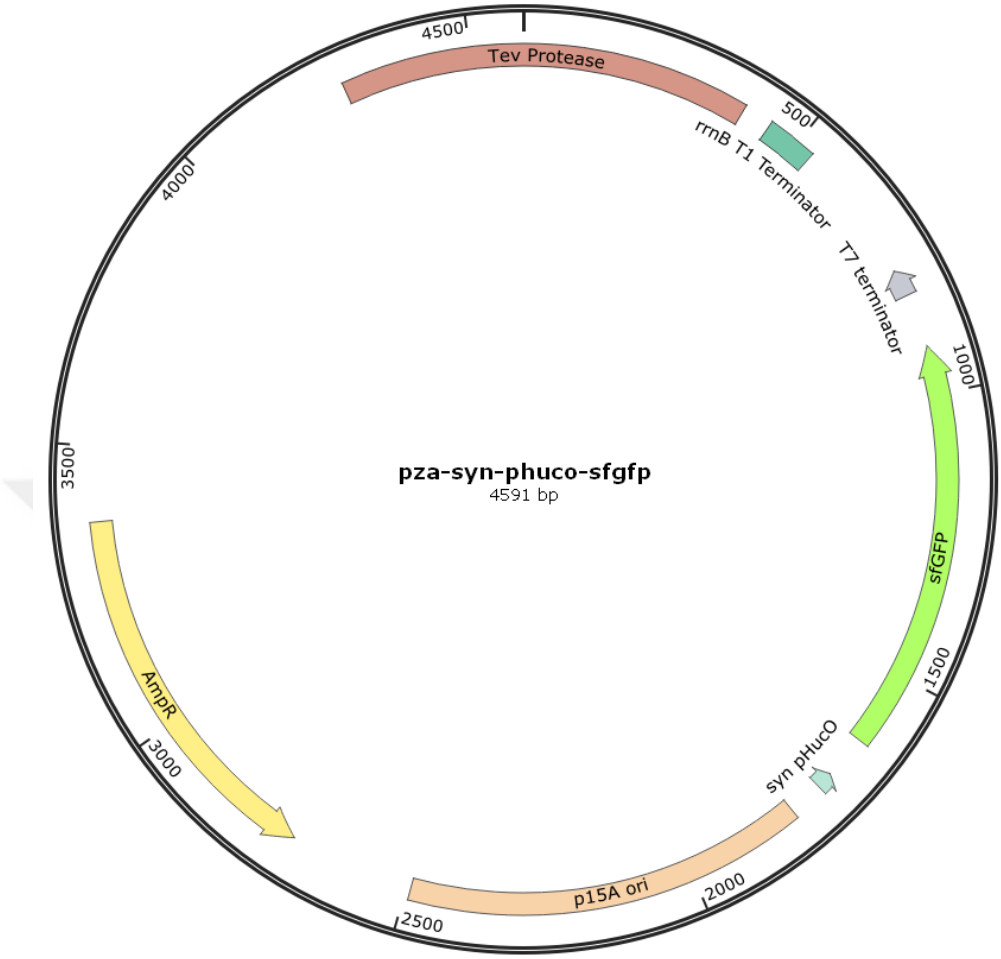

Figure C. 10: Schematic representation of pZA syn pHucO sfGFP vector.

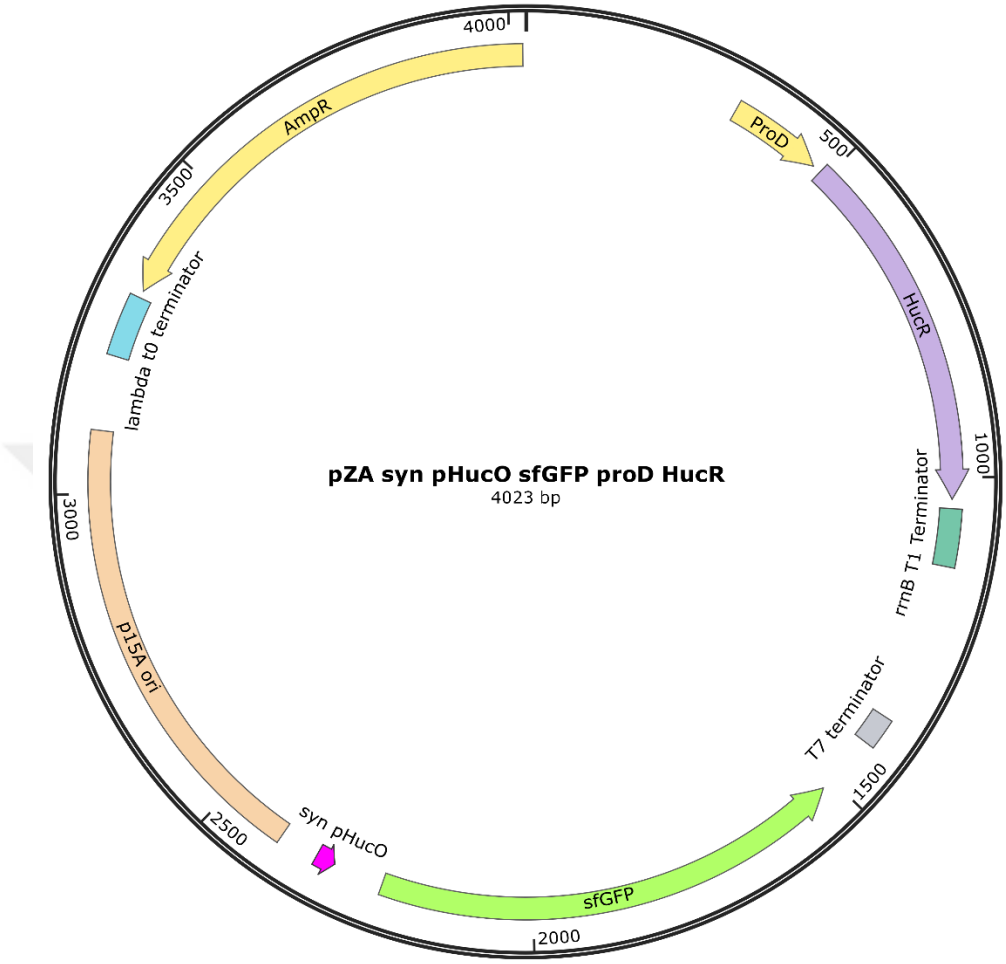

Figure C. 11: Schematic representation of pZA syn pHucO sfGFP proD HucR vector.

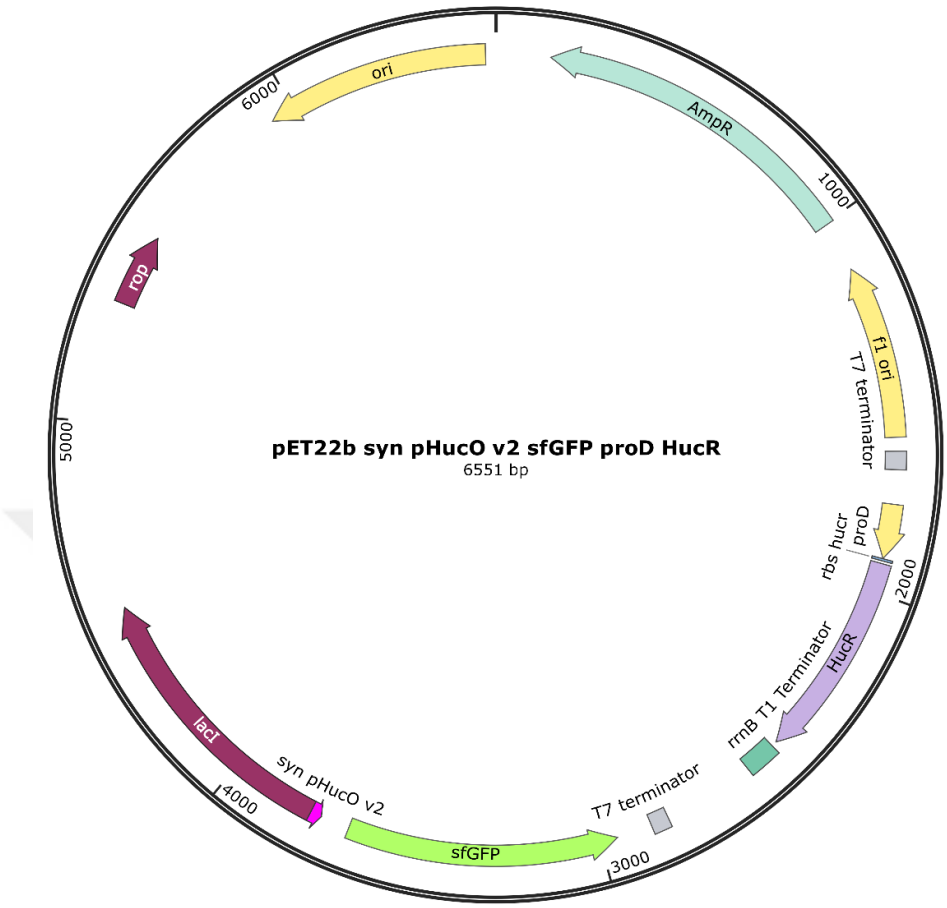

Figure C. 12: Schematic representation of pET-22b(+) syn pHucO v2 sfGFP proD HucR vector.

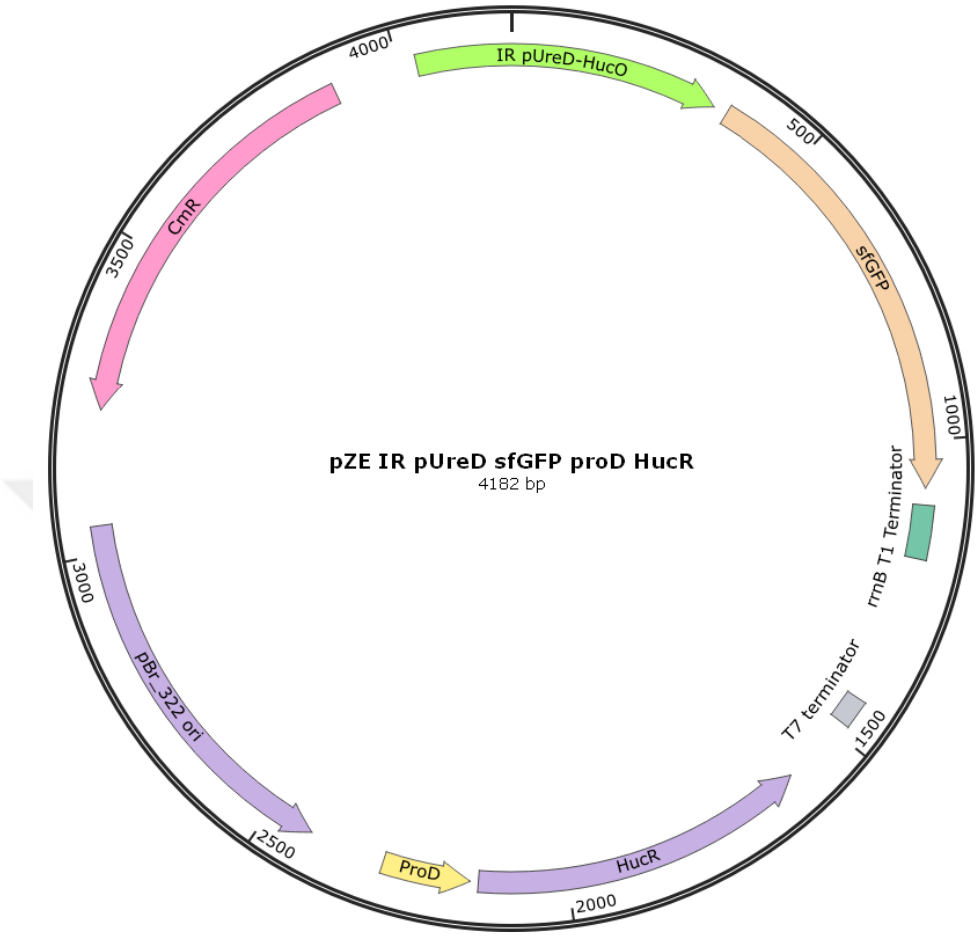

Figure C. 13: Schematic representation of pZE IR pUreD sfGFP proD HucR vector.

Figure C. 14: Schematic representation of pZE IR pUreD-HucO sfGFP proD HucR vector.

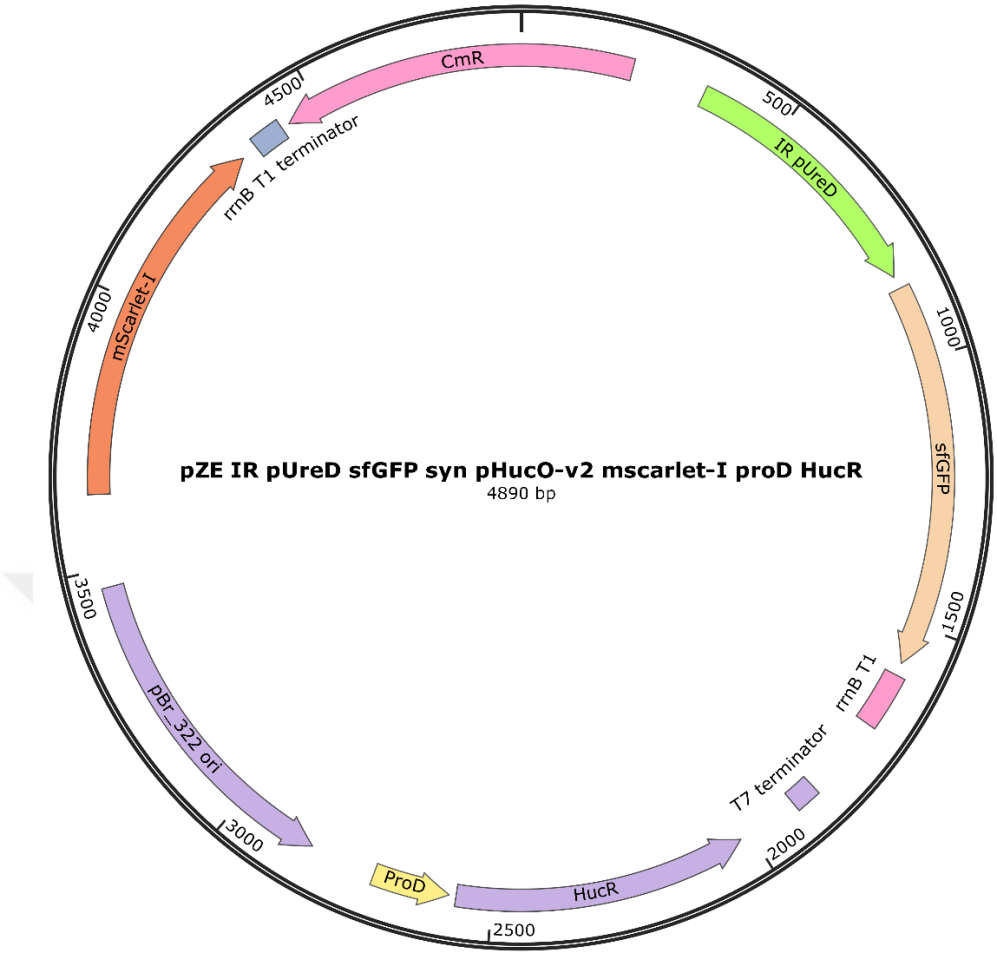

Figure C. 15: Schematic representation of pZE IR pUreD sfGFP syn pHucO-v2 mScarlet-I proD HucR vector.

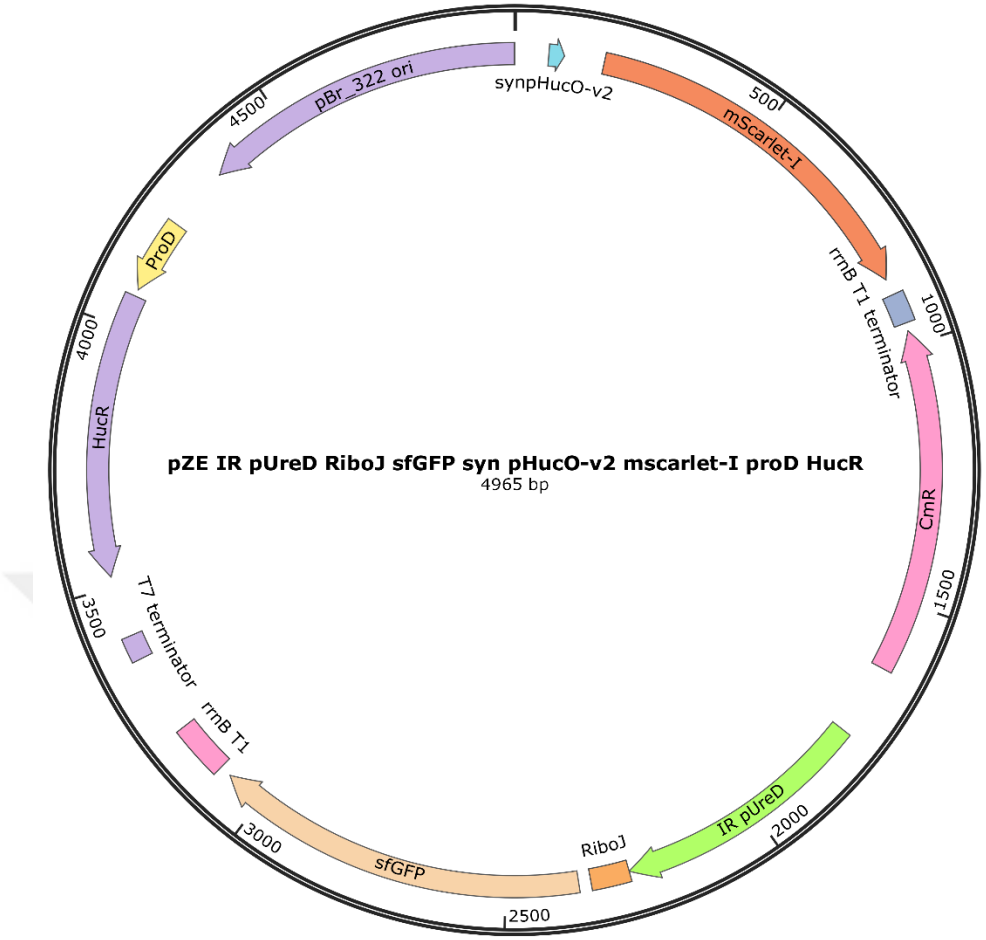

Figure C. 16:: Schematic representation of pZE IR pUreD RiboJ sfGFP syn pHucO-v2 mScarlet-I proD HucR vector

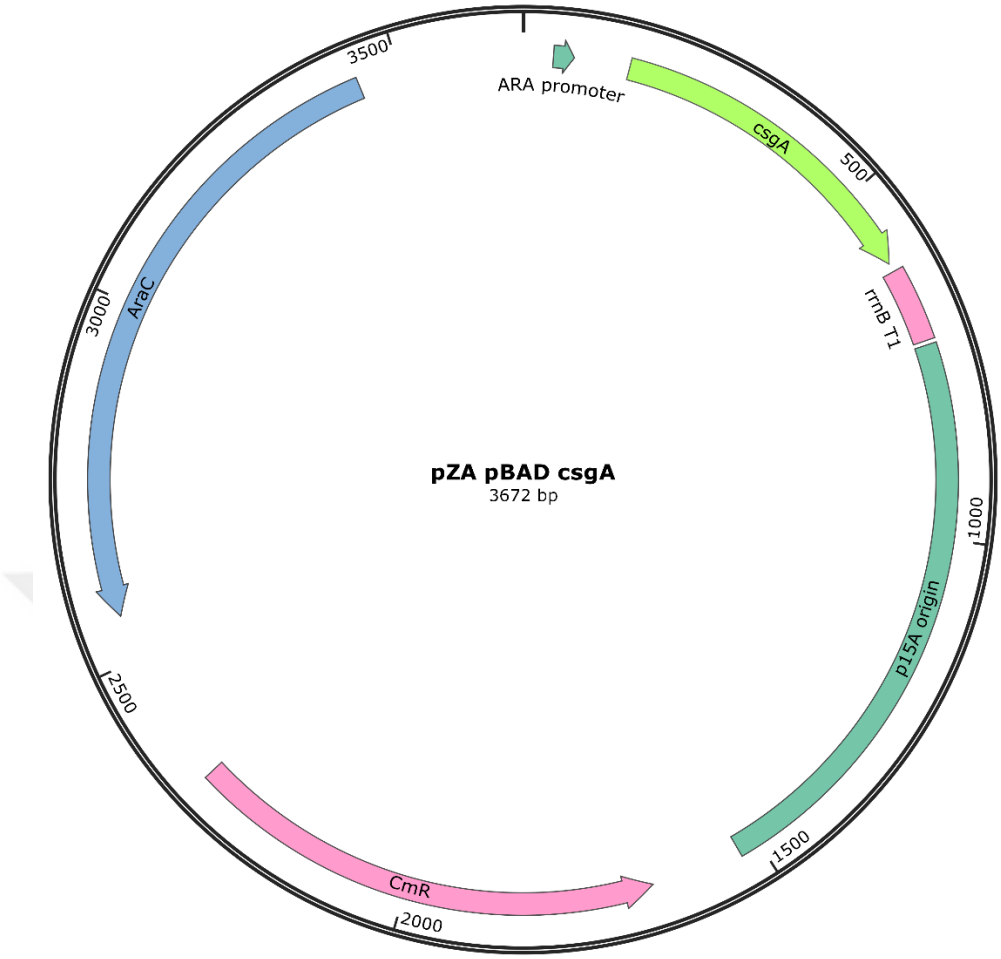

Figure C. 17: Schematic representation of pZA pBAD csgA vector.

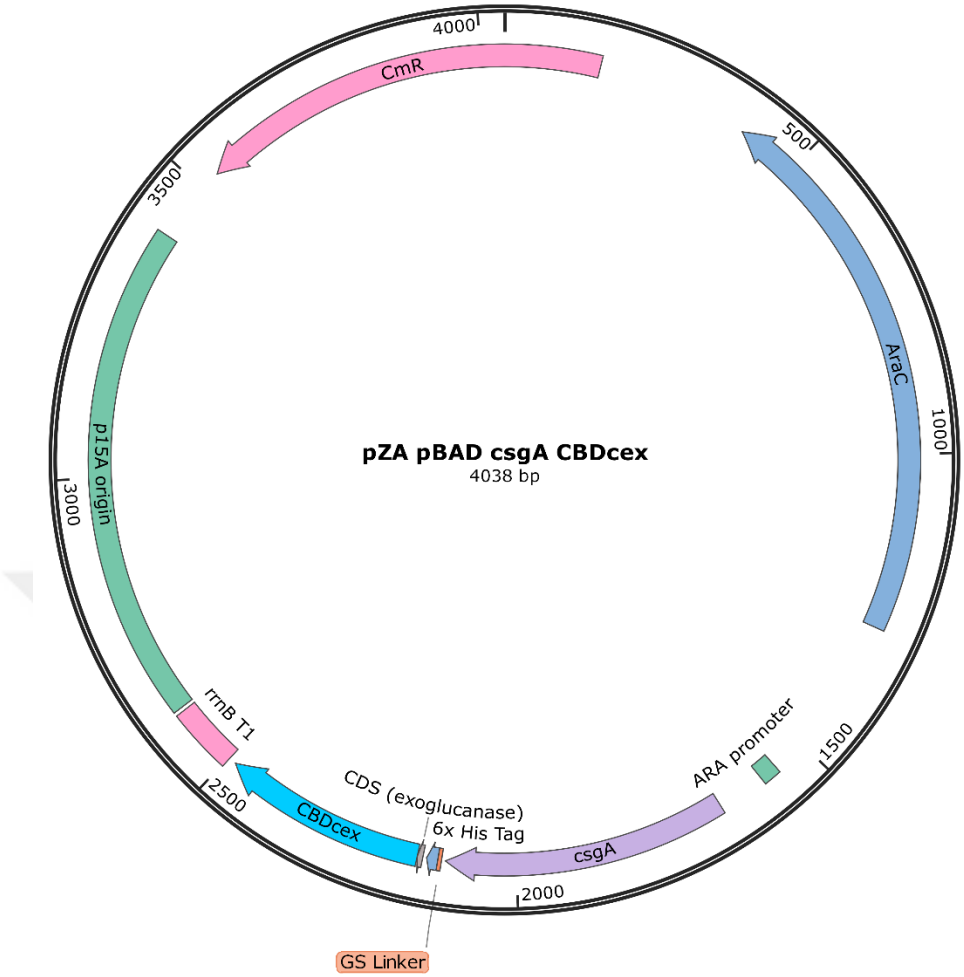

Figure C. 18: Schematic representation of pZA pBAD csgA-CBDcex vector.

APPENDIX D

Sequencing verifications of the plasmids used in this thesis

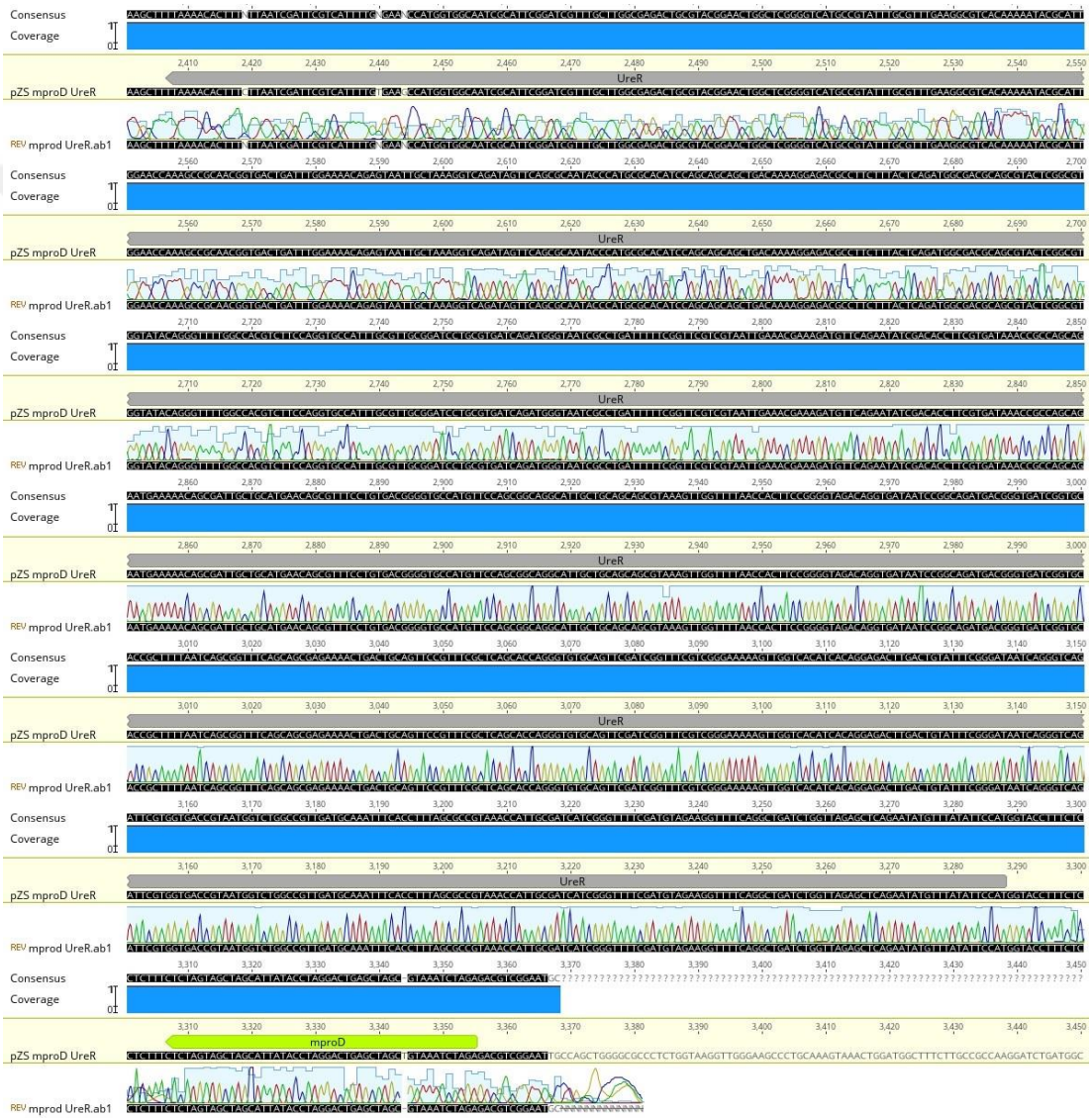

Figure D. 1: Sanger sequencing alignment with pZS mproD UreR chosen as reference.

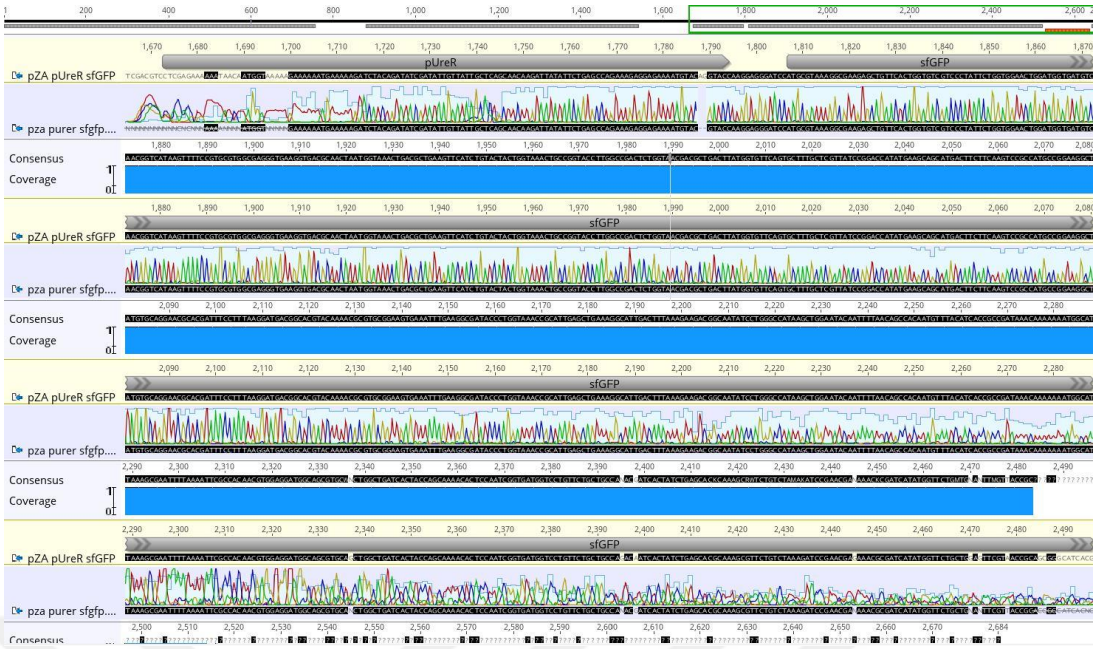

Figure D. 2: Sanger sequencing alignment with pZA pUreR sfGFP chosen as reference.

Figure D. 3: Sanger sequencing alignment with pZE pUreR sfGFP chosen as reference.

Figure D. 4: Sanger sequencing alignment with pZE IR pUreR sfGFP chosen as reference.

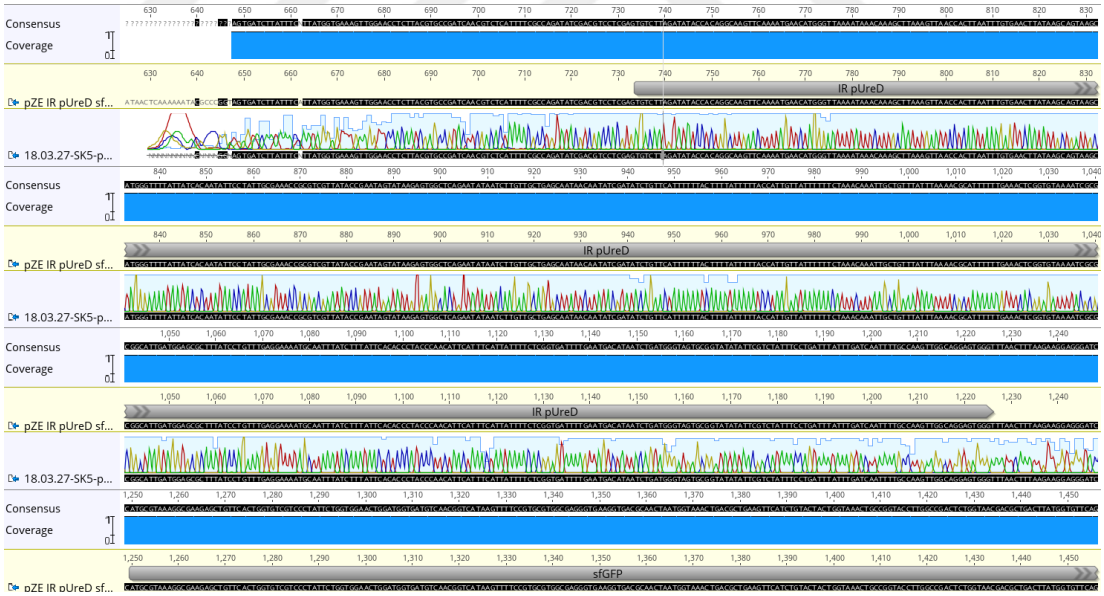

Figure D. 5: Sanger sequencing alignment with pZE IR pUreD sfGFP chosen as reference.

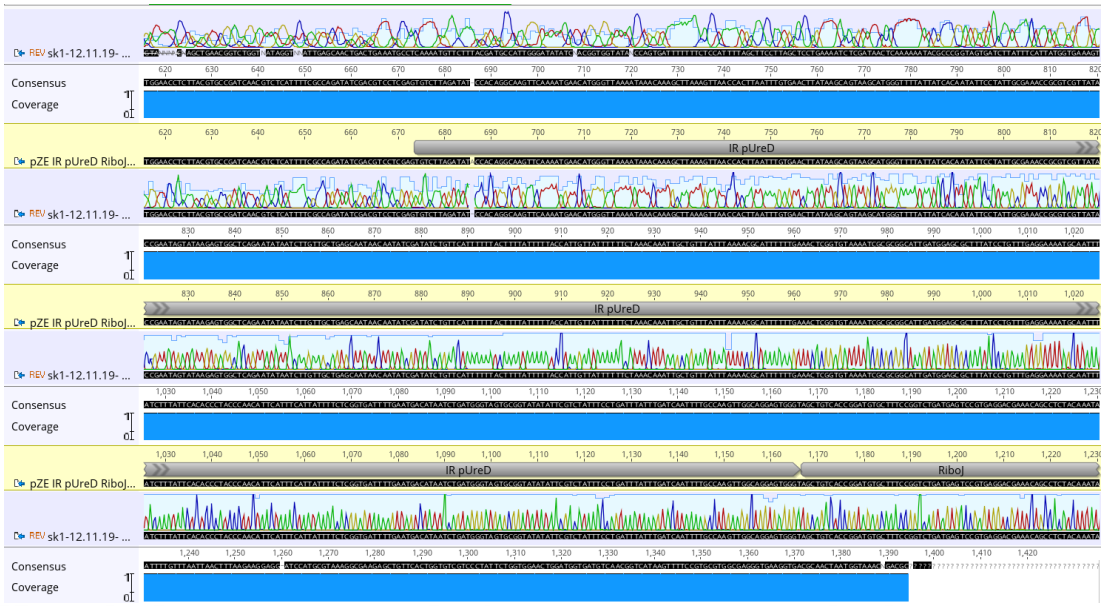

Figure D. 6: Sanger sequencing alignment with pZE IR pUreD RiboJ sfGFP chosen as reference.

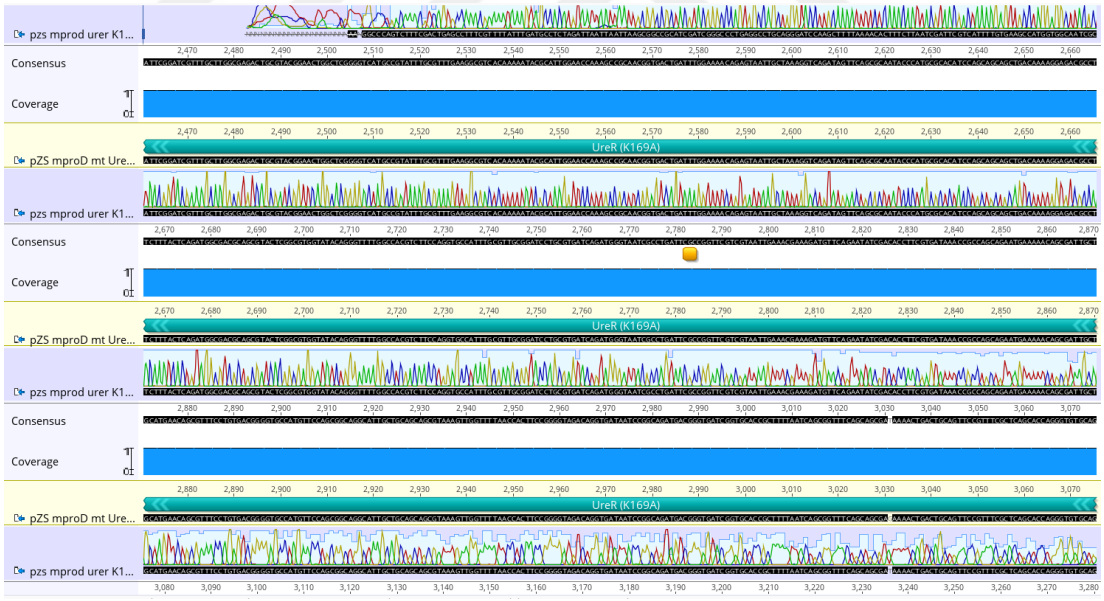

Figure D. 7: Sanger sequencing alignment with pZS mproD mt UreR (K16A) chosen as reference.

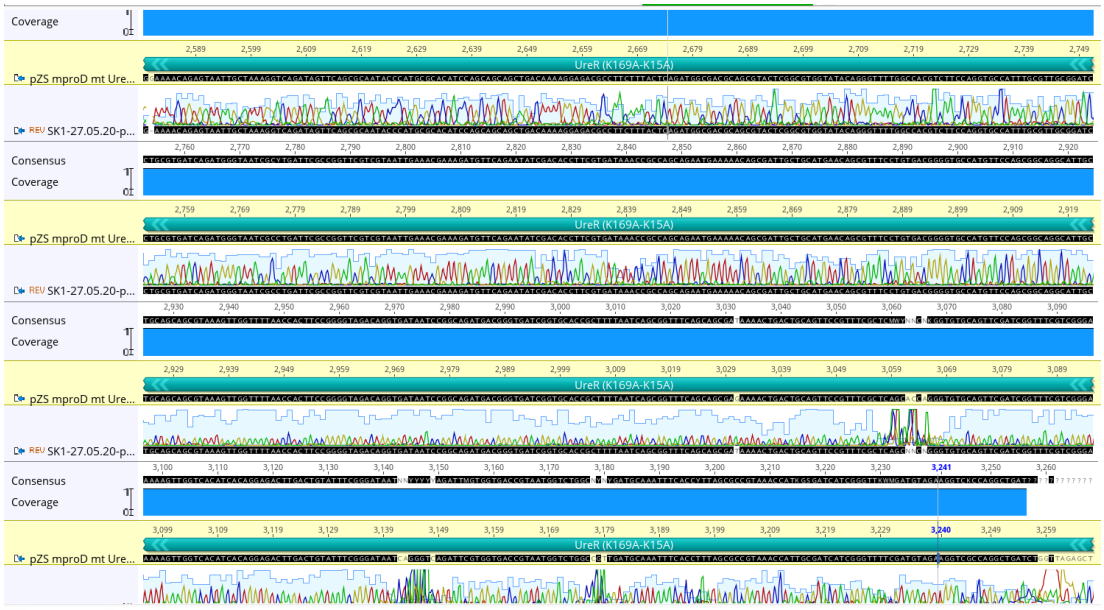

Figure D. 8: Sanger sequencing alignment with pZS mproD mt UreR (K15A-K16A) chosen as reference.

Figure D. 9: Sanger sequencing alignment with pZS mproD UACT chosen as reference.

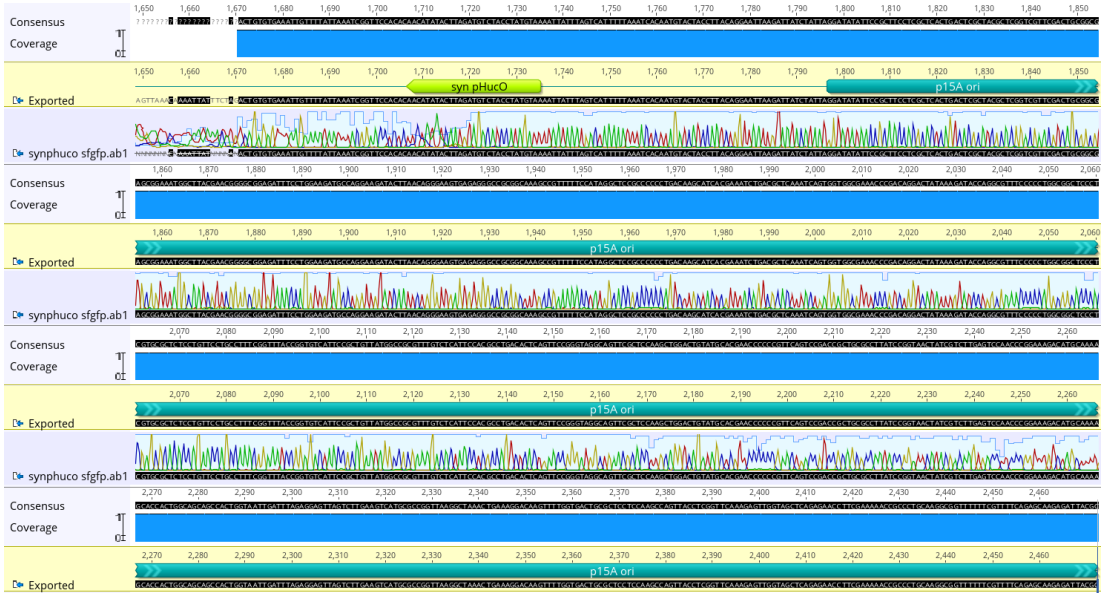

Figure D. 10: Sanger sequencing alignment with pZA syn pHucO sfGFP chosen as reference.

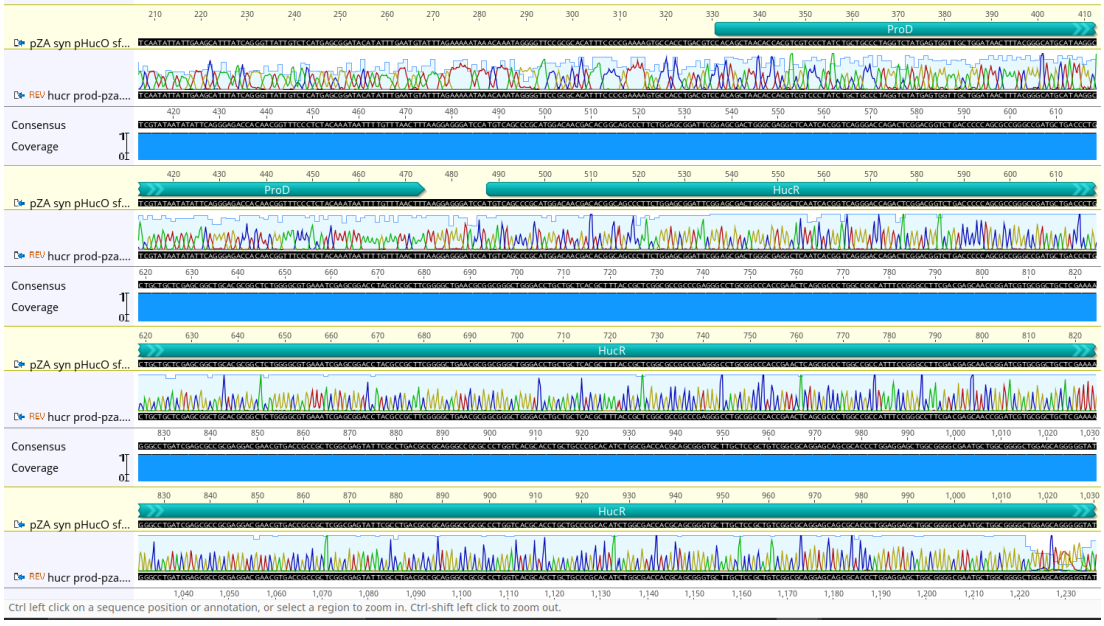

Figure D. 11: Sanger sequencing alignment with pZA syn pHucO sfGFP proD HucR chosen as reference.

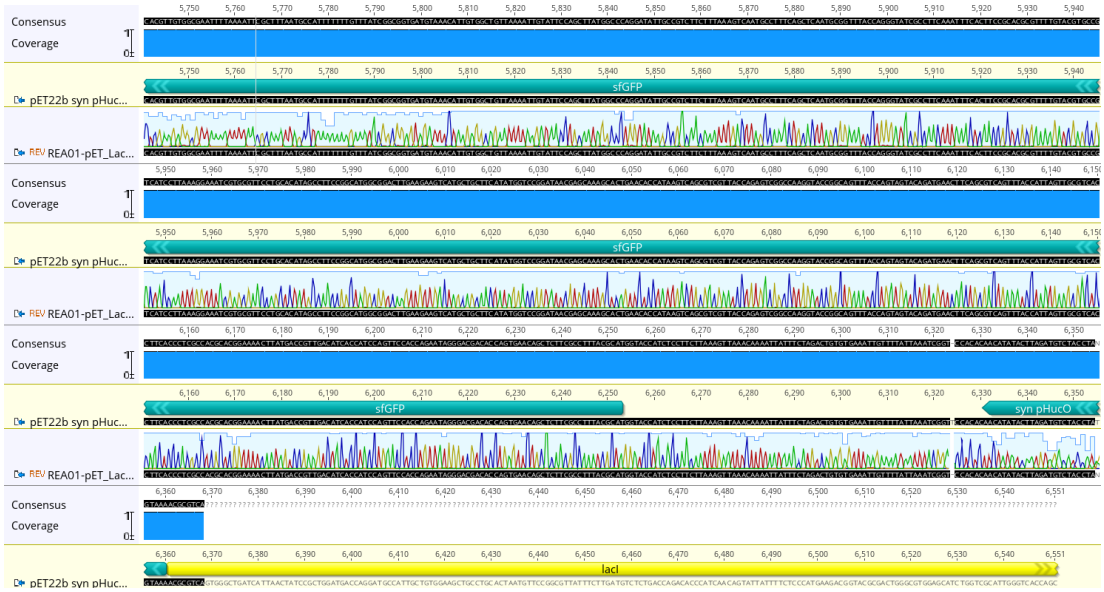

Figure D. 12: Sanger sequencing alignment with pET-22b(+) syn pHucO v2 sfGFP proD HucR chosen as reference.

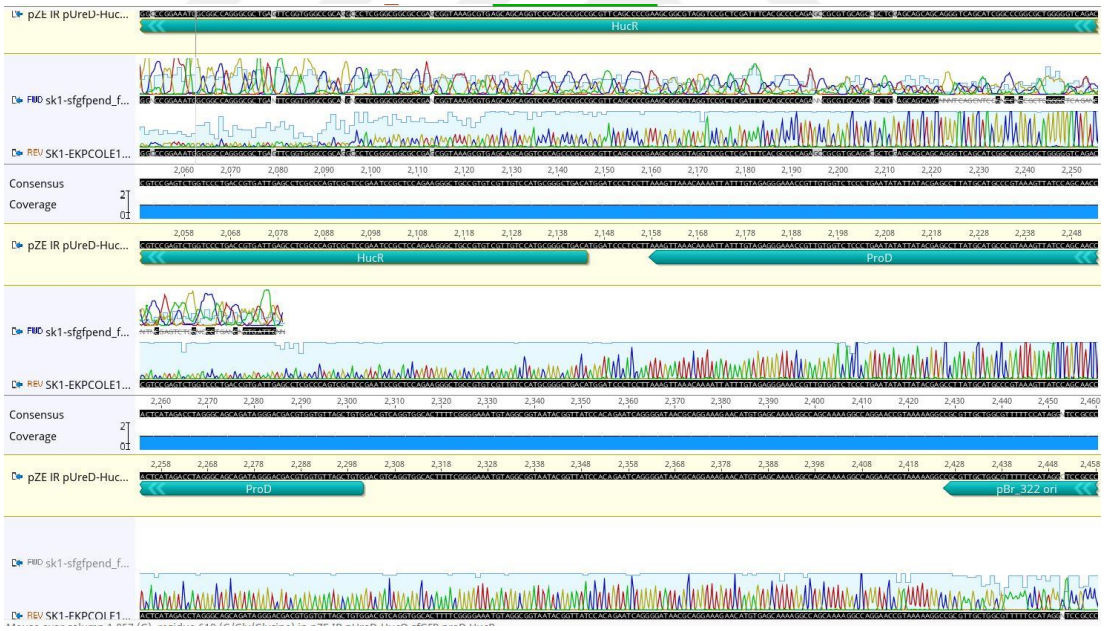

Figure D. 13: First sanger sequencing alignment with pZE IR pUreD sfGFP proD HucR chosen as reference.

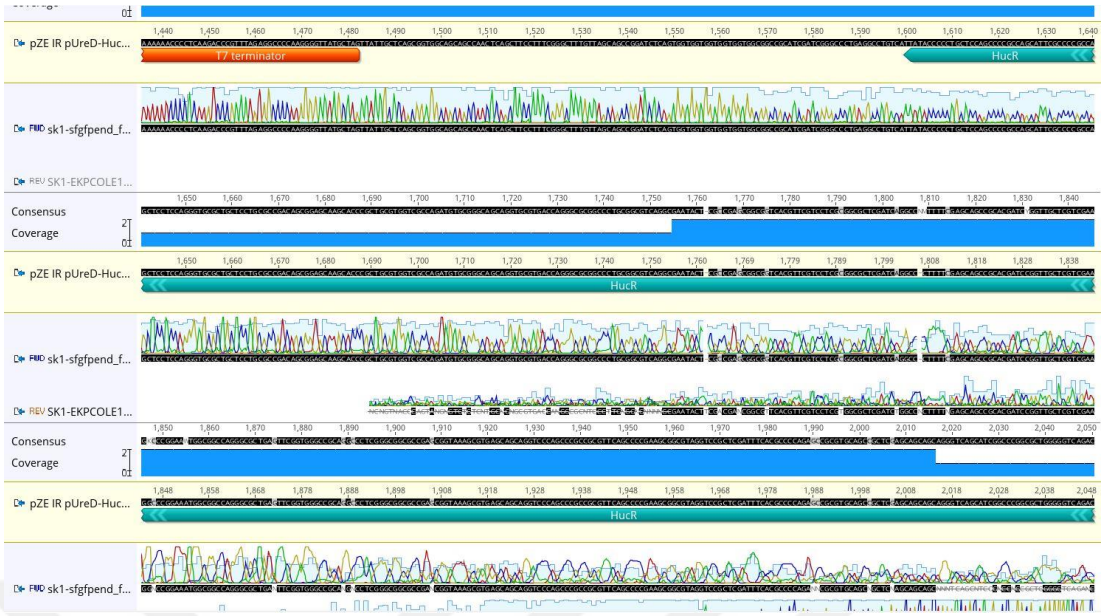

Figure D. 14: Second sanger sequencing alignment with pZE IR pUreD sfGFP proD HucR chosen as reference.

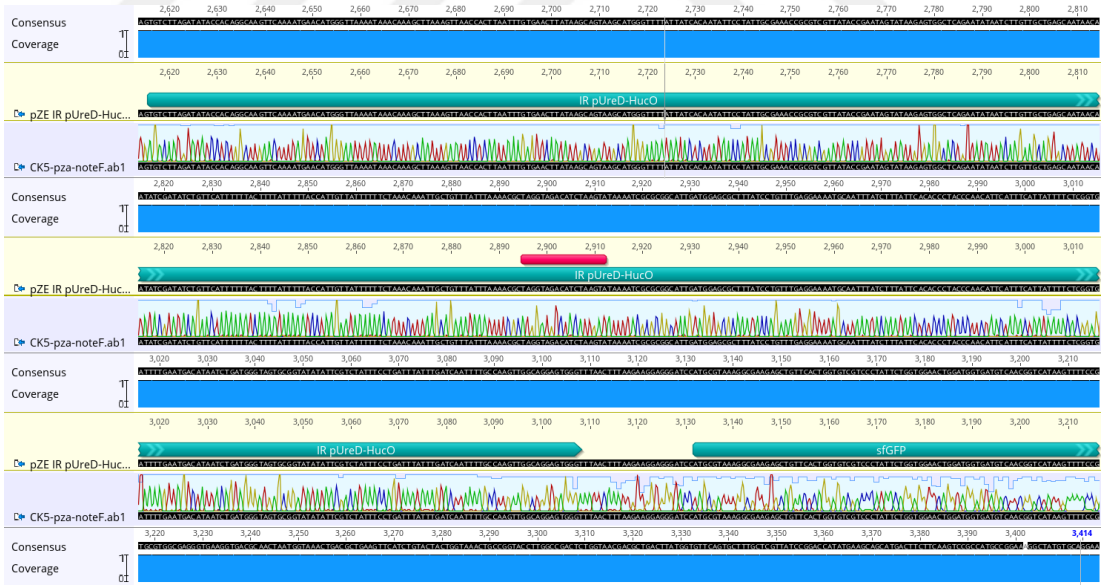

Figure D. 15: Sanger sequencing alignment with pZE IR pUreD-HucO sfGFP proD HucR chosen as reference.

Figure D. 16: Sanger sequencing alignment with pZE IR pUreD sfGFP syn pHucO mScarlet I proD HucR chosen as reference.

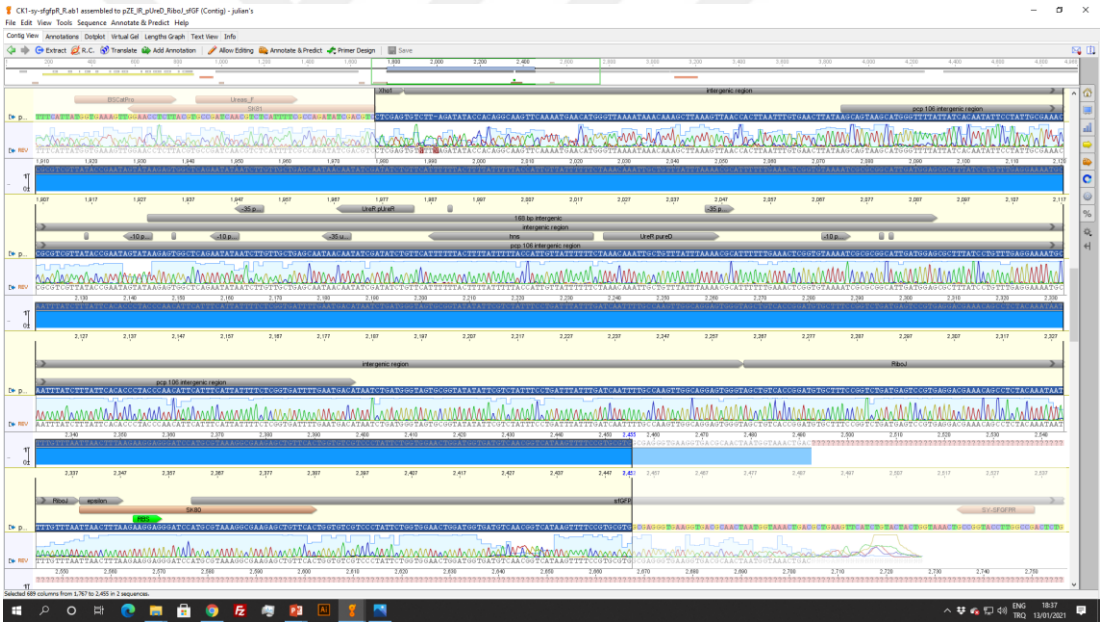

Figure D. 17: Sanger sequencing alignment with pZE IR pUreD RiboJ sfGFP syn pHucO mScarlet I proD HucR chosen as reference.

Figure D. 18: Sanger sequencing alignment with pZA pBAD csgA-CBDcex chosen as reference.

REFERENCES

1. Khalil, A.S. and J.J. Collins, *Synthetic biology: applications come of age.* Nat Rev Genet, 2010. **11**(5): p. 367-79.
2. Courbet, A., E. Renard, and F. Molina, *Bringing next-generation diagnostics to the clinic through synthetic biology.* EMBO molecular medicine, 2016. **8**(9): p. 987-991.
3. Sheth, R.U. and H.H. Wang, *DNA-based memory devices for recording cellular events.* Nature Reviews Genetics, 2018. **19**(11): p. 718-732.
4. Katz, L., et al., *Synthetic biology advances and applications in the biotechnology industry: a perspective.* Journal of industrial microbiology & biotechnology, 2018. **45**(7): p. 449-461.
5. Ruder, W.C., T. Lu, and J.J. Collins, *Synthetic biology moving into the clinic.* Science, 2011. **333**(6047): p. 1248-1252.
6. Xie, M. and M. Fussenegger, *Designing cell function: assembly of synthetic gene circuits for cell biology applications.* Nature Reviews Molecular Cell Biology, 2018. **19**(8): p. 507-525.
7. Liu, X., et al., *Design of a transcriptional biosensor for the portable, on-demand detection of cyanuric acid.* ACS synthetic biology, 2019. **9**(1): p. 84-94.
8. Archer, E.J., A.B. Robinson, and G.M. Suel, *Engineered E. coli that detect and respond to gut inflammation through nitric oxide sensing.* ACS Synth Biol, 2012. **1**(10): p. 451-7.
9. Daeffler, K.N., et al., *Engineering bacterial thiosulfate and tetrathionate sensors for detecting gut inflammation.* Mol Syst Biol, 2017. **13**(4): p. 923.
10. Ho, C.L., et al., *Engineered commensal microbes for diet-mediated colorectal-cancer chemoprevention.* Nat Biomed Eng, 2018. **2**(1): p. 27-37.
11. Danino, T., et al., *Programmable probiotics for detection of cancer in urine.* Sci Transl Med, 2015. **7**(289): p. 289ra84.
12. Watstein, D.M. and M.P. Styczynski, *Development of a Pigment-Based Whole-Cell Zinc Biosensor for Human Serum.* ACS Synth Biol, 2018. **7**(1): p. 267-275.
13. Kotula, J.W., et al., *Programmable bacteria detect and record an environmental signal in the mammalian gut.* Proc Natl Acad Sci U S A, 2014. **111**(13): p. 4838-43.
14. Kemmer, C., et al., *Self-sufficient control of urate homeostasis in mice by a synthetic circuit.* Nat Biotechnol, 2010. **28**(4): p. 355-60.
15. Duan, F. and J.C. March, *Engineered bacterial communication prevents Vibrio cholerae virulence in an infant mouse model.* Proc Natl Acad Sci U S A, 2010. **107**(25): p. 11260-4.
16. Saeidi, N., et al., *Engineering microbes to sense and eradicate Pseudomonas aeruginosa, a human pathogen.* Mol Syst Biol, 2011. **7**: p. 521.
17. Gupta, S., E.E. Bram, and R. Weiss, *Genetically programmable pathogen sense and destroy.* ACS Synth Biol, 2013. **2**(12): p. 715-23.
18. Hwang, I.Y., et al., *Reprogramming microbes to be pathogen-seeking killers.* ACS Synth Biol, 2014. **3**(4): p. 228-37.
19. Courbet, A., et al., *Detection of pathological biomarkers in human clinical samples via amplifying genetic switches and logic gates.* Sci Transl Med, 2015. **7**(289): p. 289ra83.
20. Gui, Q., et al., *The application of whole cell-based biosensors for use in environmental analysis and in medical diagnostics.* Sensors, 2017. **17**(7): p. 1623.
21. Cheng, F., X.L. Tang, and T. Kardashliev, *Transcription factor-based biosensors in high-throughput screening: advances and applications.* Biotechnology journal, 2018. **13**(7): p. 1700648.

22. De Paepe, B., et al., *Tailor-made transcriptional biosensors for optimizing microbial cell factories.* Journal of industrial microbiology & biotechnology, 2017. **44**(4-5): p. 623-645.
23. Fernandez-López, R., et al., *Transcription factor-based biosensors enlightened by the analyte.* Frontiers in Microbiology, 2015. **6**: p. 648.
24. Mannan, A.A., et al., *Fundamental design principles for transcription-factor-based metabolite biosensors.* ACS synthetic biology, 2017. **6**(10): p. 1851-1859.
25. Tang, S.Y. and P.C. Cirino, *Design and application of a mevalonate-responsive regulatory protein.* Angewandte Chemie, 2011. **123**(5): p. 1116-1118.
26. Chou, H.H. and J.D. Keasling, *Programming adaptive control to evolve increased metabolite production.* Nature communications, 2013. **4**(1): p. 1-8.
27. Cherney, L.T., et al., *Crystal structure of the intermediate complex of the arginine repressor from Mycobacterium tuberculosis bound with its DNA operator reveals detailed mechanism of arginine repression.* Journal of molecular biology, 2010. **399**(2): p. 240-254.
28. Xiao, Y., et al., *Exploiting nongenetic cell-to-cell variation for enhanced biosynthesis.* Nature chemical biology, 2016. **12**(5): p. 339-344.
29. Sedlmayer, F., D. Aubel, and M. Fussenegger, *Synthetic gene circuits for the detection, elimination and prevention of disease.* Nature biomedical engineering, 2018. **2**(6): p. 399-415.
30. Qian, S. and P.C. Cirino, *Using metabolite-responsive gene regulators to improve microbial biosynthesis.* Current opinion in chemical engineering, 2016. **14**: p. 93-102.
31. Cheng, J.K. and H.S. Alper, *Transcriptomics-guided design of synthetic promoters for a mammalian system.* ACS Synthetic Biology, 2016. **5**(12): p. 1455-1465.
32. Baig, H. and J. Madsen, *Simulation approach for timing analysis of genetic logic circuits.* ACS synthetic biology, 2017. **6**(7): p. 1169-1179.
33. Haberle, J., et al., *Suggested guidelines for the diagnosis and management of urea cycle disorders.* Orphanet J Rare Dis, 2012. **7**: p. 32.
34. Hosten, A.O., *BUN and Creatinine*, in *Clinical Methods: The History, Physical, and Laboratory Examinations*, rd, et al., Editors. 1990: Boston.
35. Taylor, A.J. and P. Vadgama, *Analytical reviews in clinical biochemistry: the estimation of urea.* Ann Clin Biochem, 1992. **29 (Pt 3)**: p. 245-64.
36. Leonard, J. and A. Morris. *Urea cycle disorders*. in *Seminars in neonatology*. 2002. Elsevier.
37. Morimoto, K., et al., *Automatic electrochemical micro-pH-stat for biomicrosystems.* Anal Chem, 2008. **80**(4): p. 905-14.
38. Jurkiewicz, M., et al., *Development of a biparametric bioanalyser for creatinine and urea. Validation of the determination of biochemical parameters associated with hemodialysis.* Analyst, 1998. **123**(6): p. 1321-7.
39. Lee, W.-Y., et al., *Sol–gel-derived thick-film conductometric biosensor for urea determination in serum.* Analytica Chimica Acta, 2000. **404**(2): p. 195-203.
40. Suman, et al., *Chronocoulometric determination of urea in human serum using an inkjet printed biosensor.* Anal Chim Acta, 2011. **697**(1-2): p. 98-102.
41. Maiuolo, J., et al., *Regulation of uric acid metabolism and excretion.* International journal of cardiology, 2016. **213**: p. 8-14.
42. Obermayr, R.P., et al., *Elevated uric acid increases the risk for kidney disease.* Journal of the American Society of Nephrology, 2008. **19**(12): p. 2407-2413.
43. Nakagawa, T., et al., *Unearthing uric acid: an ancient factor with recently found significance in renal and cardiovascular disease.* Kidney international, 2006. **69**(10): p. 1722-1725.

44. Kemmer, C., et al., *Self-sufficient control of urate homeostasis in mice by a synthetic circuit.* Nature biotechnology, 2010. **28**(4): p. 355-360.
45. Erden, P.E. and E. Kılıç, *A review of enzymatic uric acid biosensors based on amperometric detection.* Talanta, 2013. **107**: p. 312-323.
46. Obermayr, R.P., et al., *Predictors of new-onset decline in kidney function in a general middle-European population.* Nephrology Dialysis Transplantation, 2008. **23**(4): p. 1265-1273.
47. Kang, D.-H., et al., *A role for uric acid in the progression of renal disease.* Journal of the American Society of Nephrology, 2002. **13**(12): p. 2888-2897.
48. Guo, J., *Uric acid monitoring with a smartphone as the electrochemical analyzer.* Analytical chemistry, 2016. **88**(24): p. 11986-11989.
49. Walker, H.K., W.D. Hall, and J.W. Hurst, *The Oral Cavity and Associated Structures--Clinical Methods: The History, Physical, and Laboratory Examinations.* 1990.
50. Clark, V.L. and J.A. Kruse, *Clinical methods: the history, physical, and laboratory examinations.* Jama, 1990. **264**(21): p. 2808-2809.
51. Slomovic, S., K. Pardee, and J.J. Collins, *Synthetic biology devices for in vitro and in vivo diagnostics.* Proceedings of the National Academy of Sciences, 2015. **112**(47): p. 14429-14435.
52. Dattelbaum, J.D., et al., *UreR, the transcriptional activator of the Proteus mirabilis urease gene cluster, is required for urease activity and virulence in experimental urinary tract infections.* Infection and immunity, 2003. **71**(2): p. 1026-1030.
53. D'Orazio, S.E., V. Thomas, and C.M. Collins, *Activation of transcription at divergent urea-dependent promoters by the urease gene regulator UreR.* Molecular microbiology, 1996. **21**(3): p. 643-655.
54. Island, M.D. and H. Mobley, *Proteus mirabilis urease: operon fusion and linker insertion analysis of ure gene organization, regulation, and function.* Journal of bacteriology, 1995. **177**(19): p. 5653-5660.
55. Lu, T.K., A.S. Khalil, and J.J. Collins, *Next-generation synthetic gene networks.* Nature biotechnology, 2009. **27**(12): p. 1139.
56. Qi, L., et al., *RNA processing enables predictable programming of gene expression.* Nature biotechnology, 2012. **30**(10): p. 1002-1006.
57. Lou, C., et al., *Ribozyme-based insulator parts buffer synthetic circuits from genetic context.* Nature biotechnology, 2012. **30**(11): p. 1137-1142.
58. Clifton, K.P., et al., *The genetic insulator RiboJ increases expression of insulated genes.* Journal of biological engineering, 2018. **12**(1): p. 1-6.
59. Mobley, H., R. Thompson, and J. Dattelbaum, *Methods for assaying for urea and kits for use therein*. 2004, Google Patents.
60. Wilkinson, S.P. and A. Grove, *HucR, a novel uric acid-responsive member of the MarR family of transcriptional regulators from Deinococcus radiodurans.* Journal of biological chemistry, 2004. **279**(49): p. 51442-51450.
61. Moser, F., et al., *Light-controlled, high-resolution patterning of living engineered bacteria onto textiles, ceramics, and plastic.* Advanced Functional Materials, 2019. **29**(30): p. 1901788.
62. Wegst, U.G., et al., *Bioinspired structural materials.* Nat Mater, 2015. **14**(1): p. 23-36.
63. Augimeri, R.V., A.J. Varley, and J.L. Strap, *Establishing a Role for Bacterial Cellulose in Environmental Interactions: Lessons Learned from Diverse Biofilm-Producing Proteobacteria.* Front Microbiol, 2015. **6**: p. 1282.
64. Chapman, M.R., et al., *Role of Escherichia coli curli operons in directing amyloid fiber formation.* Science, 2002. **295**(5556): p. 851-5.
65. Barnhart, M.M. and M.R. Chapman, *Curli biogenesis and function.* Annu Rev Microbiol, 2006. **60**: p. 131-47.

66. Serra, D.O., G. Klauck, and R. Hengge, *Vertical stratification of matrix production is essential for physical integrity and architecture of macrocolony biofilms of E scherichia coli.* Environmental microbiology, 2015. **17**(12): p. 5073-5088.
67. Serra, D.O., A.M. Richter, and R. Hengge, *Cellulose as an architectural element in spatially structured Escherichia coli biofilms.* Journal of bacteriology, 2013. **195**(24): p. 5540-5554.
68. Florea, M., et al., *Engineering control of bacterial cellulose production using a genetic toolkit and a new cellulose-producing strain.* Proceedings of the National Academy of Sciences, 2016. **113**(24): p. E3431-E3440.
69. Wang, A.A., A. Mulchandani, and W. Chen, *Whole-cell immobilization using cell surface-exposed cellulose-binding domain.* Biotechnology progress, 2001. **17**(3): p. 407-411.
70. Ong, E., et al., *The cellulose-binding domain (CBDCex) of an exoglucanase from Cellulomonas fimi: Production in Escherichia coli and characterization of the polypeptide.* Biotechnology and bioengineering, 1993. **42**(4): p. 401-409.
71. Gupta, M.N., *Methods for affinity-based separations of enzymes and proteins*. 2002: Springer Science & Business Media.
72. Cui, M., et al., *Modular genetic design of multi-domain functional amyloids: Insights into self-assembly and functional properties.* Chemical science, 2019. **10**(14): p. 4004-4014.
73. Reichhardt, C., et al., *Congo red interactions with curli-producing E. coli and native curli amyloid fibers.* PloS one, 2015. **10**(10): p. e0140388.
74. Kan, A., et al., *Congo red fluorescence for rapid in situ characterization of synthetic curli systems.* Applied and environmental microbiology, 2019. **85**(13).
75. Yuk, H., et al., *Skin-inspired hydrogel–elastomer hybrids with robust interfaces and functional microstructures.* Nature communications, 2016. **7**(1): p. 1-11.
76. Aroguz, A.Z., et al., *Alginate/polyoxyethylene and alginate/gelatin hydrogels: preparation, characterization, and application in tissue engineering.* Applied biochemistry and biotechnology, 2014. **173**(2): p. 433-448.
77. Hagen, K., *Science policy and concomitant research in synthetic biology—Some critical thoughts.* Nanoethics, 2016. **10**(2): p. 201-213.
78. Schmidt, M., *Diffusion of synthetic biology: a challenge to biosafety.* Systems and synthetic biology, 2008. **2**(1-2): p. 1-6.
79. Yang, G., et al., *Assessment of the characteristics and biocompatibility of gelatin sponge scaffolds prepared by various crosslinking methods.* Scientific reports, 2018. **8**(1): p. 1-13.
80. Long, H., et al., *Preparation and characteristics of gelatin sponges crosslinked by microbial transglutaminase.* PeerJ, 2017. **5**: p. e3665.
81. Halloran, D.O., et al., *An injectable cross-linked scaffold for nucleus pulposus regeneration.* Biomaterials, 2008. **29**(4): p. 438-447.
82. Lien, S.-M., L.-Y. Ko, and T.-J. Huang, *Effect of pore size on ECM secretion and cell growth in gelatin scaffold for articular cartilage tissue engineering.* Acta biomaterialia, 2009. **5**(2): p. 670-679.
83. Valade, D., et al., *Polyacrylamide hydrogel membranes with controlled pore sizes.* Journal of Polymer Science Part A: Polymer Chemistry, 2013. **51**(1): p. 129-138.